GEND-INF- 092 — V1
January 1990
Cy 1

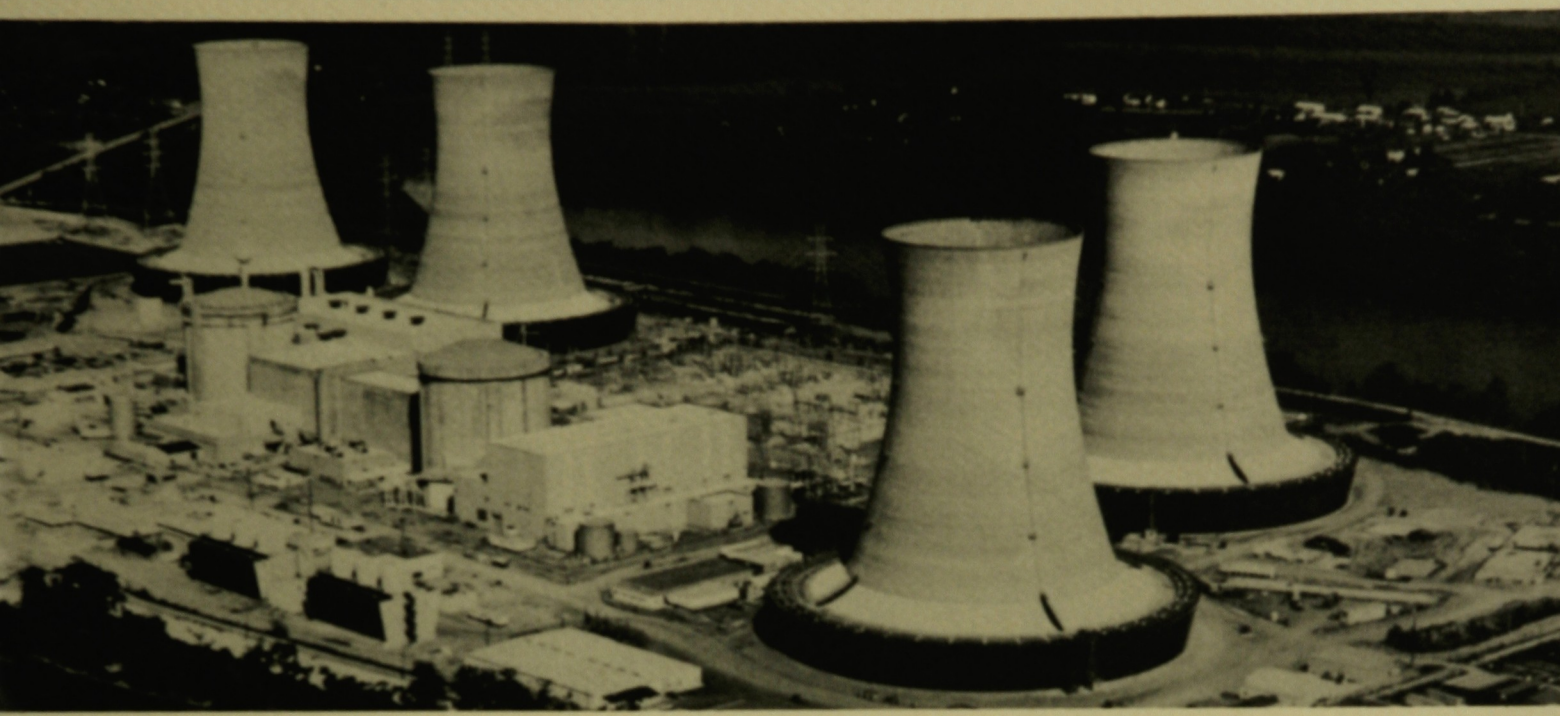

This is an informal report intended for use as a preliminary or working document

GEND
General Public Utilities • Electric Power Research Institute • U.S. Nuclear Regulatory Commission • U.S. Department of Energy

TMI-2 CORE BORE EXAMINATIONS
VOLUME 1

Douglas W. Akers
Charles S. Olsen
Bruce A. Pregger

Malcolm L. Russell
Richard K. McCardell

Prepared for the
U.S. Department of Energy
Three Mile Island Operations Office
Under Contract No. DE-AC07-76ID01570

GEND-INF-092

TMI-2 CORE BORE EXAMINATIONS
VOLUME 1

Douglas W. Akers
Charles S. Olsen
Malcolm L. Russell
Richard K. McCardell
Bruce A. Pregger

Published January 1990

EG&G Idaho, Inc.
Idaho Falls, Idaho 83415

Prepared for the
U.S. Department of Energy
Idaho Operations Office
Under DOE Contract No. DE-AC07-76ID01570

ABSTRACT

Nine core bore samples were examined from the lower part of the damaged reactor core at Three Mile Island. These core samples indicated the presence of a central consolidated core region composed of prior-molten debris above a region of partial fuel assemblies. The consolidated region was composed of a central region of prior-molten fuel debris surrounded by hard crusts. This document presents the results of the physical, metallurgical, and radiochemical examinations of the core bore samples and evaluates these results as they relate to the progression of core damage and fission-product behavior in this region of the reactor core. The results indicate the mechanisms that cause the retention of significant quantities of fission products (e.g., ^{125}Sb and ^{106}Ru) in the prior-molten materials in the central core region.

EXECUTIVE SUMMARY

As part of the Three Mile Island Unit 2 (TMI-2) Accident Evaluation Program conducted by EG&G Idaho, Inc. at the Idaho National Engineering Laboratory (INEL) for the U.S. Department of Energy, samples from the lower part of the damaged TMI-2 reactor core were obtained to characterize damage in this part of the reactor vessel. Core boring of the damaged reactor core was selected as the appropriate means of acquiring samples of the solid structure of prior-molten core materials and rod stubs beneath the upper debris bed. The core boring operation provided access into the lower plenum for visual inspection in regions previously inaccessible to closed circuit television.

The core boring operation was performed in July 1986 using a special computer-controlled device that used commercially available core boring machinery from the mining/geology industry. The core-bore drill was designed to cut a continuous 6.1-cm-dia core from the lower core region. However, as part of the consolidated region proved to be friable, portions of the samples broke up and were washed out of the containers. Thus, the actual samples recovered consisted of nine 6.3-cm cores containing fuel rod segments, crust sections, and fragments of debris. A series of photographic and visual inspections were performed of the open holes from the core bores to help characterize the lower core region.

The primary goal of sampling the lower core was to characterize the chemical, physical, and spatial distribution of materials in the lower core region. Samples were obtained from all regions of the lower core. The core bores provided two samples from the center of the core, two samples from near mid-radius, and six samples from around the core periphery. Only nine of these cores contained sample material. Access into the lower plenum for video inspection was obtained at three core inspection locations.

The initial characterization following disassembly was to produce full-length mosaic photographs of the samples in their as-received condition. Other characterizations were bulk sample weights and immersion

densities on all intact samples. The fragments were then sectioned to provide samples for the metallurgical and radiochemical examinations.

Nine of the ten core bores were examined, yielding a total of 130.5 kg of debris. The debris included fuel rod segments (115.8 kg) and loose, prior-molten debris (14.7 kg). The loose debris included samples of upper, lower, and peripheral crust regions and debris from the consolidated central core region between the crusts.

The visual examinations indicated that most of the lighter core bores (i.e., <13 kg) from near the center of the core consisted of short fuel rod sections. The mosaic photographs of each of the core bores indicate substantial damage to the relatively intact fuel rods below the consolidated prior-molten region; however, video examinations of the lower core region indicate that this damage was due to the core boring operation and that the fuel rods in the lower core were relatively intact and had not been exposed to high temperatures. The fuel rods varied in lengths, but in general, they ranged from 60 cm near the center of the core to 120 cm near the core periphery. The fuel rod cladding was not appreciably oxidized and showed substantial ductility, as indicated by the bent and twisted rods. There were indications of melting near the top surface of a few of the Ag/In/Cd control rods in the peripheral core bores; however, the visual examinations indicate that the intact rods at all core locations were not exposed to sufficiently high temperatures to melt the lower melting point materials such as the Ag/In/Cd control rods.

Above the intact fuel rods was the central consolidated region of the core surrounded by upper, lower, and peripheral crusts. Five of the core bores contained eight examples of the crust regions. Cores from the central part of the core contained examples of both top and bottom crust layers. The top crust was composed mostly of ceramic material with metallic inclusions that were either finely dispersed globules or relatively large regions of metallics deposited in the ceramic crust.

The metallographic examinations of the core bore samples indicated that the upper and peripheral crust material, as well as the material from the

central consolidated region, was very similar. Samples from these regions can basically be described as being a mixture of metallic and ceramic melts, with some segregation of metallic and ceramic phases. This segregation is due in some cases to immiscible metallic melts, particularly Ag-In and Fe-Cr-Ni, and sometimes the segregation is simply due to melts flowing over and through previously solidified melt material. Examples of metallic melts flowing through cracks in the solidified ceramic melt material are certainly evident in samples from the upper crust, which suggests that metallic melts from higher in the reactor core flowed down over the solidified upper crust. This also indicates that the melt progression was incoherent and took place over time.

Fuel liquefaction by zircaloy melts was observed in regions of the upper crust, which indicates temperatures in excess of 2200 K; however, the presence of $(U,Zr)O_2$ melt regions indicates that temperatures in some areas of the upper and peripheral crusts exceeded 2810 K prior to solidification. Localized temperatures within material in the center of the consolidated region exceeded the 3120 K melting point of the UO_2 fuel, as evidenced by large voids and porosity in some fuel pellet remnants. Average temperatures in the central consolidated region were certainly above 2810 K, in order to form the molten $(U,Zr)O_2$ that eventually flowed out of a breach in the crust and relocated to the lower vessel head.

In contrast to the other regions, the lower crust consisted primarily of metallic melts which flowed down and surrounded intact fuel pellet stacks. This metallic melt material can be assumed to represent material which relocated early in the melt progression. The lowest extent of this material probably solidified near the lowest water level during the accident. Oxidized cladding remnants were dissolved by these metallic melts, and any unoxidized zircaloy (portions were probably unoxidized based upon the lack of any significant zircaloy oxidation in the intact rod regions just below the lower crust) would probably have liquefied as a result of eutectic interactions between the zircaloy, silver, iron, and nickel. These interactions become significant above approximately 1400 K, with complete solidification of these materials expected by approximately

1200 K. Minor amounts of fuel liquefaction by the metallic melts were observed, which suggests localized maximum peak temperatures of approximately 2200 K. Based upon this information, a best estimate average temperature for the lower crust material is approximately 1300-1500 K.

The thickness of the crust varied from 4.5 to 11.5 cm, with the thickest amount being measured in the upper crust. These data suggest a relatively uniform crust thickness, which might be expected if it is assumed that this crust contained a molten pool of material of relatively uniform temperature. The density of samples from the upper and peripheral crusts varied from 7.6 to 9.7 g/cm^3, which reflects a consolidated mixture of $(U,Zr)O_2$ and metallic materials, whereas the density of the lower crust varied from 7.0 to 7.6 g/cm^3, which reflects the presence of significant amounts of zircaloy melt. The density of samples from the central consolidated region ranged from 5.5 to 8.8 g/cm^3, which reflects the segregation of immiscible metallic and ceramic melts.

The condition of the intact rod segments below the lower crust indicates that very little zircaloy oxidation occurred in this region, and that the rods remained ductile. Temperatures varied as a function of reactor core position and axial heights, but in general the temperatures were relatively cool. Molten control rod material indicated temperatures in excess of 1073 K on the upper endtips of some of the intact control rod segments on the periphery of the core, whereas the as-fabricated condition of the zircaloy cladding in many parts of this region indicated temperatures were below the recrystallization temperature of 920 K. The fuel rod lengths varied from approximately 60 cm near the center of the core to approximately 120 cm near the periphery of the core. These data suggest that the lowest water level during the accident was approximately 60 cm above the lower end fitting in the center of the reactor core. The presence of longer rod segments in the peripheral regions suggests that the lower crust solidified in a hemispherical shape, reflecting the cooler temperatures which would generally be expected in the peripheral regions for a given axial elevation.

The radiochemical examination data indicated that the upper and peripheral crusts were primarily ceramic material with some metallic material. The examinations indicated that the metallic portion of the upper crust was mostly made up of structural materials with lesser amounts of zirconium. For zirconium, the data from the ceramic regions range from 10 to 20 wt%; the average is 13 wt%, which indicates that zirconium is depleted in the upper crust relative to the core average concentration of 18 to 19 wt%.

Control materials were measurable in both metallic and ceramic material samples of the upper and peripheral crusts with an average silver concentration of about 3 wt%, which is greater than the expected core average concentration of silver (1.9 wt%). Indium and cadmium were both also measurable with indium at approximately 3 times the core average concentration. The nickel/molybdenum ratios in the upper crust suggest that the Inconel grid spacers contributed to the formation of the crusts along with some stainless steel.

The bulk of the uranium enrichment data for the upper crust suggests that the upper crust is a composite of the 1.98% and 2.64% enriched assemblies with a very homogeneous distribution of the fuel material from the two assembly enrichments. Also, the high relative retentions for the low volatile fission products suggest that the fuel material forming the upper crust came from a relatively high burnup region of the core and that the upper crust was not formed by fuel material from the upper periphery of the core.

The ^{90}Sr data for the upper crust indicate a wide range of concentrations with no apparent distinction between metallic and ceramic samples. The data indicate mobility of this radionuclide with no obvious correlation with elemental composition or other radionuclide characteristics. Comparisons with the elemental analysis results were also performed for ^{125}Sb and ^{106}Ru. These comparisons indicate an increase in metallic content generally correlated with large increases in ^{125}Sb and ^{106}Ru content.

Examinations for the high volatiles ^{129}I and ^{137}Cs indicate retention of these fission products in both metallic and ceramic materials. Comparisons indicate retentions in the ceramic phase that are approximately 5%, whereas in the metallic phase the uranium-based normalized retentions are about 35%. However, the concentration data are similar in both types of material, which indicates that the high retentions in the metal phases are an artifact of the normalization to uranium content which is low in the metallic samples.

The lower crust generally is composed of relatively intact columns of fuel pellets embedded in a metallic mixture. The intact columns contain some veins of metallic materials that extend into the cracks in some fuel pellets. The elemental data indicate that zirconium is concentrated in the crust and that tin is not transported with the zirconium and may tend to form accumulations separate from the zirconium in the lower crust. The average concentration data for the lower crust indicate that iron is the principal structural element present (average 11 wt%) and that it ranges up to 34 wt% in the metallic parts of the crust. Lesser concentrations of nickel (average 5.5 wt%) and chromium (average 1.6 wt%) are also present (the average zirconium content is 30 wt% in the metallic region).

The presence of significant amounts of molybdenum in the lower crust at ratios appropriate for Inconel suggests that Inconel was a significant contributor to the formation of the crust.

The average retention of low volatiles for the ceramic and metallic regions of the lower crust are between 130 and 134%. These retentions (i.e., >100%) indicate that the fuel material forming the lower crust came from a relatively high burnup region of the core.

For the medium volatiles, the data suggest that the bulk of the ^{90}Sr has been retained in the ceramic regions with only small amounts present in the metallic regions of the lower crust. For ^{125}Sb and ^{106}Ru, comparisons were performed with the concentrations of elemental

constituents of the crust; no correlations were observed with the exception that a general increase in metallic content generally correlated with an increase in ^{125}Sb and ^{106}Ru content.

The samples obtained from the central core region debris are quite heterogeneous; many samples are either metallic or ceramic, and some samples are a mixture of the two types of material. Examination of the data indicate that the least volatile control material, silver, was measurable in both metallic and ceramic material samples at an average concentration of about 2.9 wt%, with a range of concentrations from 0.07 to 34 wt%. Also, indium was measurable in all samples at concentrations averaging 0.9 wt% (core average 0.3 wt%), with the data ranging from 0.05 to 7.6 wt%. Cadmium was measurable in only about one-half of the samples obtained from the central core, principally the metallic ones. It is suggested that cadmium at relatively low concentrations alloyed with other materials, thereby reducing its vapor pressure substantially and causing retention in the reactor vessel.

Extrapolation of the elemental and radionuclide concentrations in the core bore samples to the volumes and masses of the upper and lower crusts and the consolidated region indicates that a significant fraction of the zirconium and metallic content of the core relocated to form the lower crust and that a substantial part of the metallic material in the central part of the core did not oxidize, but remained as metallic materials during the accident.

Examination of the radionuclide data indicates that the low and medium volatiles were retained in the core region. However, a large portion of the core inventories of ^{106}Ru and ^{125}Sb (medium volatiles) were retained in the core as metallic inclusions. Most of the high volatile inventory of the molten portion of the core was released with only a few percent of inventory retained in the prior molten debris.

ACKNOWLEDGMENTS

Many people contributed both to the acquisition and examination of the core bore samples. Acquisition of the samples was a joint effort between GPU Nuclear Corporation and EG&G Idaho, Inc. Design and fabrication of the core boring machine, which performed admirably, was the responsibility of M. R. Martin and B. B. Kaiser, with support from engineers and technicians at the Idaho National Engineering Laboratory (INEL). Without the support of the GPU Nuclear staff at TMI-2, the core boring operations would not have been accomplished. Special thanks go to G. R. Eidam for his efforts in these operations. Upon receipt of the core bores at the INEL, the initial photovisual characterization and sampling was performed by the staff of the Nuclear Materials Evaluation Organization at the TAN, ARA, and TRA hot cells. The metallographic examinations were performed by M. L. Lindstrom and P. M. Stephens; the Scanning Electron Microscopy (SEM) was performed by B. A. Pregger. The radiochemical examinations were performed by A. W. Marley and the Radiochemistry staff at TRA. Additional work was performed by L. A. Weinrich and M. W. Huntley.

CONTENTS

ABSTRACT ii

EXECUTIVE SUMMARY iii

ACKNOWLEDGMENTS x

1. INTRODUCTION 1-1

2. EXAMINATION PLAN AND ANALYSIS METHODS 2-1

2.1. Sample Acquisition 2-2

2.2 Sample Selection 2-2

2.3 Sample Examinations 2-4

3. EXAMINATION RESULTS AND DISCUSSION 3-1

3.1 Upper Crust Examination Results 3-6

3.1.1 Visual and Metallurgical Examinations 3-6
3.1.2 Upper Crust Bulk Composition 3-16
3.1.3 Upper Crust Radiochemical Examinations 3-29

3.2 Lower Crust Examination Results 3-41

3.2.1 Visual and Metallurgical Examinations 3-41
3.2.2 Lower Crust Bulk Composition 3-47
3.2.3 Lower Crust Radiochemical Examinations 3-64

3.3 Peripheral Crust Examination Results 3-73

3.3.1 Visual and Metallurgical Examinations 3-73
3.3.2 Peripheral Crust Bulk Composition 3-77
3.3.3 Peripheral Bulk Radiochemical Examinations 3-87

3.4 Central Core Consolidated Region Examination Results 3-94

3.4.1 Visual and Metallurgical Examinations 3-94
3.4.2 Central Core Bulk Composition 3-103
3.4.3 Central Core Region Radiochemical Examinations ... 3-114

3.5 Intact Core Component Examination Results 3-123

3.5.1 Visual and Metallurgical Examinations..... 3-123
3.5.2 Lower Core Structural Material Bulk Composition 3-131
3.5.3 Lower Core Structural Material Radiochemical Analyses 3-131

3.6 Fission Gas Analysis 3-134

4. CONTRIBUTIONS TO UNDERSTANDING THE TMI-2 ACCIDENT 4-1

4.1 Core Damage Progression 4-5

4.2 Bulk Core Materials Distribution 4-8

4.2.1 Fuel Materials 4-8
4.2.2 Control Materials 4-12
4.2.3 Structural Materials 4-15

4.3 Fission Product Behavior 4-18

4.3.1 Low Volatiles 4-19
4.3.2 Medium Volatiles 4-22
4.3.3 High Volatiles 4-26

5. CONCLUSIONS AND OBSERVATIONS 5-1

6. REFERENCES 6-1

APPENDIX A--TMI-2 LOWER CORE REGION SAMPLE SELECTION A-1

APPENDIX B--SAMPLE PREPARATION AND EXAMINATION METHODS B-1

APPENDIX C--VISUAL EXAMINATIONS C-1

APPENDIX D--DENSITY AND POROSITY DATA D-1

APPENDIX E--OPTICAL METALLOGRAPHY AND SEM DATA E-1

APPENDIX F--BETA-GAMMA AUTORADIOGRAPHY DATA F-1

APPENDIX G--ELEMENTAL ANALYSIS RESULTS G-1

APPENDIX H--RADIOCHEMICAL EXAMINATION RESULTS H-1

APPENDIX I--DATA QUALIFICATION I-1

APPENDIX J--QUANTITATIVE WDS ANALYSIS..... J-1

FIGURES

1. TMI-2 core end-state configuration 1-2

2. Core bore sampling locations 1-4

3. Mosaic photographs of the core bore samples 3-3

4. Cross section of upper crust from K09-P2 3-7

5. Transverse cross section from D08-P3 3-8

6. Typical ceramic melt structure in the upper crust (K9-P2) 3-9

7. ZrO_2 - Fe_3O_4 phase diagram 3-11

8. Transverse cross section from G08-P11 3-12

9. Coarse dendritic structure in metallic melt in G08-P11 3-13

10. Penetration of metallic material along fuel crack in G08-P11 3-14

11. Grain boundary porosity in fuel in G08-P11 3-15

12. K09-P2-C sampling locations 3-17

13. G08-P11-B sampling locations 3-19

14. D08-P3-A sampling locations 3-21

15. Metallic melt surrounding and penetrating fuel pellet stacks in K09-P1 3-42

16. Cladding oxidation and dissolution near fuel pellet in K09-P1 ... 3-43

17. SEM analysis of fuel dissolution in metallic melt (K09-P1) 3-44

18. UO_2 precipitates in metallic melt in lower crust (K09-P1) 3-48

19. UO_2 precipitates in metallic melt in lower crust (K09-P1) 3-49

20. Backscattered electron image of UO_2 precipitates in metallic melt (K09-P1) 3-50

21. SEM analysis of UO_2 precipitates in metallic melt (K09-P1) 3-51

22. K09-P1-C sampling locations 3-55

23. D08-P1-C sampling locations 3-56

24. D08-P2-A sampling locations 3-57

25. Morphology of ceramic melt in peripheral crust (G12-P1) 3-74

26. Mottled structure in ceramic melt of peripheral crust (G12-P1) .. 3-75

27. Longitudinal cross section through peripheral crust sample 007-P4 3-76

28. 007-P4-C sampling locations 3-78

29. G12-P1-D2 sampling locations 3-79

30. Metallic melt particle from central core region (009-P1) 3-95

31. Partially molten fuel pellets in central core region (G12-P4) ... 3-97

32. Pores in partially molten fuel pellet (G12-P4) 3-98

33. Mottled structure in $(U,Zr)O_2$ melt in central core region (G08-P10) 3-99

34. Second phase along $(U,Zr)O_2$ grain boundaries in central core region (G08-P10) 3-99

35. Backscattered electron image of iron, chromium, nickel eutectic phases in $(U,Zr)O_2$ grain boundaries (G08-P10) 3-100

36. Backscattered electron image of UO_2 crystal growth inside pore in ceramic matrix (G12-P9) 3-101

37. Secondary electron image of polyhedral UO_2 crystals in pores (G12-P9) 3-102

38. Fuel microstructure in fuel rod segment (D04-R9-2B) 3-124

39. As-fabricated zircaloy cladding in intact region just below lower crust (K09-R5-5L) 3-125

40. Zirconium hydrides in zircaloy cladding in intact region just below lower crust (K09-R5-5L) 3-126

41. Intact Ag-In-Cd in control rod segment K09-R13-2B 3-128

42. Molten control rod material near top of rod segment N12-R7-10Y .. 3-129

43. Cladding cracks at interaction zone of G08-R3 instrument tube ... 3-130

TABLES

1. TMI-2 reactor core composition 2-6

2. TMI-2 core bore cores examination program summary 2-7

3. TMI-2 core bore rocks examination program summary 2-9

4. TMI-2 post drilling rocks examination summary 2-12

5. TMI-2 core bore rods examination summary 2-13

6. Core bore sample weights 3-2

7. Upper crust average composition 3-23

8. Upper crust fuel material (U, Zr, Sn) weight percent ratios 3-24

9. Upper crust control material (Ag, In, Cd) weight ratios 3-25

10. Upper crust structural material (Fe, Cr, Ni, and Mo) weight ratios 3-28

11. Core material volatility groups 3-30

12. Upper crust average radionuclide concentrations 3-33

13. Upper crust uranium-235 enrichment 3-34

14. ORIGEN2 predicted radionuclide concentrations 3-36

15. Radionuclide retention in the upper crust 3-37

16. Radionuclide retention in metallic and ceramic samples 3-38

17. Lower crust average composition 3-59

18. Lower crust fuel material (U, Zr, Sn) weight ratios 3-60

19. Lower crust control material (Ag, In, Cd) weight ratios 3-63

20. Lower crust metallic material (Fe, Cr, and Ni) weight ratios 3-65

21. Lower crust average radionuclide concentrations 3-67

22. Lower crust uranium-235 enrichment 3-68

23. Radionuclide retention in the lower crust 3-70

24. Radionuclide retention in metallic and ceramic samples 3-71

25. Peripheral crust average composition 3-81

26. Peripheral crust fuel material (U, Zr, Sn) weight ratios 3-82

27. Peripheral crust control material (Ag, In, Cd) weight ratios 3-84

28. Peripheral crust structural material (Fe, Cr, and Ni) weight ratios 3-86

29. Peripheral crust average radionuclide concentrations 3-88

30. Peripheral crust uranium-235 enrichment 3-89

31. Radionuclide retention in the peripheral crust 3-91

32. Average radionuclide retention in metallic and ceramic samples 3-92

33. Core central region average composition 3-104

34. Central core region fuel material (U, Zr, Sn) weight ratios 3-106

35. Central core region control material (Ag, In, Cd) weight ratios 3-108

36. Central core region metallic material (Fe, Cr, and Ni) weight ratios 3-112

37. Central core region average radionuclide concentrations 3-115

38. Central core region uranium-235 enrichment 3-116

39. Radionuclide retention in the central core region 3-119

40. Average radionuclide retention in metallic and ceramic samples 3-121

41. Structural sample composition 3-132

42. Structural material surface radionuclide concentrations 3-133

43. Central core region average radionuclide concentrations 3-135

44. Sample locations for intact pellet and debris fission gas analyses 3-136

45. Estimated postaccident core materials distribution 4-2

46. Estimated ceramic and fuel material content of the lower core ... 4-9

47. Fuel material distributions in the molten pool 4-10

48. Control material distributions in the molten pool 4-13

49. Structural material distributions in the molten pool 4-16

50. Low volatile fission product distribution in the molten pool 4-20

51. Medium volatile fission product distribution in the molten pool 4-23

52. High volatile fission product distribution in the molten pool ... 4-27

TMI-2 CORE BORE EXAMINATIONS

1. INTRODUCTION

The Three Mile Island Unit 2 (TMI-2) pressurized water reactor (PWR) underwent a prolonged loss of coolant accident (LOCA) on March 28, 1979, that resulted in severe damage to the reactor core. As a consequence of the TMI-2 accident, numerous aspects of light water reactor (LWR) safety have been questioned, and the U.S. Nuclear Regulatory Commission (NRC) has embarked on a thorough review of reactor safety issues, particularly the causes and effects of severe core damage accidents. The nuclear community acknowledges the importance of examining TMI-2 in order to understand the nature of the core damage. Immediately after the accident, four organizations with interests in both plant recovery and acquisition of accident data formally agreed to cooperate in these areas. These organizations [General Public Utilities Nuclear Corporation (GPU Nuclear-owner/operator of TMI), Electric Power Research Institute (EPRI), the NRC, and the U.S. Department of Energy (DOE) collectively known as GEND] are presently involved in postaccident evaluations of TMI-2. The DOE is providing a portion of the funds for reactor recovery (in those areas where accident recovery knowledge will be of benefit to the LWR industry in the United States). In addition, DOE is funding acquisition and examination of samples obtained from the damaged reactor core.

The end-state configuration of the TMI-2 core just after the accident as determined by closed circuit television (CCTV), mechanical probing, and core-boring operations[1] is illustrated in Figure 1. Current estimates indicate that approximately 19% of the original core mass formed an upper layer of debris supported by a hard crust.[2] Below the upper debris bed, there was a consolidated mass (approximately 25% of the total core mass) composed of an upper crust, peripheral or side crust of differing composition, a central core region of the consolidated mass, and a lower crust. Below the consolidated mass, there were standing fuel rod segments. Also, a portion of the core mass (14%) flowed down onto the lower reactor

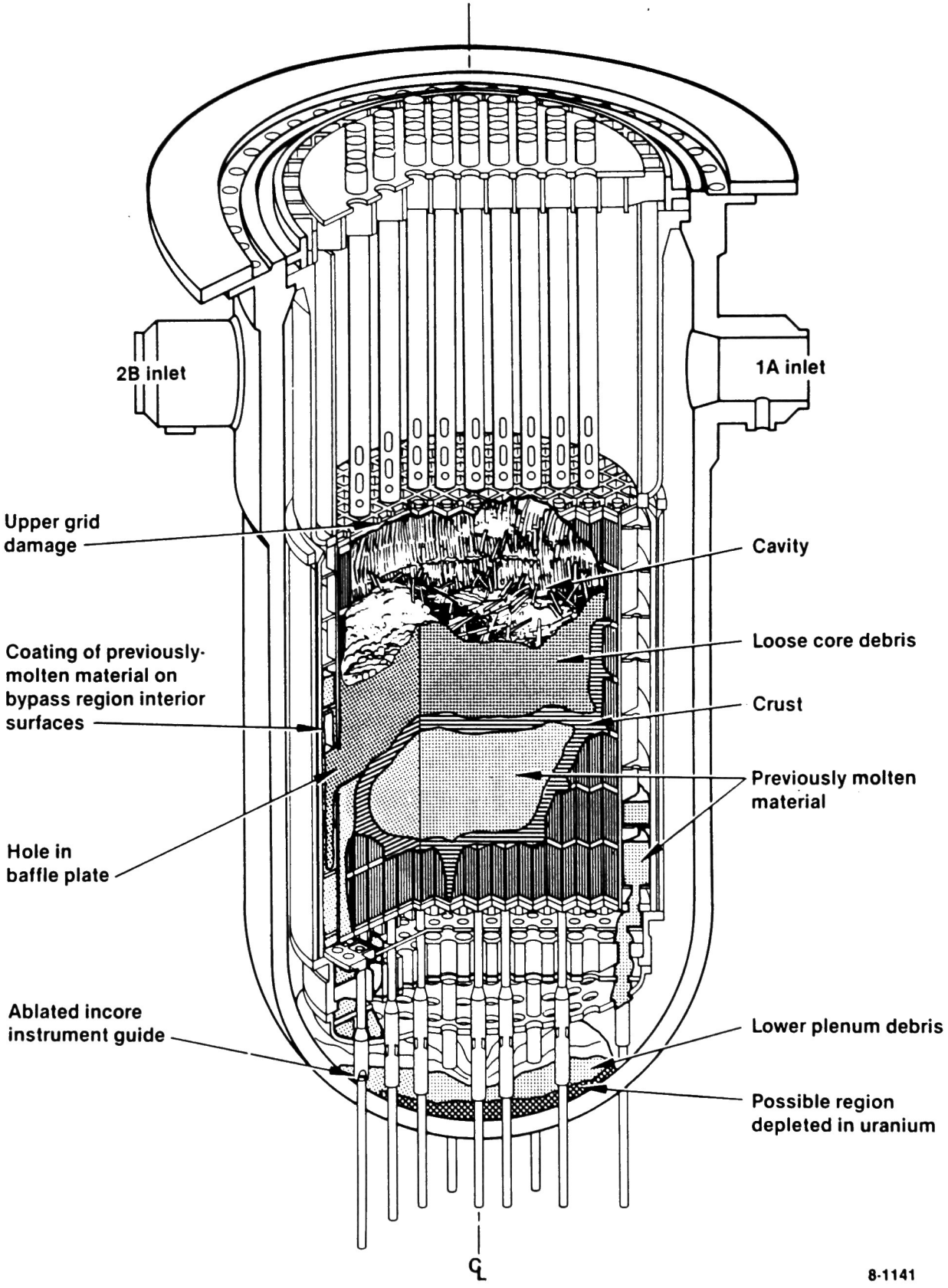

Figure 1. TMI-2 core end-state configuration.

vessel head. The CCTV examinations of the debris deposited on the lower reactor vessel head were used to estimate the volume of deposited material.[3]

As part of the TMI-2 Accident Evaluation Program (AEP)[4,5] that is being conducted by EG&G Idaho, Inc. at the Idaho National Engineering Laboratory (INEL) for the DOE, samples of the lower reactor core were obtained by a core-boring operation[6] to characterize damage to the lower core region below the hard crust and debris bed shown in Figure 1. Core boring of the damaged reactor core was selected as the appropriate means of acquiring samples of the solid structure of prior-molten core materials and rod stubs beneath the upper debris bed. The samples were obtained from well-defined locations within the core and core support assembly; the core-boring operation provided access into the lower plenum for visual inspection in regions previously inaccessible to CCTV.

The core-boring operation performed in July 1986 was done with a special computer-controlled, electro-mechanical device that used commercially available core-boring machinery from the mining/geology industry. The core-bore drill was designed to cut a continuous 6.1-cm-dia core from the lower core region. In practice, the consolidated region of the core was friable and much of the core bore material was washed out during drilling. Thus, sample recovery consisted of nine 6.3-cm-dia cores of crust layers and fragments. The precise original axial position of the debris in the TMI-2 core bores could not be determined, creating uncertainty about the original location of the samples.

The primary goal of the core-boring operation was to obtain the physical samples necessary to spatially characterize the current chemical and physical state and distribution of core materials in the lower core region. The 10 assembly locations at which core boring was performed are shown in Figure 2. This pattern provides east-west and southwest-northeast diametral cross-sectional samples, as well as two radial sample cross sections from core center to the north and another to the southeast. A north-south sample line was also established on the eastern side of the

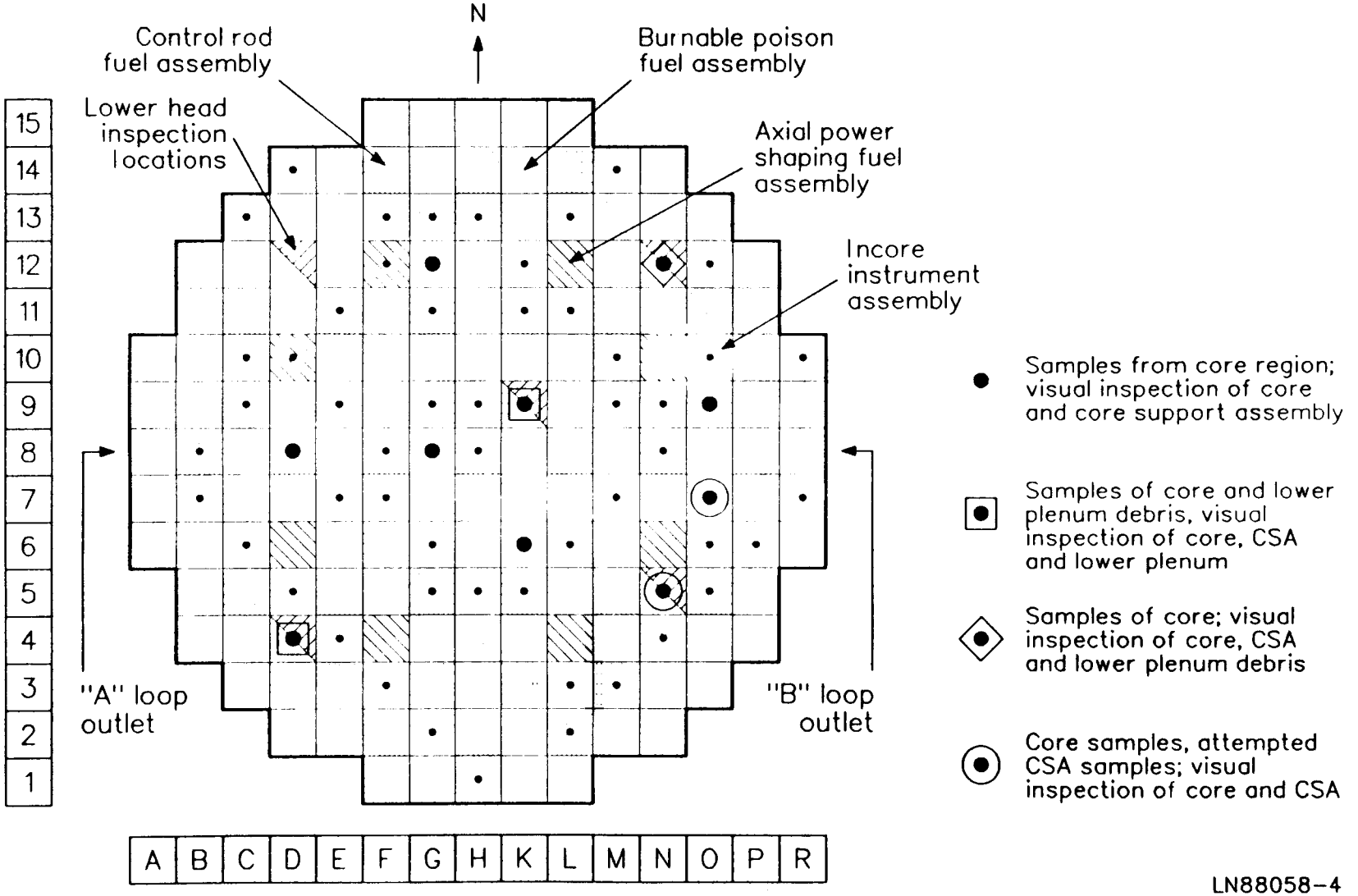

Figure 2. Core bore sampling locations.

core. These 10 core bores provided two samples from the center of the core, two samples from near mid-radius, and six samples from around the core periphery. (Note: Only nine of ten cores contained any sample material.) Access into the lower plenum for video inspection was obtained at three inspection locations (N12, D4, and K9). A summary of the core-boring operations is provided in Reference 6, including drilling sequence, the rationale for selection of drilling locations, and the major findings obtained during the drilling operation.

The TMI-2 lower core samples include samples from both the consolidated region and the fuel assemblies (rod bundles) that retained their original geometry below and around the consolidated region. Samples for examination (187 kg) were collected on three occasions during and after the core-boring operation:

- Nine core samples were obtained in July 1986 as part of the core-boring operations. No sample was contained in the K06 core bore.

- Central core region particle samples were obtained after the consolidated region had been pulverized by drilling 409 holes in an overlapping pattern with a solid-faced bit.

- Loose debris was obtained in late January 1987 after removal of most of the pulverized core material that remained in the core region above the rod bundle geometry after the overlapping hole drilling.

A summary of the history of the TMI-2 AEP's Sampling and Examination Program, including examinations performed and principle results, is discussed in References 1, 2, 4, 5, and 7. Preaccident operation of the TMI-2 reactor and the description of the core components including the core, control rod and burnable poison fuel assemblies, and the core composition are discussed in References 8 and 9. The accident scenario (i.e., the progression of the accident) is discussed in numerous documents, including

References 1 and 7. The gamma spectroscopy measurements performed on the intact core bores before sampling and analysis are discussed in Reference 10.

Due to the large amount of material data obtained on the core-bore samples, the report on the examinations has been divided into two volumes. Volume 1 includes the the text of the main report. Volume 2 includes Appendixes A through J.

2. EXAMINATION PLAN AND ANALYSIS METHODS

Acquisition and examination of the debris from the lower reactor core is one of the tasks identified in the TMI-2 AEP's Sample Acquisition and Examination Plan[7] that describes the technical/scientific data that were required from examination of samples from the TMI-2 reactor core. The general objectives of the TMI-2 Accident Evaluation Program are to understand:

- The physical and chemical states of the TMI-2 core and related structures, and the external influences that affected the accident

- What happened during the accident, which includes developing a qualified data base and standard problem of the TMI-2 accident to benchmark severe accident analysis codes and methodologies

- The relationship between the phenomena and processes controlling the accident and the important severe accident/source term technical issues.

An additional objective is to obtain data to aid in defueling the reactor. From these general objectives, an examination plan was developed for the lower reactor core region to obtain data to address the following specific informational needs:

- Physical morphology of the debris (weight, density, shape)

- Composition and chemical form (if possible) of the debris (fuel, cladding, control material, structural material, and reaction products) and the peak temperatures to which those materials were exposed

- Distribution and retention of radionuclides in the debris.

2.1 Sample Acquisition

Samples were acquired at several periods during the core-boring operation and after the core boring and drilling operations were completed. Possible sample locations were limited, as shown in Figure 2 and discussed in Reference 6. These limitations included the following:

- Drilling was not permitted in instrumented fuel assemblies because of safety considerations related to potential failure of the instrument penetration nozzle weld joints in the lower head.

- Drilling in the outer two rows of fuel assemblies was not possible because of hardware interface restrictions.

The core samples obtained were 6.3 cm in dia and up to 150 cm in length. The three periods when samples were obtained produced the following material from the lower core region:

Collection Date	Sample Mass (kg)	Sample Description
July 1986 (core bores)	130	Cores, rocks, and fragments from the consolidated region, rods and tubes from below the consolidated region, and a lower end fitting core from 10 core positions, as identified in Figure 2.
December 1986	53	Rocks and fragments from the consolidated region at core positions F6, H8 and M11.
Late January 1987	4	Rocks and fragments from the consolidated region at core positions H9 and K9.

2.2 Sample Selection

The selection of samples for examination was accomplished using a screening process during the initial photography and examination of the

samples. The screening criteria included size, distinctive features, and density--as the core-bore cores, rocks, and fragments were discovered to have a large range (5.4 to 9.7 g/cm^3) in density, indicating a range of compositions and porosity.

The nine 6.1-cm-dia cores from the core bores were subdivided into 66 subsections, as described in Appendix A. Mosaic photographs of each of the core bores are shown in Section 3.

Approximately 100 rock-size particle samples were initially selected from the fragments of consolidated core material from the core bores on the basis of size (2.5 cm in some dimension) or distinctive feature. The 25 samples for INEL destructive examinations were selected from the 100 samples based on photographs and weights of all samples and density measurements on 41 samples. The 25 samples were prioritized with emphasis on average and extremes of the density range.

Forty-two rod and tube samples were initially selected from the core bores on the basis of representativeness and/or interaction with other core materials. The 42 tubes were sectioned into 122 4-in.-long subsections. Twenty-four of these subsections were selected for the INEL examination program.

Debris from the consolidated region at core positions F6, H8 and M11 was transported to INEL in TMI-2 fuel canister D-174. The debris from each core position was in its own debris bucket. The 10 largest pieces from each debris bucket were selected for examination, with the exception of a large rock (240 kg) from core position M11 that was believed to be a piece of the horseshoe ring.[11] The 240-kg rock was too large to handle with existing equipment and was returned to storage. A disfigured rod previously overheated and the upper extremity of a core instrument string were also discovered in the debris and photographed.

The debris from the consolidated region at core positions H9 and K9 were packaged in two shielded canisters (pigs) and transported to INEL in a

CNS 1-13II-C Cask. The 10 largest pieces from the two pigs were selected for examination.

Sufficient samples were stockpiled to provide sample collections for examination by an NRC program at Argonne National Laboratory-East (ANL-E), an Organization for Economic Cooperation and Development (OECD) Committee for the Safety of Nuclear Installations (CSNI) program at seven laboratories in foreign countries (i.e., France, United Kingdom, Federal Republic of Germany, Sweden, Switzerland, CEC, and Canada), a Korean program, and a Japanese program. The distribution of samples to the examination programs and additional information about the sample selection process are discussed in Appendix A.

2.3 Sample Examinations

The methods and procedures used for the lower core sample examinations were, in most instances, standard laboratory techniques with necessary modifications to adapt them to the physical characteristics of the samples and to remote analysis because of the high radiation levels.

The initial characterization following disassembly of the core-bore samples was to produce full-length mosaic photographs of the samples in their as-received condition (mosaic photographs in Section 3). Other initial characterizations were bulk sample weights, and immersion densities on all particles >2.5 cm. The particles were then sectioned to provide samples for the metallurgical and radiochemical examinations. The grinding and polishing of sample cross sections for the optical metallography examinations was performed in a hot cell. Microcores were also removed for the Scanning Electron Microscopy (SEM) and radiochemical examinations. Details of the polishing and preparation of the metallurgical samples are discussed in Appendix B, and a discussion of the SEM calibration methods is presented in Appendix J.

Samples weighing between 20 and 200 mg were removed from the microcores and were transported to the radiochemical laboratories for analysis. The

intact samples were examined using delayed neutron analysis to determine ^{235}U and ^{238}U content, and some samples were analyzed via gamma spectroscopy to determine gamma-emitting radionuclide content. The samples were then dissolved using a pyrosulfate fusion technique in a closed system for the retention and measurement of the volatile constituents (i.e., ^{129}I). Iodine-129 and ^{90}Sr tracers were added to the intact sample before dissolution, and a tellurium tracer was added after dissolution to determine losses of these radionuclides during the dissolution and subsequent separations. A brief description of the analysis methods used for the lower core debris samples is presented in Appendix B.

Elemental analyses were performed on aliquots of the dissolved radiochemical samples. The elemental analyses were performed using inductively coupled plasma spectroscopy for the elements present in the core as identified in Table 1. Also listed is the average as-fabricated composition of the TMI-2 core.

The sample identifications and the analyses performed on each of the lower core region samples are summarized in Tables 2 through 5. Tables 2 through 5 also indicate which samples are identified for examination at other laboratories.

TABLE 1. TMI-2 REACTOR CORE COMPOSITION

Material (weight)	Element	Weight Percent	Material (Weight)	Element	Weight Percent
UO_2	U-235[a]	22.265	Inconel-718	Ni[a]	51.900
(94,029 kg)	U-238[a]	85.882	(1211 kg)	Cr[a]	19.000
(531.9 kg)[b]	O	11.853	(6.8 kg)[b]	Fe[a]	18.000
				Nb[a]	5.553
Zircaloy-4	Zr[a]	97.907		Mo[a]	3.000
(23,177 kg)	Sn[a]	1.60		Ti	0.800
(125 kg)[b]	Fe[a]	0.225		Al[a]	0.600
	Cr[a]	0.125		Co	0.470
	O	0.095		Si[a]	0.200
				Mn[a]	0.200
Type-304	Fe[a]	68.635		N	0.130
stainless	Cr[a]	19.000		Cu	0.100
steel	Ni[a]	9.000			
(676 kg) and	Mn[a]	2.000	Ag-In-Cd	Ag[a]	80.0
unidentified	Si[a]	1.000	(2749 kg)	In[a]	15.0
stainless	N	0.130	(43.5 kg)[b]	Cd[a]	5.0
steel	C	0.080			
(3960 kg)	Co[a]	0.080	B_4C-Al_2O_3	Al[a]	34.33
(16.8 kg)[b]			(626 kg)	O	30.53
			(0 kg)[b]	B[a]	27.50
				C	7.64
			Gd_2O_3-UO_2	Gd[a]	10.27
			(131.5 kg)	U[a]	77.72
			(0 kg)[b]	O	12.01

Average Core Composition

Element	Composition (Weight Percent)	Element	Composition (Weight Percent)
U	65.8	In	0.3
Zr	18.0	Sn	0.3
O	8.5	Al	0.2
Fe	3.0	B	0.1
Ag	1.8	Cd	0.1
Cr	1.0	Mn	0.8
Ni	0.9	Nb	0.04

a. Elements for which ICP analysis was performed.

b. Weight of material in a control rod fuel assembly.

TABLE 2. TMI-2 CORE BORE EXAMINATION PROGRAM SUMMARY

Core Number	Section ID	Photo.	Disposition	Weight Density g/cm³	Metallurgy						Radiochemical							
						Etch		SEM										
					Macro	Zr	UO_2	EDX	WDX	Auto-Rad	Gamma Spect.	^{129}I	^{90}Sr	Is	Fiss.-Part.	Fiss. Gas	Gamma Tomog.	Elem. Chem. Anal.
DOB-P1 (Lower Crust)		X	X	7.05														
	A	X	CSNI-KFK															
	B	X	ANL-E															
	C	X									3	3	3	3	3			3
	D	X			X													
	E	X	CSNI-France															
	F	X	CSNI-Canada															
DOB-P2 (Agglom)		X	X	7.6														
	A-1	X									2	2	2	2	2			2
	A-2	X			X												1	
	A-3	X	CSNI-JRC															
	B	X	CSNI-JRC															
	C	X	Japan															
	D	X	Japan															
	E	X	Korea															
DOB-P3 (Upper Crust)		X	X	9.7														
	A-1	X	CSNI-JRC															
	A-2	X	CSNI-Canada															
	A-3	X	Japan															
	A-4	X	Japan															
	A-5	X	Japan															
	B	X	CSNI-UK															
	C	X	CSNI-Sweden															
	D-1	X									2	2	2	2	2			2
	D-2	X			X			1	1									
	D-3	X	Japan															
	D-4	X	Japan															
	E	X	Japan															
GOB-11 (Upper Crust)		X	X	8.2														
	A	X	Japan															
	B	X									3	3	3	3	3			3
	C (disk)	X			X			2	2							2		
	D	X	Japan															
	E (long)	X			X						3	3	3	3	3			3
	F	X																
	G	X	Japan															
	H	X	CSNI-Switzerland															
	I	X			X													
	J	X																
	K	X	Japan															

TABLE 2. Continued

Core Number	Section ID	Photo.	Disposition	Weight Density g/cm³	Metallurgy					Radiochemical							
					Macro	Etch Zr	Etch UO_2	SEM EDX	SEM WDX	Auto-Rad	Gamma. Spect.	^{129}I	^{90}Sr	Te	Fiss.-Fert.	Fiss. Gas	Gamma Tomog.	Elem. Chem. Anal.
G12-P1		X	X	7.6														
(Homogen	A	X	ANL-E															
Ceramic)	B	X	CSNI-KFK															
	C-1	X	CSNI-UK															
	C-2	X	CSNI-Sweden															
	D-1	X	CSNI-France															
	D-2	X									2	2	2	2	2	X	2	2
	D-3	X			X			1	1									
	D-4	X	Japan															
	D-5	X	CSNI-Canada															
	E	X	Japan (remn.)								3T	3T	3T	3T	3T			3T
K09-P1		X	X	7.2														
(Lower	A	X																
Crust)	B	X	CSNI-UK															
	C	X	Korea (remn.)							X	4	4	4	4	X	X		4
	D				X			4	3								4	
	E	X	ANL-E															
	F	X	CSNI-KFK														1	
	H	X	CSNI-Canada															
K09-P2		X	X	7.9														
(Upper	A	X	CSNI-KFK															
Crust)	B	X	CSNI-UK															
	C	X	Korea (remn.)							X	4	4	4	4	X	X		4
	D	X			X			2	2								2	
	E	X	ANL-E															
	F	X	CSNI-Switzerland															
007-P4		X		8.8														
(Agglom)	A	X	Japan															
	B	X	CSNI-KFK															
	C	X									4T	4T	4T	4T	4T			4T
	D	X			X													
	E	X	CSNI-JRC															
	F	X	Japan															

TABLE 3. TMI-2 CORE BORE ROCKS EXAMINATION PROGRAM SUMMARY

Rock Number	INEL Prior	Photo.	Disposition	Weight Density g/cm³	Metallurgy						Radiochemical							
					Etch			SEM		Auto-Rad	Gamma. Spect.	^{129}I	^{90}Sr	Ie	Fiss.-Fert.	Fiss. Gas	Gamma Tomog.	Elem. Chem. Anal.
					Macro	Zr	UO_2	EDX	WDX									
D04-P2-D		X	ANL-E															
D04-P2-A	21	X		8.9	X						T	T	T	T	T			T
D04-P2-B		X	CSNI-UK															
D04-P2-C		X		9.4	Japan													
D04-P1-B		X	CSNI-KFK															
D04-P1-A	X																	
D08-P4-A	16	X		8.7	X						1T	1T	1T	1T	1T			1T
D08-P4-D		X	ANL-E															
D08-P4-B		X	CSNI-Canada															
D08-P4-C	17	X		7.8	X						2	2	2	2	2			2
G08-P10-A	11	X		8.2	X			1	1	1	2	2	2	2	2		1	2
G08-P7-A	10	X		7.4							1	1	1	1	1			1
G08-P9-A	23	X		7.3	X						T	T	T	T	T			T
G08-P6-B	8	X		7.6	X			1	1	2	2	2	2	2	2		1	2
G08-P5-B	12	X		8.0	X						1,T	1,T	1,T	1,T	1,T			1,T
G08-P8-A	24	X		7.4	X						T	T	T	T	T			T
G08-P4-B		X	ANL-E															
G08-P4-A		X		7.5	CSNI-KFK													
G08-P5-A		X	CSNI-KFK															
G08-P8-C		X	CSNI-Switzerland															
G08-P8-B		X																
G08-P7-B		X	ANL-E															
G08-P7-C	9	X		8.8	X				1	1	1T	1T	1T	1T	1T			1T
G08-P9-B		X	ANL-E															
G08-P6-A		X		7.7	Japan													
G12-P9-A	13	X		7.7	X		X	1	1	1	2	2	2	2	2		1	2
G12-P4-A	22	X		7.8	X						T	T	T	T	T			T
G12-P8-A		X	ANL-E															
G12-P10-A		X	CSNI-JRC															
G12-P2-B	14	X		8.5	X		X				2T	2T	2T	2T	2T			2T
G12-P10-B		X	CSNI-Sweden															
G12-P8-B		X		7.7	Japan													
G12-P2-E		X	CSNI-JRC															
G12-P3-A		X		7.7	Japan													
G12-P2-D		X		8.3	Japan													
G12-P7-A		X																
G12-P6-A		X																
G12-P4-B		X																
G12-P6-E		X	CSNI-JRC															
G12-P5-A		X																
G12-P9-B		X	CSNI-JRC															
G12-P2-C		X																
G12-P10-D		X																

TABLE 3. Continued

Core Number	Section ID	Photo.	Disposition	Weight Density g/cm^3	Metallurgy						Radiochemical							
					Macro	Etch Zr	Etch UO_2	SEM EDX	SEM WDX	Auto-Rad	Gamma. Spect.	^{129}I	^{90}Sr	Te	Fiss.-Fert.	Fiss. Gas	Gamma Tomog.	Elem. Chem. Anal.
G12-P10-C		X	CSNI-KFK															
G12-P2-A		X																
G12-P8-C		X																
G12-P6-B		X																
G12-P9-C		X																
G12-P6-C		X																
G12-P10-E		X																
G12-P9-D		X																
G12-P6-D		X																
G12-P3-B		X																
G12-P8-D		X	Korea (remn.)															
K09-P3-L		X	ANL-E															
K09-P4-G		X	CSNI-Canada															
K09-P4-E		X																
K09-P4-D	7	X		6.9	X	X		1	1	1	2	2	2	2	2			2
K09-P3-A	25	X		7.6	X						T	T	T	T	T			T
K09-P4-F		X																
K09-P3-D	5	X		7.4	X			1	1		1			1	1	X		1
K09-P3-M		X		7.5	CSNI-France													
K09-P4-H	4	X		6.7	(Inadvertent Return to Storage)													
K09-P4-N		X																
K09-P3-C			Korea															
K09-P3-J		X																
K09-P4-L		X																
K09-P4-M		X	ANL-E															
K09-P4-J		X	ANL-E															
K09-P3-F	6	X		7.8	X			1	1	1	1	1	1	1	1			1
K09-P3-H		X																
K09-P4-B		X		7.4	X													
K09-P4-A		X	Korea															
K09-P3-G		X	CSNI-UK															
K09-P3-I		X		7.5														
K09-P3-E		X																
K09-P4-I		X																
K09-P1-B		X																
K09-P3-B		X	CSNI-KFK															
K09-P4-K		X																
K09-P3-K		X																
K09-P4-C		X	CSNI-KFK															
N05-P1-D	19	X		8.3	X						2T	2T	2T	2T	2T		1	2T
N05-P1-H	2	X		9.1	X			1	1		1T	1T	1T	1T	1T			1T
N05-P1-F		X	Japan															
N05-P1-A	18	X		8.0	X						2T	2T	2T	2T	2T			2T

TABLE 3. Continued

Core Number	Section ID	Photo.	Disposition	Weight Density g/cm³	Metallurgy					Radiochemical							
					Macro	Etch Zr	Etch UO_2	SEM EDX	SEM WDX	Auto-Rad	Gamma Spect.	^{129}I	^{90}Sr	Is	Fiss.-Part.	Fiss. Gas	Gamma Tomog.	Elem. Chem. Anal.
M05-P1-E		X	CSNI-JRC															
M05-P1-G		X																
M05-P1-B		X	CSNI-KFK															
M05-P1-C		X																
M12-P1-A		X	AML-E															
M12-P1-B		X	Japan															
007-P6	1	X		5.4	X			1	1		2	2	2	2	2		2	2
007-P5		X	CSNI-France															
007-P8-B		X	CSNI-KFK															
007-P8-C		X																
007-P8-A		X																
007-P1-A	20	X		7.6	X						T	T	T	T	T			T
007-P3		X	CSNI-KFK															
009-P1-A	3	X	Japan	6.9	X			1	1		2	2	2	2	2			2
009-P1-B	15	X		7.2	X						1,T	1,T	1,T	1,T	1,T			1,T

TABLE 4. TMI-2 POST DRILLING ROCKS EXAMINATION SUMMARY

Rock Number	Photo.	Density g/cm	Examinations: Metallurgy: Macro	Metallurgy: Etch: Zr	Metallurgy: Etch: UO_2	Metallurgy: SEM: EDX	Metallurgy: SEM: WDX	Radiochemical: Auto-Rad	Radiochemical: Gamma. Spect.	Radiochemical: ^{129}I	Radiochemical: ^{90}Sr	Radiochemical: Te	Radiochemical: Fiss.-Fert.	Radiochemical: Fiss. Gas	Radiochemical: Gamma Tomog.	Radiochemical: Elem. Chem. Anal.
F6-P1	X	7.5														
F6-P2	X	7.3														
F6-P3	X	7.7														
F6-P4	X	7.3														
F6-P5	X	7.3														
F6-P6	X	7.3														
F6-P7	X	7.4														
F6-P8	X	7.5														
F6/H8-P1	X	7.7														
F6/H8-P2	X	7.5														
F6/H8-P3	X	6.6														
F6/H8-P4	X	7.5														
F6/H8-P5	X	6.5														
F6/H8-P6	X	6.7														
F6/H8-P7	X	7.9														
F6/H8-P8	X	8.5														
F6/H8-P9	X	6.5														
F6/H8-P10	X	6.9														
M11-Big-Rock	X	Returned to fuel														
	X	canister D-174														
M11-P1	X	7.5	Japan													
M11-P2	X	7.6														
M11-P3	X	8.0														
M11-P4	X	7.3														
M11-P5	X	7.9														
M11-P6	X	7.8														
M11-P7	X	8.2														
M11-P8	X	8.2														
M11-P9	X	7.9														
M11-P10	X	8.4	Japan													
H9/K9-P1	X	8.0														
H9/K9-P2	X	7.1														
H9/K9-P3	X	7.9														
H9/K9-P4	X	7.7	Japan													
H9/K9-P5	X	7.0	Japan													
H9/K9-P6	X	8.1	Japan													
H9/K9-P7	X	7.5														
H9/K9-P8	X	7.1														
H9/K9-P9	X	7.3	Korea													
H9/K9-P10	X	7.9														

TABLE 5. TMI-2 CORE BORE RODS EXAMINATION SUMMARY

Rod/Tube Number	Sample No.	Type	Video Survey	Length (in.)	Examinations: Metallurgy: Macro	Metallurgy: Etch: Zr	Metallurgy: Etch: UO_2	Metallurgy: SEM: EDX	Metallurgy: SEM: WDX	Fiss. Gas	Burn Up	Surface Deposits: Gamma. Spect.	Surface Deposits: ^{129}I	Surface Deposits: ^{90}Sr	Surface Deposits: Te	Elem. Chem.	Density
D04-R1		IT	X	31													
D04-R8:		CR/GT	X	48													
	-2			4	X												
	-4			4	X												
	-6			4	X												
	-8			4	X	1	1										
D04-R9:		FR	X	49													
	-2			4	X	X	X			X	X	X	X	X		X	
	-4			4	X												
	-6			4	X	X	X			X	X	1	1	1	1	1	
	-8			4	X	X	X										
D04-R12:		FR	X	48													
	-2			4	Japan												
	-4			4	Japan												
	-6			4	Japan												
D08-R4		FR	X	27												X (Gd)	
D08-R6		FR	X	24													
D08-R7		CR/GT	X	33													
D08-R8		IT	X	20													
G08-R3:		IT	X	22													
	-2			4	X	X						1(BPR) 1(GT)	1(BPR) 1(GT)	1(BPR) 1(GT)	1(BPR) 1(GT)	2 1(GT)	X(Al_2O_3-B_4C)
	-4			4	X	X											
	-6			4	X	X	1					1(GT)	1(GT)	1(GT)	1(GT)	1(GT)	
G08-R6		FR	X	25													
				4	Japan												
G08-R9:	-2	FR	X	25	Japan												
	-2			4	X					X		X	X	X		X	
	-4			4	X					X		X	X	X		X	
	-6			4	X	X											
G08-R11:		BPR/GT	X	12													
G12-R2		FR	X	44													
G12-R4:		FR	X	42													
	-2			4	ANL-E												
	-4			4	ANL-E												
	-6			4	ANL-E												
G12-R8:		FR	X	42													
	-8			4	CSNI-Canada												

TABLE 5. Continued

Rod/Tube Number	Sample No.	Type	Video Survey	Length (in.)	Examinations: Metallurgy: Macro	Metallurgy: Etch: Zr	Metallurgy: Etch: UO_2	Metallurgy: SEM: EDX	Metallurgy: SEM: WDX	Fiss. Gas	Burn Up	Surface Deposits: Gamma. Spect.	Surface Deposits: ^{129}I	Surface Deposits: ^{90}Sr	Surface Deposits: Te	Elem. Chem.	Density
G12-R12:		IT	X	45	Japan												
	-2			4	Japan												
	-4			4	Japan												
	-6			4	Japan												
	-8			4	Japan												
G12-R13:		BPR/GT	X	35													
	-4			4	CSNI-FRG												
G12-R16:		BPR/GT	X	39													
	-2			4	CSNI-FRG												
	-4			4	CSNI-FRG												
K09-R1		FR	X	7													
K09-R4:		IT	X	16													
	-2			4	Japan												
	-4			4	Japan												
K09-R5:		FR	X	17													
	-2			4	X												
	-4			4	X	X	X					1	1	1	1	1	
	-5			4	X	X	X										
K09-R9:		FR	X	16													
	-2			4	ANL-E												
	-4			4	ANL-E												
	-5			4	ANL-E												
K09-R13:		CR/GT	X	20													
	-2			4	X												
	-4			4	X												
	-6			4	X												
K09-R14:		FR	X	20													
	-4			4	CSNI-UK												
	-5			4	CSNI-UK												
N05-R2:		FR	X	47													
	-2			4						X	X	X	X	X		X	
	-8			4						X	X	X	X	X		X	
N05-R5		FR	X	47													

TABLE 5. Continued

Rod/Tube Number	Sample No.	Type	Video Survey	Length (in.)	Examinations: Metallurgy: Macro	Metallurgy: Etch: Zr	Metallurgy: Etch: UO_2	Metallurgy: SEM: EDX	Metallurgy: SEM: WDX	Fiss. Gas	Burn Up	Surface Deposits: Gamma Spect.	Surface Deposits: ^{129}I	Surface Deposits: ^{90}Sr	Surface Deposits: Tc	Surface Deposits: Elem. Chem.	Density
N05-R7:		BPR/GT	X	48													
	-2			4	ANL-E												
	-4			4	ANL-E												
	-6			4	ANL-E												
	-8			4	ANL-E												
N05-R15:		IT	X	24													
	-2			4	X	X											
N12-R4:		FR	X	44													
	-2			4	Japan												
	-4			4	Japan												
	-6			4	Japan												
N12-R7:		CR/GT	X	46								2	2	2	2	2	
	-2			4	Japan												
	-4			4	Japan												
	-6			4	Japan												
	-8			4	Japan												
	-10			4	X												
N12-R9		FR	X	45													
N12-R11		FR	X	45													
N12-R13:		CR/GT	X	21													
	-2			4	ANL-E												
	-4			4	ANL-E												
	-6			2	ANL-E												
007-R3		FR	X	27													
007-R4		IT	X	27													
007-R5		FR	X	26													
007-R7:		CR/GT	X	29													
	-6			4	X			X	X								
009-R6		FR	X	29													
009-R7		CR/GT	X	43													
009/R8		CR/GT	X	43													
009/R11		FR	X	27													

a. Type code: BPR--burnable poison rod, CR--control rod, FR--fuel rod, GT--guide tube, and IT--instrumentation tube.

3.0 EXAMINATION RESULTS AND DISCUSSION

This section presents the significant results of the physical, metallurgical, chemical, and radionuclide analyses performed on the samples obtained from the lower reactor vessel. The discussion is divided into analyses of samples from the upper crust, lower crust, peripheral crust, central core region, and intact regions. Additional details from these examinations are provided in the appendices.

The nine core bores from the lower reactor vessel were first visually examined and weighed. A total of 130.7 kg of fuel debris was obtained from the nine core bores as shown in Table 6. The total sample weight includes the weight of fuel rods (116 kg) and the loose debris (14.7 kg). Particles larger than 2.5 cm made up most of the debris (79% or 11.5 kg). The high fraction of large-sized particles may be due to flushing the smaller particles out of the core bores during the drilling operation.

Mosaic photographs of each of the core bores are shown in Figure 3. At the bottom of each core bore is a jamming collar covering the lower spacer grid. This collar prevented the loss of fuel rods and debris from the core bore during the coring operations and handling. Examination of the intact debris around the core bore holes indicated that the damage to the fuel rod segments occurred during the coring operation.[6] The fuel rods varied in length from approximately 60 cm near the center of the core to approximately 120 cm near the core periphery. The fuel rod cladding was not appreciably oxidized and showed substantial ductility, as indicated by the bent and twisted rods. There were indications of melting near the tops of a few Ag-In-Cd control rods in the peripheral core bores.

Above the intact fuel rod segments was a previously molten region consisting of a central consolidated region surrounded by a solidified crust.[6] Five of the core bores contained eight examples of the crust regions. Cores from the central part of the reactor core (K09, G08, and D08) contained examples of both top and bottom crust layers. The top crust was composed mainly of ceramic material with metallic inclusions that were either finely dispersed globules or relatively large masses. The lower

TABLE 6. CORE BORE SAMPLE WEIGHTS

Core Bore	Total Mass (kg)	Loose Debris[a] Mass (g)	Large Particle[b] Mass (g)	Number of Particles
D04	19.1	77	77	6
D08	18.1	2287	2092	7
G08	12.7	3476	3232	16
G12	15.9	2638	1731	30
K09	10.9	4951	3209	30
N05	17.0	114	114	8
N12	13.9	146	146	2
007	10.7	936	896	7
009	12.4	89	50	2
TOTALS	130.7	14714	11547	108

a. Total loose debris.

b. Mass of large loose particles (>2.5 cm).

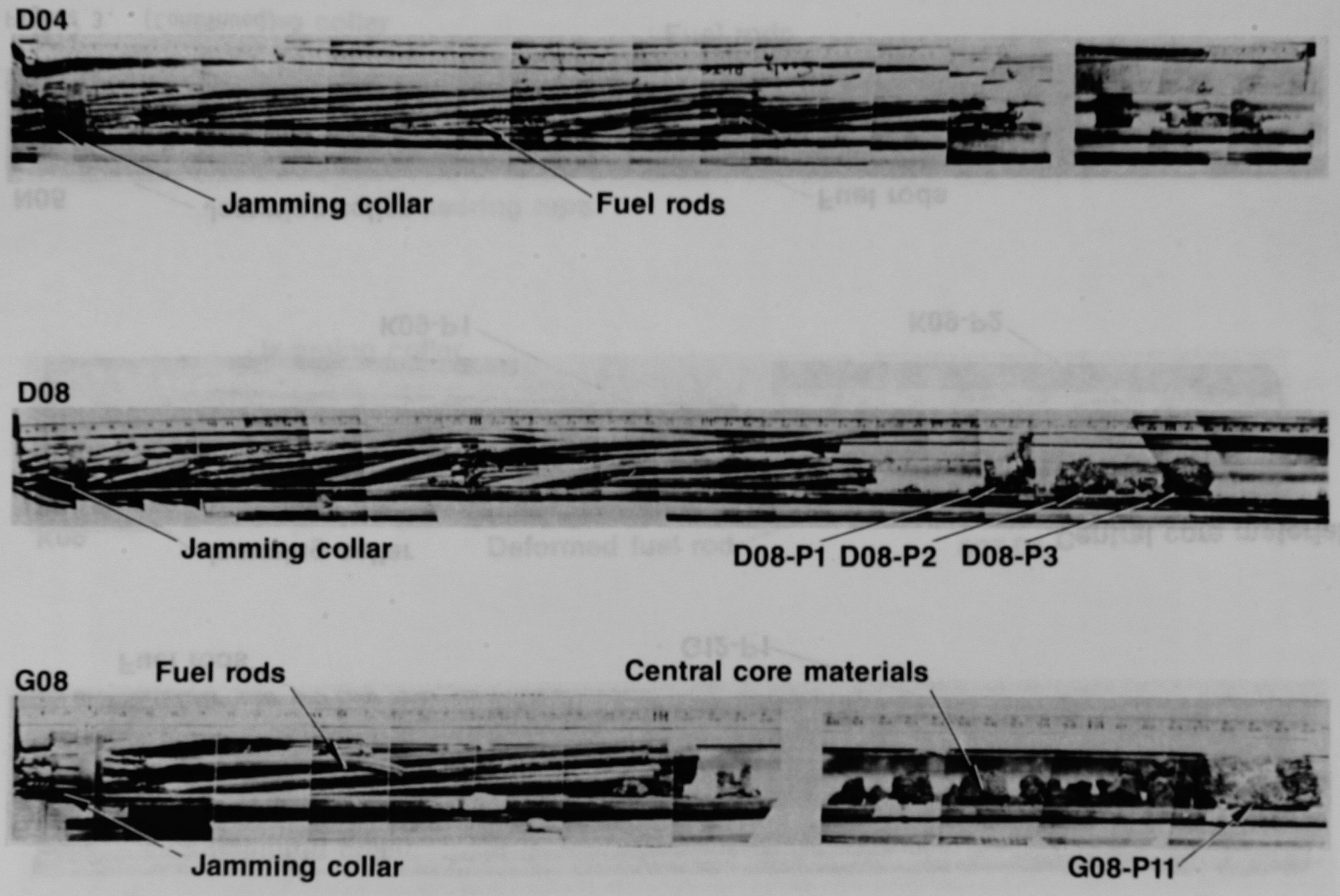

Figure 3. Mosaic photographs of the core bore samples.

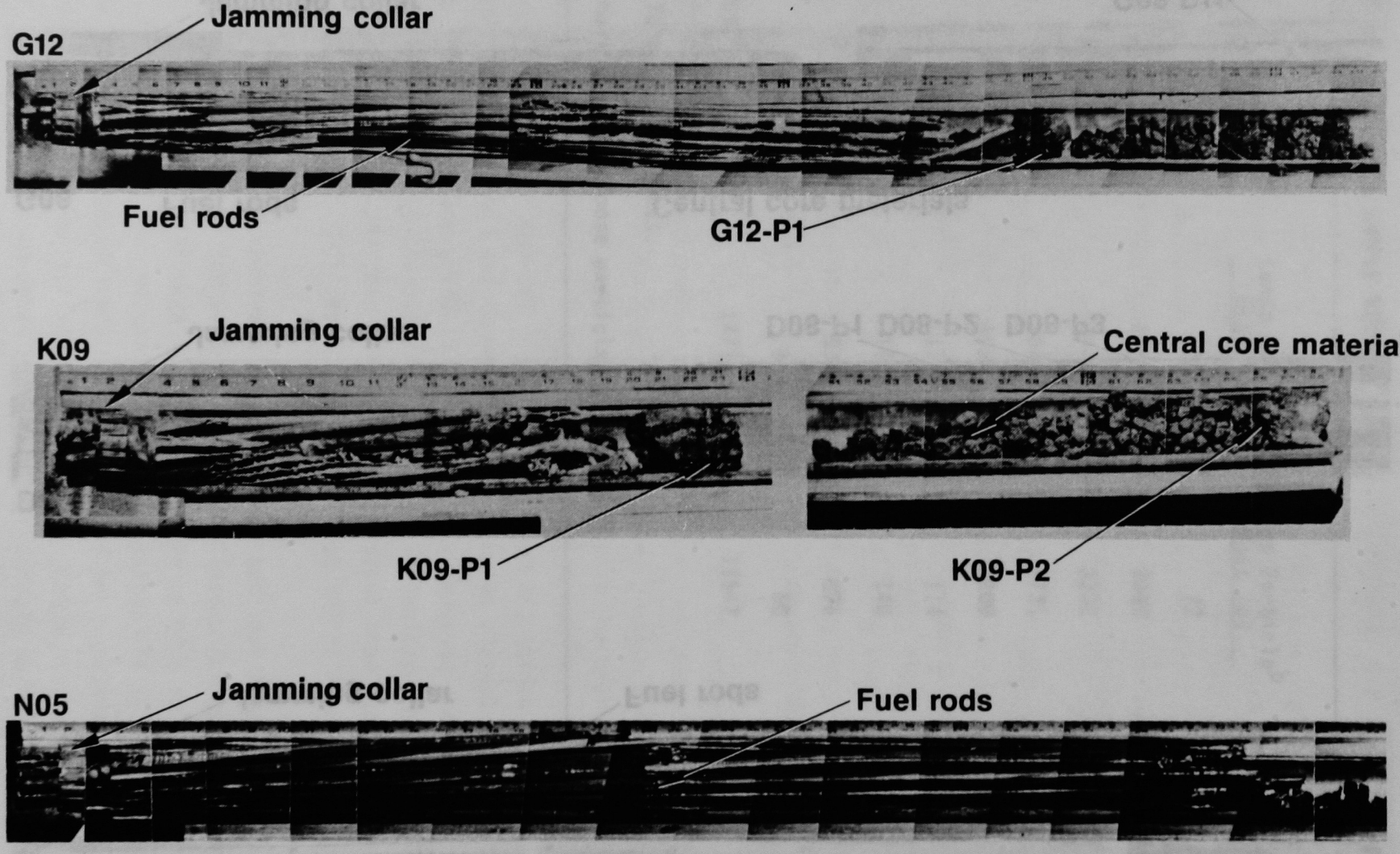

Figure 3. (Continued)

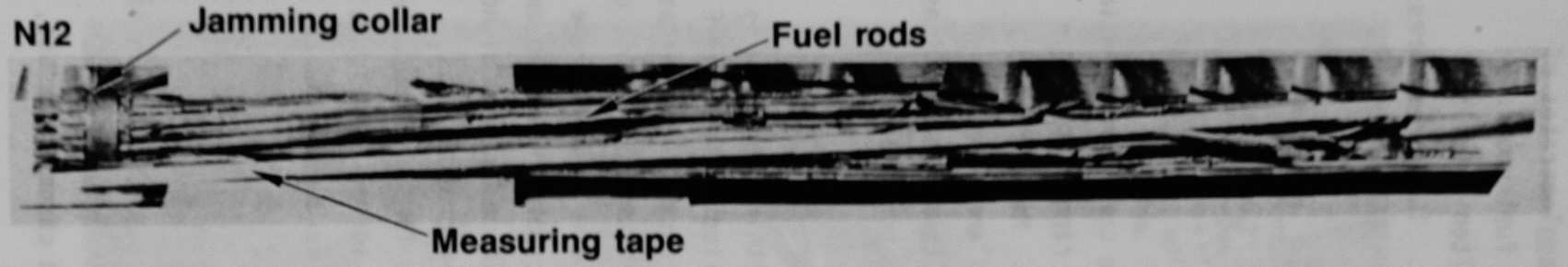

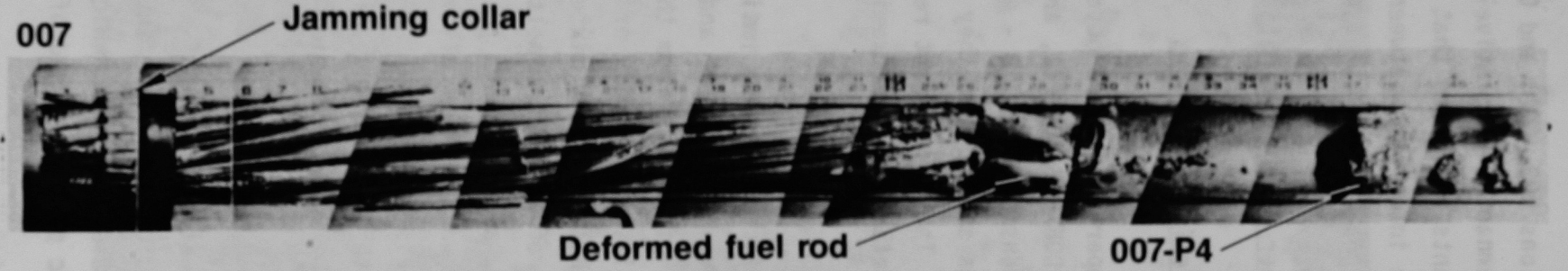

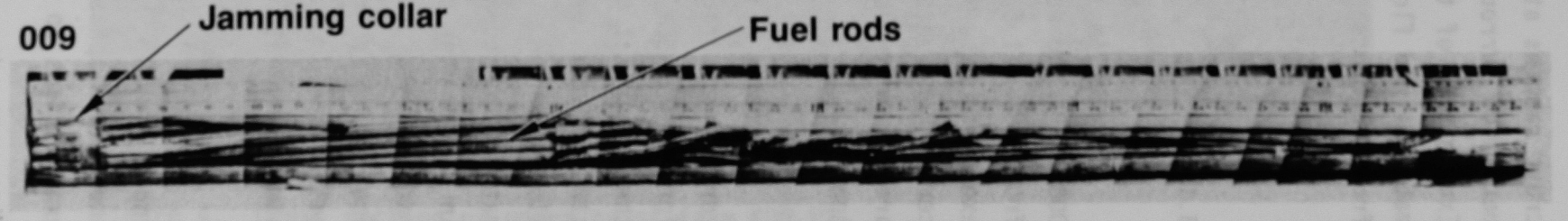

Figure 3. (Continued)

crust samples at core locations K09, G08, and D08 were agglomerates of metallics surrounding the remnants of relatively intact fuel rods. Examination of the rod remnants indicated that prior-molten metallic material had flowed into the interfaces between pellets. The cores bores from locations G12 and 007 contained examples of the peripheral crust.

3.1 Upper Crust Examination Results

3.1.1 Visual and Metallurgical Examinations

Three samples of the upper crust were obtained from core bore locations D08, G08, and K09. Samples D08-P3, G08-P11, and K09-P2 ranged in length from 4.5 - 11.5 cm, and in density from 7.8 - 9.7 g/cm^3. Metallographic examinations of these samples showed that they contained areas of both ceramic and metallic melts. The significant results of these examinations are summarized below, with details of the examinations described in Appendix E.

In many cases the metallic melts were immiscible within the $(U,Zr)O_2$ ceramic melt regions, as shown in Figure 4, and as detailed in Appendix E for several SEM examinations of samples from the upper crust. In many cases these metallic globules consisted primarily of control materials (Ag,In) or structural materials (Fe,Cr,Ni), although mixtures of these elements were also observed. The presence of a metallic melt within cracks in the ceramic matrix, as shown in Figure 5, also suggests that metallic melts from higher in the reactor core flowed down over the solidified upper crust. This material was probably stainless steel from the upper end fittings and upper fuel assembly grid, along with zircaloy and silver high in the core, that melted due to heat produced by steam oxidation of zircaloy during the 2B pump transient.

Figure 6 shows the typical structure of the ceramic material in the upper crust. This figure indicates significant porosity and fracturing of the ceramic phase. A mottled black phase, which was identified from SEM examinations to be a eutectic phase composed of iron and chromium oxides,

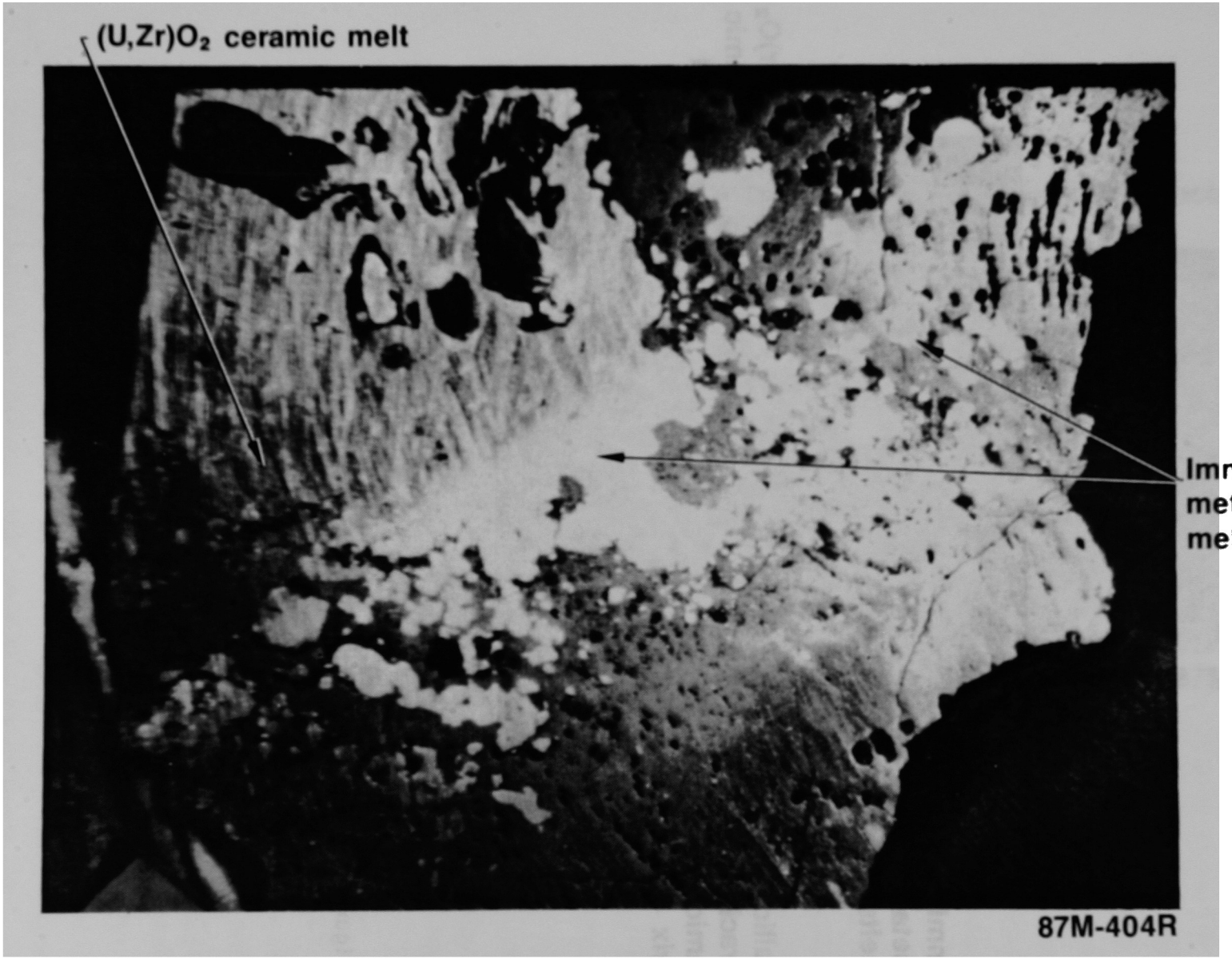

Figure 4. Cross section of upper crust from K09-P2.

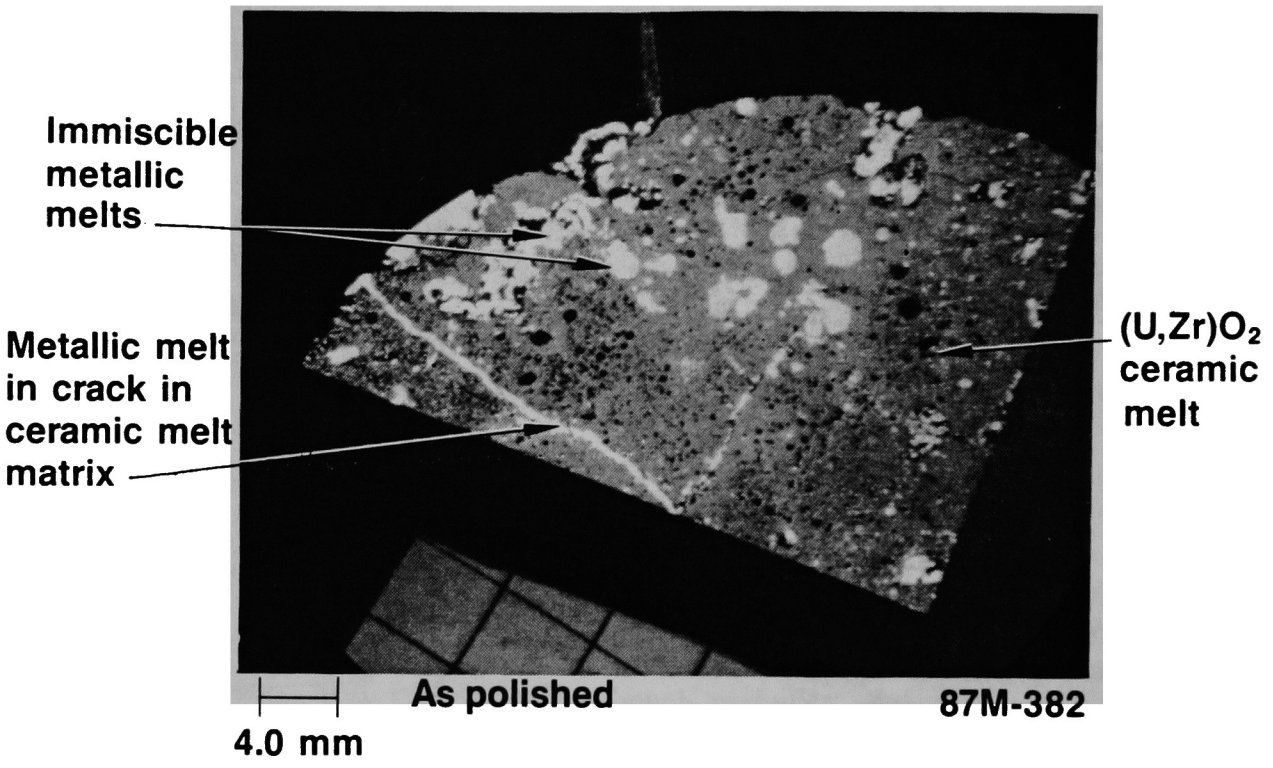

Figure 5. Transverse cross section from D08-P3.

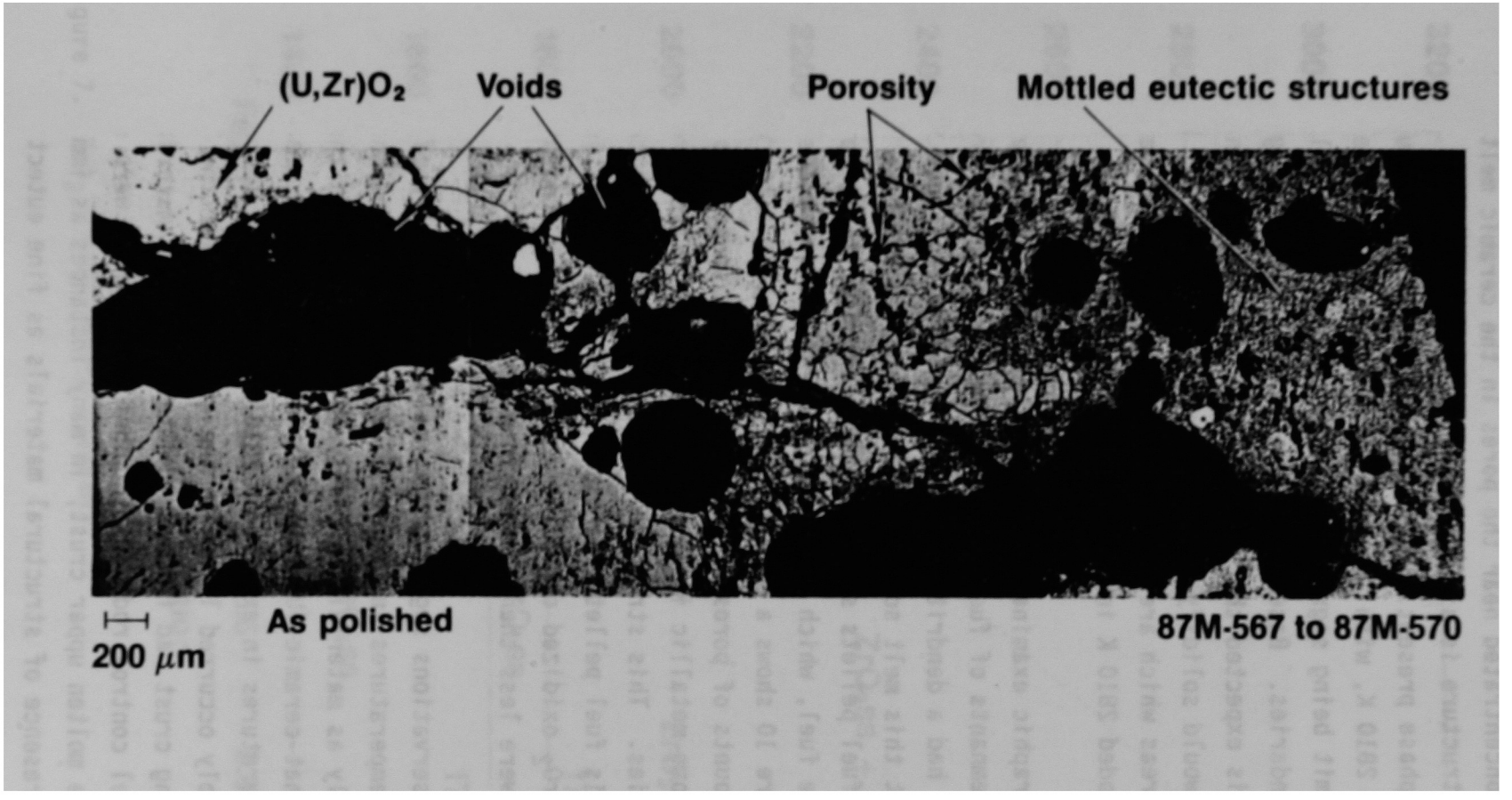
(U,Zr)O2
Voids
Porosity
Mottled eutectic structures
200 μm
As polished
87M-567 to 87M-570

seems to be concentrated near the pores in the ceramic melt regions the structure is single-phase $(U,Zr)O_2$ with only a the eutectic phase present. Upon cooling, the $(U,Zr)O_2$ wou solidified by 2810 K, with iron and chromium oxides in exce solubility limit being segregated to the material which sol the grain boundaries. Based upon the ZrO_2-Fe_3O_4 phase diag Figure 7, it is expected that $(U,Zr)O_2$ melts containing con these oxides would solidify at temperatures below 2810 K. I presence of areas which are primarily $(U,Zr)O_2$ suggests tha probably exceeded 2810 K in the upper crust.

Metallographic examination of sample G08-P11 showed me surrounding remnants of fuel rods as shown in Figure 8. Ar metallic melt had a dendritic structure as shown in Figure indicates that this melt solidified over a period of time. shape of the fuel pellets suggests that zirconium in the me dissolving the fuel, which indicates temperatures in excess 2200 K. Figure 10 shows a metallic melt penetrating along with large amounts of porosity at the fuel grain boundaries Figure 11. Some metallic inclusions are present in the por grain boundaries. This structure suggests that very high t existed in this fuel pellet, perhaps approaching fuel melti presence of ZrO_2 oxidized cladding remnants Figure 8 indica temperatures were less than 2960 K in nearby areas.

These observations suggest that molten zircaloy liquef the fuel at temperatures in excess of 2200 K in some region crust, probably as material initially relocated downward th region, but that ceramic $(U,Zr)O_2$ melt existed in other are crust at temperatures in excess of 2810 K. These high temp regions probably occurred later in the accident, after the and surrounding crust had formed. Molten structural materi stainless steel control rods and Inconel spacer grids were throughout the molten upper crust, in many instances as imm melts. The presence of structural materials as fine eutect

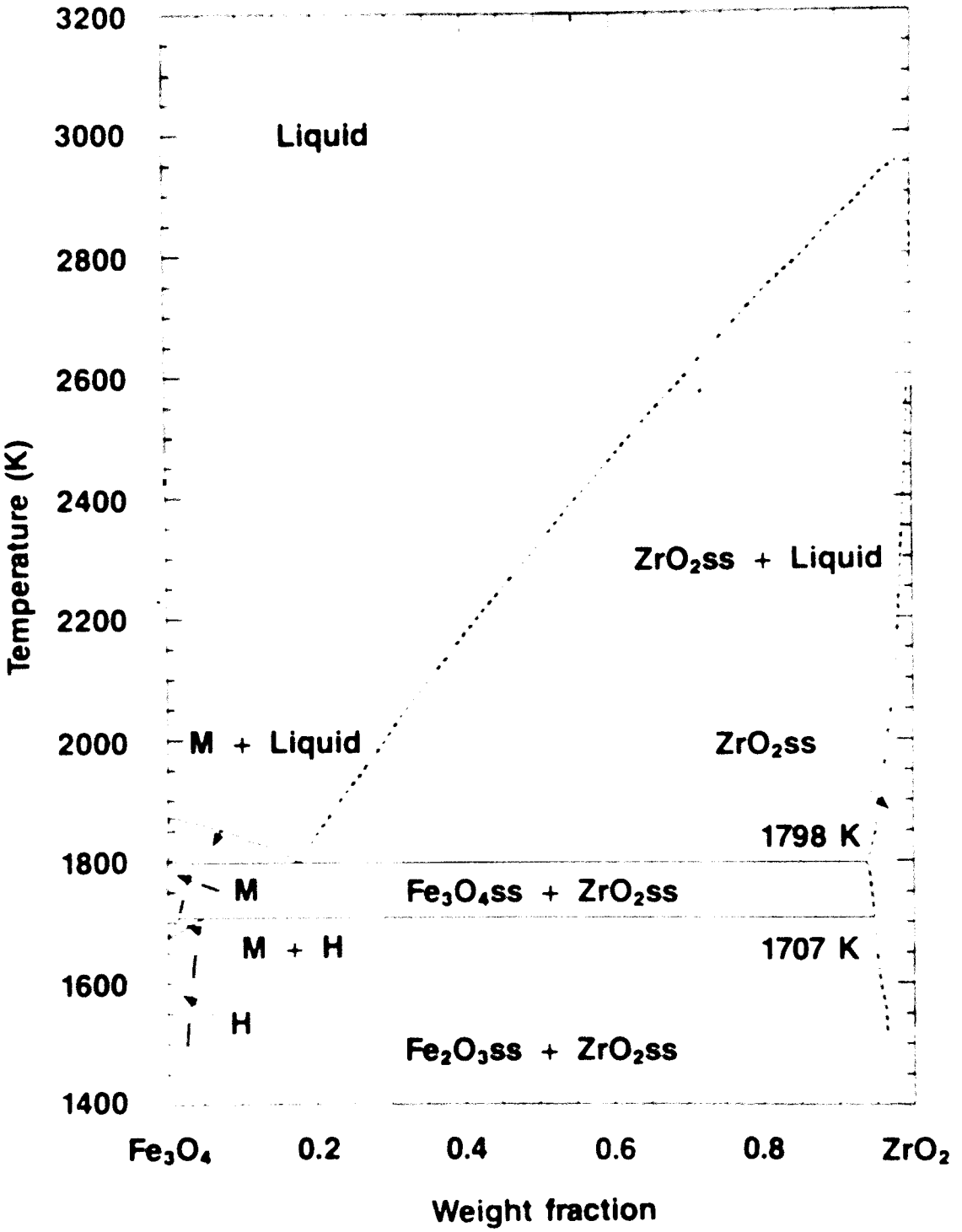

Figure 7. ZrO_2 - Fe_3O_4 phase diagram.

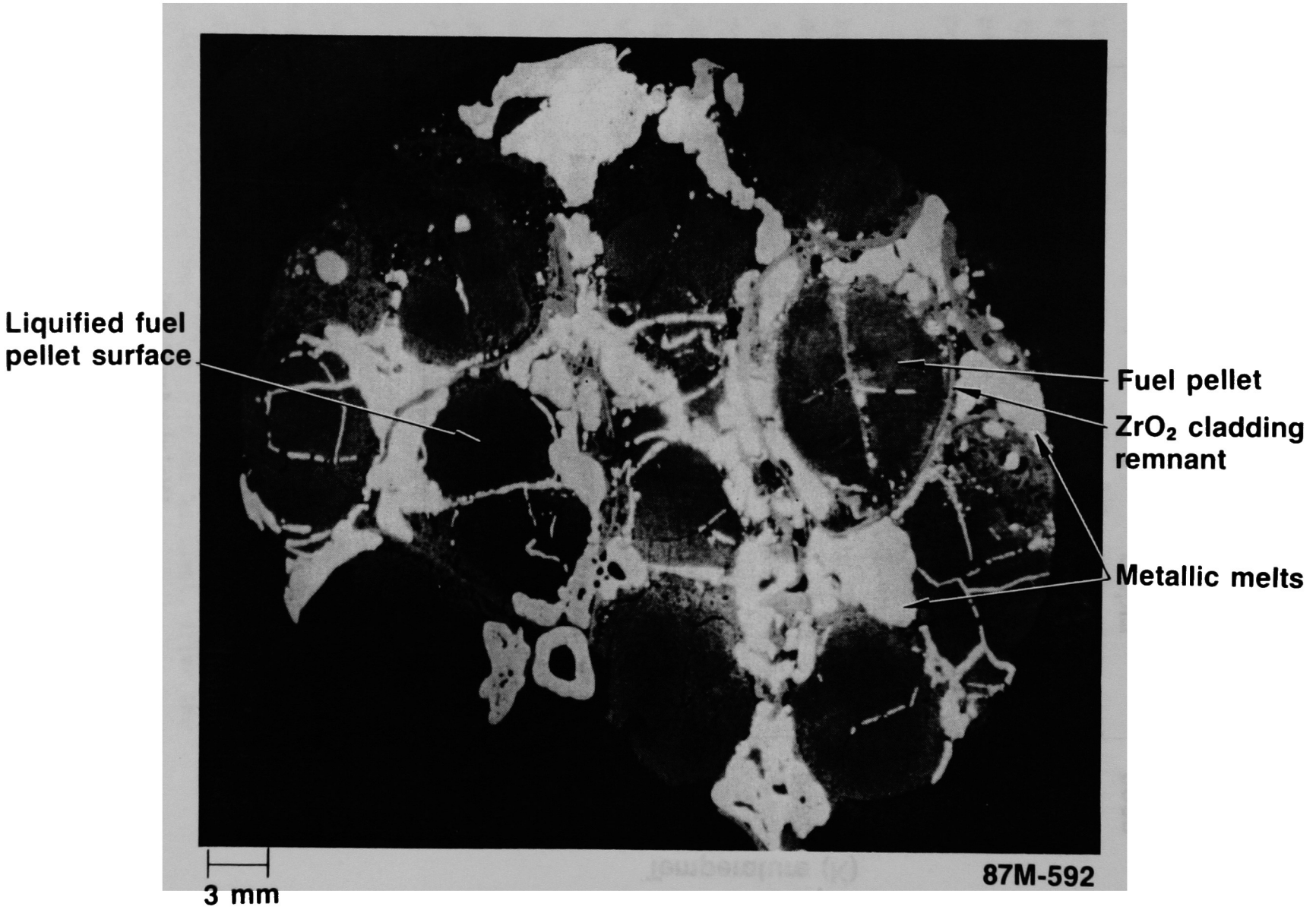

Figure 8. Transverse cross section from G08-P11.

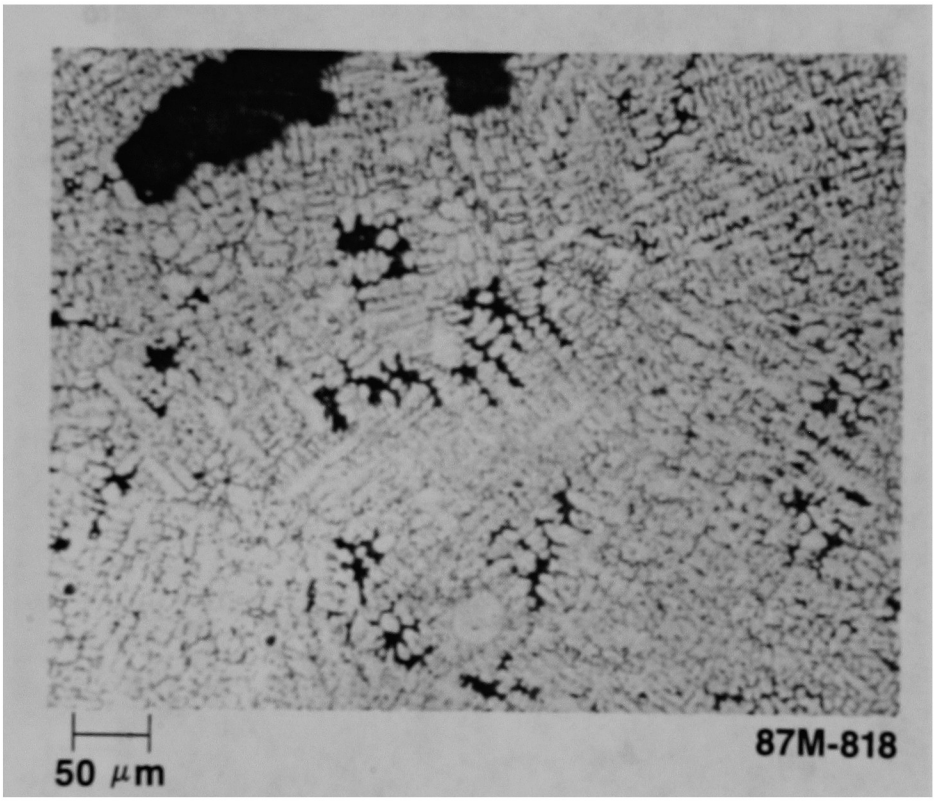

Figure 9. Coarse dendritic structure in metallic melt in G08-P11.

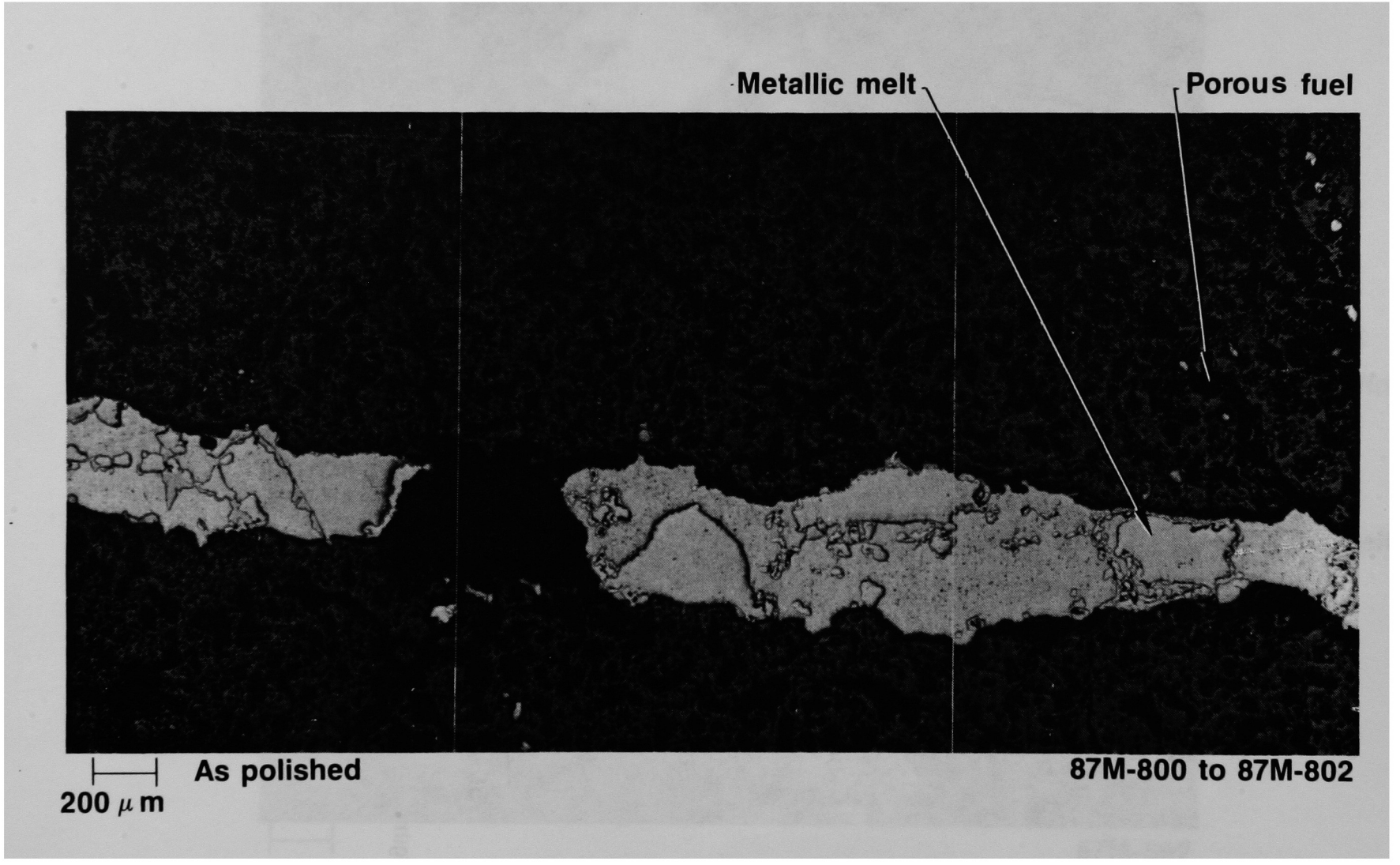

Figure 10. Penetration of metallic material along fuel crack in G08-P11.

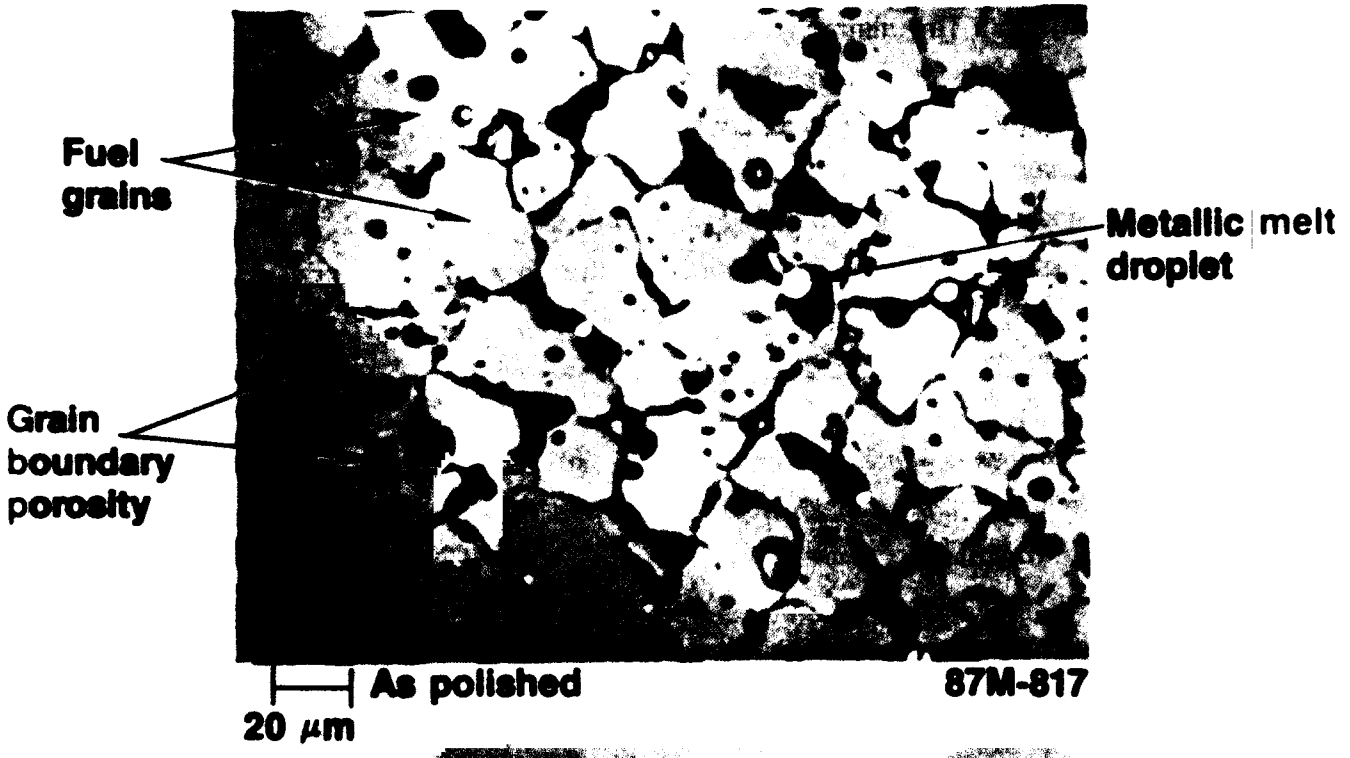

Figure 11. Grain boundary porosity in fuel in G08-P11.

the ceramic melt region indicates that there was mixing of these molten materials when the crust was formed; however, the presence of metallic melts in cracks within the solidified crust indicates that metallic melts continued to form and relocate after the upper crust had formed. The presence of dendritic metallic melts in some areas suggests that the upper crust cooled slowly, which agrees with thermocouple data that indicated temperatures in the upper debris bed remained above 1000 K for up to three days following the accident. The heterogeneous nature of the upper crust indicates that it formed as a result of incoherent melt progressions. The upper crust was relatively thin, ranging from 4.5 - 11.5 cm on the samples which were examined. The density measurements ranged from 7.8 - 9.7 g/cm^3, which indicates that despite the presence of significant amounts of closed porosity in some areas, as determined from the metallographic examinations, the upper crust was generally a very consolidated mass of intact and previously molten materials. This is also apparent from simple visual observations of the upper crust samples.

3.1.2 Upper Crust Bulk Composition

Elemental analyses were performed on dissolved microcores from sample locations in the upper crust. Analyses were performed for 17 elements that constitute the principal components of the TMI-2 core. For comparison, Table 1 lists the average core composition of each of the core constituents (Reference 9) and the average core composition of the TMI-2 core, including the oxygen content of the uranium, but excluding oxygen that might be present due to the oxidation of zircaloy and structural materials. Samples were examined from three regions of the upper crust (core locations K09-P2, G08-P11, and D08-P3). The elemental analysis results for these samples are listed in Appendix G, Tables G1 through G4.

K09-P2, an axial cross section of the crust, is from the central portion of the reactor core. Figure 12 shows the cross section and the locations sampled. Sample location No. 1 is located in the metallic region near the top of the crust; sample locations No. 2 and No. 3 are located at the interface between the metallic and previously molten fuel material; and

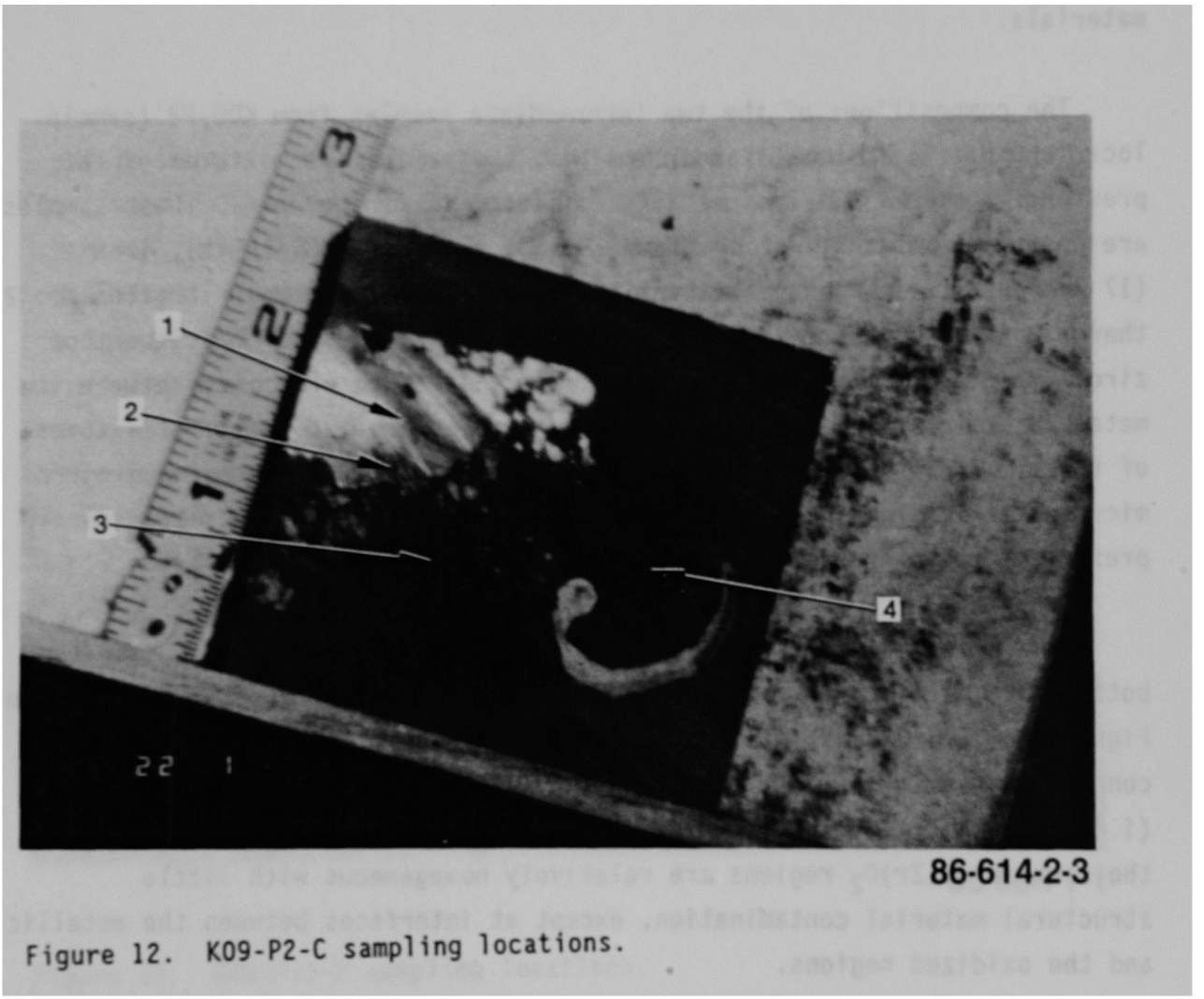

Figure 12. K09-P2-C sampling locations.

sample location No. 4 is from the previously molten fuel material portion of the cross section near the bottom of the crust. Examination of Table G1 indicates that the metallic region (Sample No. 1) is composed principally of iron (53 wt%) and nickel (24 wt%) with significant amounts of tin (3.7 wt%), chromium (3.7 wt %) and control material [silver (2.1 wt%) and indium (1.8 wt%)]. However, this sample and presumably the metallic portion of the upper crust contains little zirconium, which suggests that the metallic inclusions in this part of the core were formed primarily from structural materials.

The compositions of the two intermediate samples from K09-P2 (sample locations No. 2 and No. 3) indicate that the samples are mixtures of the previously molten fuel and metallic constituents of the core. These samples are composed primarily of uranium (33 wt%), zirconium (8-11 wt%), iron (17 wt%), and some control material. Surprisingly, at sample location No. 2 there is a concentration of 9 wt% copper, which is a trace constituent of zircaloy and Inconel. These data suggest that at the interface between the metallic and oxidized fuel regions, the samples are heterogeneous mixtures of the previously molten fuel and structural materials. Scanning electron microscope examinations indicate that the structural metallic materials are present as metallic globules deposited in the previously molten fuel.

The previously molten fuel region of cross section K09-P2-C near the bottom of the crust is typified by the sample at location No. 4, as shown in Figure 12. This sample is composed primarily of uranium and zirconium at concentrations similar to those found in intact fuel rods or assemblies (i.e., 70 wt% uranium and 20 wt% zirconium). These data would suggest that the ceramic $(U,Zr)O_2$ regions are relatively homogeneous with little structural material contamination, except at interfaces between the metallic and the oxidized regions.

At the G08 core location, two samples from the upper crust were examined: G08-P11-B, a transverse section; and G08-P11-E, a longitudinal section. The transverse section, which appears to be ceramic fuel material with metallic striations, is shown in Figure 13. The photograph indicates

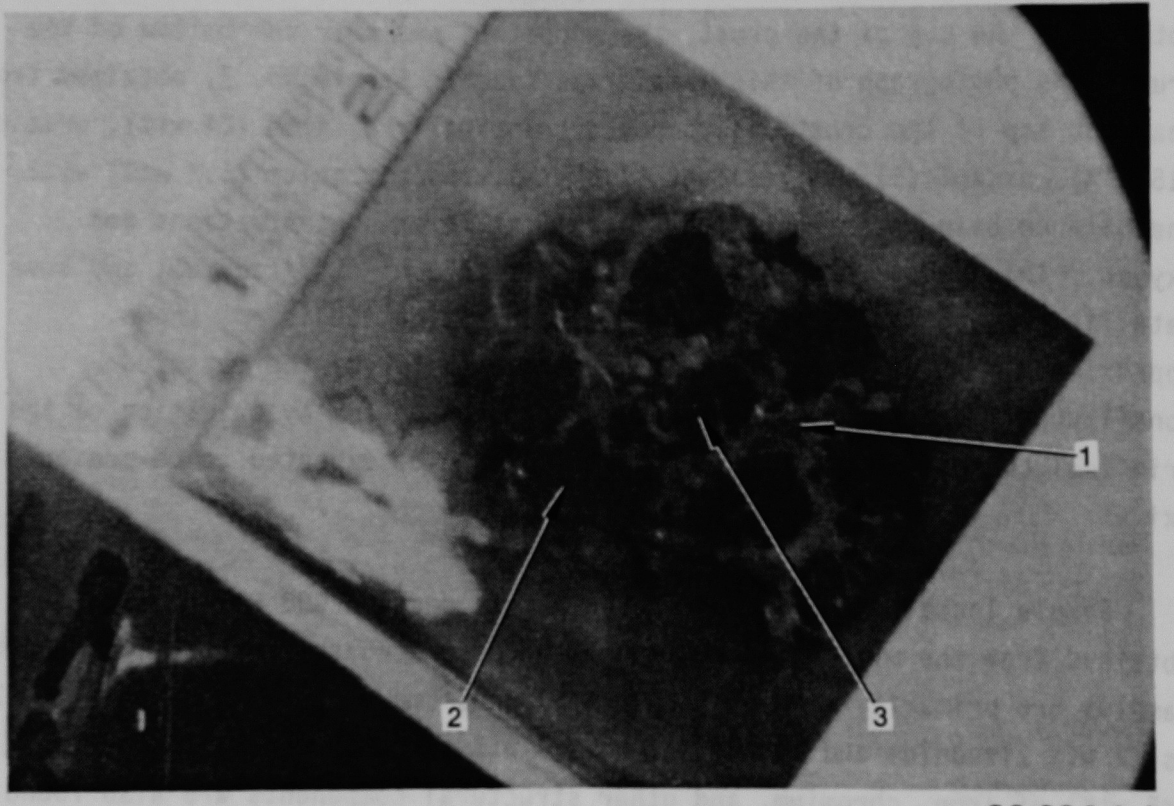

Figure 13. G08-P11-B sampling locations.

that sample location No. 1 should be primarily metallic, and sample locations No. 2 and 3 should be primarily fuel. However, the elemental examination results indicate that all three samples are primarily uranium (51-67 wt%) and zirconium (17-23 wt%) with little structural material present. Further visual examination of the G08-P11-B cross section after the analysis results had been reviewed indicated that a thin layer of metallic material (that was probably removed during coring) had been spread over the fuel material where core sample No. 1 was obtained.

In the longitudinal cross section, G08-P11-E, three samples were obtained: the top of the crust, the midpoint, and near the bottom of the crust. No photograph of this sample was taken. Sample No. 1, obtained from near the top of the crust, is composed principally of iron (24 wt%), uranium (15 wt%), nickel (11 wt%), silver (7.8 wt%), and zirconium (5.2 wt%) with the balance being other core constituents at lower concentrations and oxygen. This sample probably contains a mixture of oxidized fuel and some metallic components; however, the degree of oxidation is not known. Approximately 75 wt% of the sample is accounted for by the measured constituents, and the remainder would be accounted for by oxidation of the principal constituents of the sample that would be expected to be present as oxides.

Sample locations Nos. 2 and 3 from cross section G08-P11-E were obtained from the middle and bottom of the upper crust, respectively. Both samples are primarily uranium (65-70 wt%) and some zirconium. Sample No. 2 is 22 wt% zirconium and sample No. 3 is 4 wt% zirconium. Small amounts (<5 wt%) of iron, chromium, and other structural components are also found in these samples.

Figure 14 shows the D08-P3-A cross section and the two locations where samples were obtained. This sample is composed principally of uranium (60 wt%) and zirconium (11 -14 wt%) with some structural and control materials present in sample No. 1.

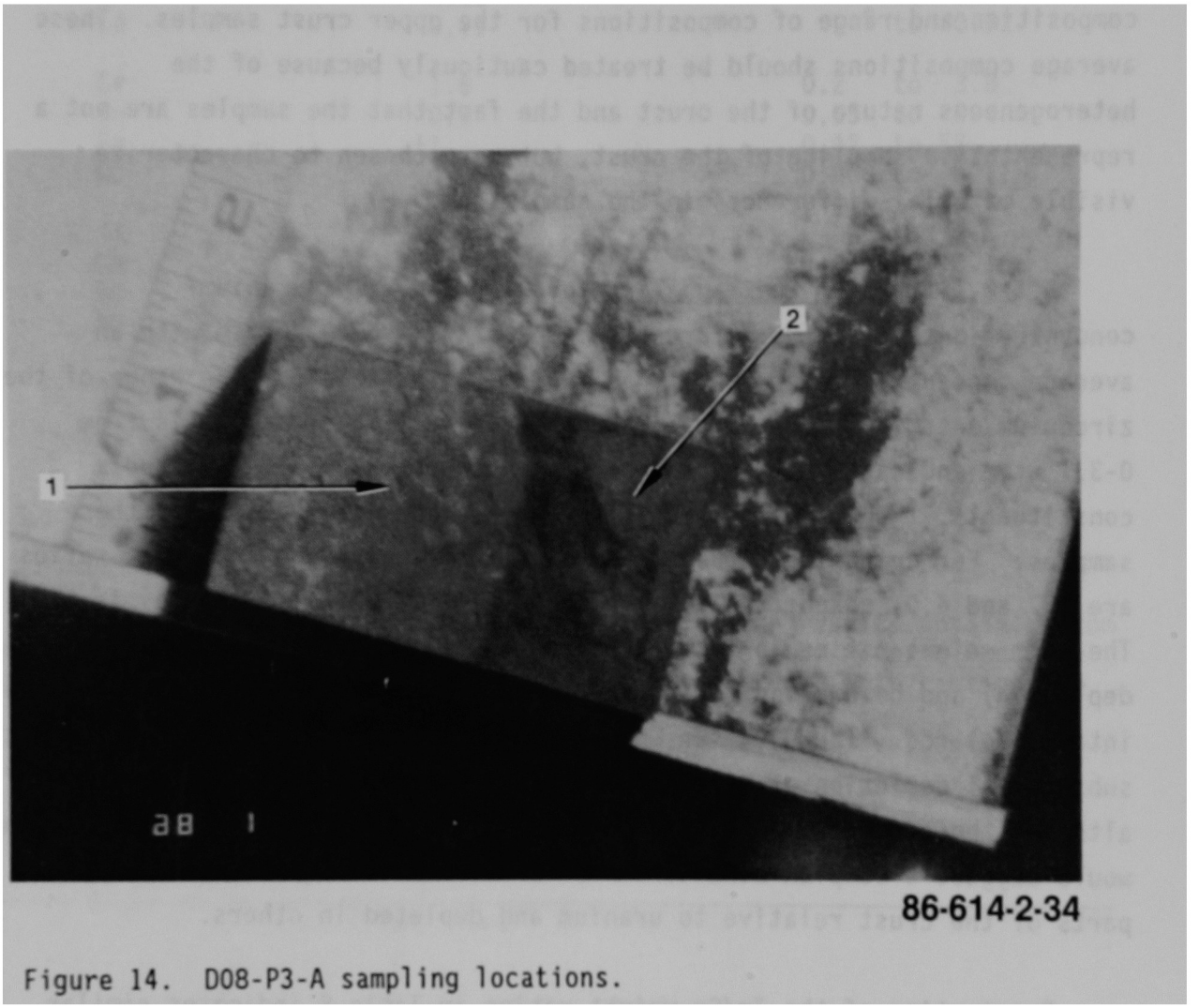

Figure 14. D08-P3-A sampling locations.

Of the samples examined, only K09-P2 sample location Nos. 1 to 3, and G08-P11-E sample location No. 1 (15 wt% uranium) can be considered primarily metallic samples (<50 wt% uranium) with the remaining samples being mixtures of U,Zr ceramic and structural metallic materials. The prior-molten uranium and zirconium samples are similar in composition to the melted fuel material found in other parts of the core, and the primary metallic constituents of the crust are iron, nickel, silver, and indium. Table 7 lists the average composition and range of compositions for the upper crust samples. These average compositions should be treated cautiously because of the heterogeneous nature of the crust and the fact that the samples are not a representative sampling of the crust, but were chosen to characterize visible material differences in the samples.

3.1.2.1 Uranium Fuel and Zircaloy Cladding. The uranium concentrations in the upper crust samples range from 0-70 wt% with an average concentration of 49 wt%, as indicated in Table 7. The range of the zirconium data is from 0-22 wt%, and the range of the tin data is from 0-3.7 wt%, indicating a wide range of compositions for all fuel rod constituents. Table 8 lists the U/Zr and Zr/Sn weight ratios for these samples. For comparison, the core average and fuel rod U/Zr weight ratios are 3.7 and 4.0, respectively. The Zr/Sn weight ratio in zircaloy is 61. The U/Zr weight ratios in Table 9 are both above (indicating zirconium depletion) and below (indicating accumulation of zirconium) the ratio for an intact fuel rod. The data for G08-P11-E, No. 3 (a high U/Zr ratio) suggests substantial depletion of zirconium near the bottom of the crust layer, although the same behavior is not apparent at the K09 location. These data would suggest a complex behavior where zirconium is concentrated in some parts of the crust relative to uranium and depleted in others.

Examination of the Zr/Sn weight ratios in Table 8 indicates similar behavior to that observed for the U/Zr weight ratios with widely varying ratios both above and below the as-manufactured ratio in zircaloy. Examination of the results for the primarily metallic samples suggests that the zirconium does not appear to concentrate in the metallic parts of the crust,

TABLE 7. UPPER CRUST AVERAGE COMPOSITION[a]
(wt%)

Element	Average Composition[b]	Range
Ag	3.2	0.05 to 9.32
Al	0.21	0.08 to 0.44
B	0.12	--[c] to 0.26
Cd	0.11	--[c] to 0.32
Cr	1.6	0.2 to 3.8
Cu	0.9	0.05 to 9.4
Fe	11	0.42 to 53
Gd	0.06	0.006 to 0.11
In	1.0	--[c] to 2.6
Mn	0.06	0.03 to 0.16
Mo	0.44	--[c] to 2.15
Nb	0.14	--[c] to 0.32
Ni	5.2	0.07 to 14.5
Si	0.56	0.13 to 1.5
Sn	1.1	--[c] to 3.7
Te	0.03	--[c] to 0.09
U	49.0	--[c] to 70
Zr	20.4	--[c] to 22

a. This table presents the average of the examination results obtained from the upper crust; however, due to the heterogeneity of the material and the small number of samples examined, these data must be used with caution.

b. The average concentration is calculated using only real values and is averaged without zero values.

c. Lowest value below analytical detection limit.

TABLE 8. UPPER CRUST FUEL MATERIAL (U, Zr, Sn) WEIGHT PERCENT RATIOS

Sample ID	U/Zr Ratio[a]	Zr/Sn Ratio[b]
K09-P2-C		
No. 1[c]	--[d]	--[d]
No. 2[c]	3.7	5.1
No. 3[c]	2.9	9.2
No. 4	3.6	--[d]
G08-P11-B		
No. 1	3.8	153
No. 2	2.9	18
No. 3	2.7	213
G08-P11-E		
No. 1[c]	2.9	1.6
No. 2	2.9	288
No. 3	18	11
D08-P3-A		
No. 1	4.3	8.3
No. 2	5.4	78

a. The core average U/Zr weight ratio is 3.7 assuming oxidation of the zircaloy and the weight ratio for a fuel rod is 4.0.

b. The average Zr/Sn ratio in zircaloy cladding is 61.

c. Samples are primarily metallic. Additionally samples K09-P2-C Nos. 2 and 3 are both approximately 32 wt% uranium but contain substantial amounts of structural material.

c. Component not detected.

TABLE 9. UPPER CRUST CONTROL MATERIAL (Ag, In, Cd) WEIGHT RATIOS

Sample ID	Ag/In Ratio[a]	Ag/Cd Ratio[b]	In/Cd Ratio[c]
K09-P2-C			
No. 1[d]	1.2	18	16
No. 2[d]	5.9	98	81
No. 3[d]	5.8	81	14
No. 4	--[e]	5.0	--[e]
G08-P11-B			
No. 1	0.4	--[e]	--[e]
No. 2	4.0	26	6.5
No. 3	2.8	--[e]	--[e]
G08-P11-E			
No. 1[d]	4.4	24	5.5
No. 2	4.7	--[e]	--[e]
No. 3	2.7	95	35
D08-P3-A			
No. 1	2.6	31	12
No. 2	0.6	28	47

a. The Ag/In weight ratio is 5.3 in intact control rod alloy.

b. The Ag/Cd weight ratio is 16 in intact control rod alloy.

c. The In/Cd ratio is 3.0 in intact control rod alloy.

d. A component of the comparison was below the detection limit of the analysis method.

but is present probably as metallic inclusions in the oxidized U,Zr portion of the crust.

3.1.2.2 Control Rod Materials. Control rod materials, including the relatively volatile cadmium, were measurable in most of the upper crust samples. Examination of the data in Tables G1 through G4 and 7 indicates that the least volatile control material, silver, was measurable in all samples at an average concentration of about 3 wt% with a range of concentrations from 0.05 to 9 wt%. However, as discussed in Appendix G, the quantity of silver indicated may be less than was actually present in the sample due to the possible precipitation of this element during the elemental analysis procedure. Therefore, the silver data should be treated as suspect when drawing conclusions.

Indium was measurable in all samples at concentrations averaging 1.0 wt% with the bulk of the data ranging from 0.5 to 2.0 wt%. The core average concentration of this element is 0.3 wt%. The indium appears to be primarily concentrated in those metallic samples near the top of the crust.

Cadmium was measurable in 9 of the 12 samples obtained from the upper crust. The concentrations ranged from 0.01 to 0.3 wt%, with an average concentration of about 0.1 wt%. This concentration is similar to the core average concentration of 0.12 wt%. The presence of the significant amounts of cadmium (boiling point 1040 K) in most samples suggests that the cadmium was not at high temperatures for a long period of time, and/or alloying may have significantly reduced its vapor pressure.

Table 9 presents the weight ratios for Ag/In, Ag/Cd and In/Cd for the upper crust samples. The Ag/In weight ratios indicate a range from 0.4 to 6 with most of the results below the as-fabricated ratio of 5.3. Examination of the results indicates that there is no apparent distinction between metallic and ceramic samples with ratios both below and near the as-fabricated ratios. Although these data may be an artifact of the precipitation of silver, these data would suggest that indium probably is retained to a greater extent than silver. Examination of the Ag/Cd and

In/Cd ratios indicates ratios substantially greater than 16 and 3.0, the as-manufactured ratios. These data indicate that cadmium has been partially lost from the debris relative to silver and the In/Cd ratios suggest a similar behavior for cadmium relative to indium.

3.1.2.3 Poison Rod Materials. Poison rod materials measurable in the upper crust included aluminum, boron, and gadolinium. Aluminum was measurable in all samples at concentrations averaging 0.2 wt%, which is the same as the core average concentration. Boron from the poison rods and reactor coolant is present in most samples at concentrations between 0.05 and 0.25 wt%. Gadolinium is also present in the upper crust in a range of concentrations from 0.03 to 0.1 wt%. This concentration is greater than the average concentration of 0.01 wt%, which indicates accumulation of this element in the upper crust samples.

3.1.2.4 Structural Materials. Measurements were made for all structural material constituents of the core (i.e., iron, chromium, nickel, manganese, niobium, and molybdenum). The average concentration data in Table 7 indicates that iron is the principal structural material present and that it ranges up to 53 wt% in some samples. Lesser concentrations of nickel (average - 5.2 wt%) and chromium (average - 1.6 wt%) are also present. Examination of the ratio data for the principal components of the metallic crust (Table 10) indicates that the iron/Cr ratios are greater than those found in stainless steel and Inconel, and that the iron nickel ratios are between those of stainless steel and Inconel. The binary phase diagrams[12] indicate melting temperatures of ~1770 K for the binary couples Fe Cr, ~1720 K for Fe Ni, and ~1760 K for Ni Cr; however, as indicated by the Fe/Cr ratios, chromium is depleted in the upper crust samples relative to iron. Chromium would be expected to oxidize more readily because of a relatively low oxidation potential, as compared with iron and nickel. SEM examination indicates the presence of oxidized chromium in the (U,Zr)O ceramic samples, with some dissolved in the oxide matrix and some in eutectic mixtures at grain boundaries, probably as a chromate. The presence of molybdenum in the upper crust samples suggests that the metallic crust was composed of the Inconel grid spacers, as molybdenum is not present in

TABLE 10. UPPER CRUST STRUCTURAL MATERIAL (Fe, Cr, Ni and Mo) WEIGHT RATIOS[a]

Sample I.D.	Fe/Cr Ratio	Fe/Ni Ratio	Ni/Cr Ratio	Ni/Mo Ratio
K09-P2-C				
No. 1	14.5	2.3	6.4	11
No. 2	51	1.1	4.4	37
No. 3	9.2	7.9	3.9	--
G08-P11-E				
No. 1	6.3	2.83	2.8	11

a. The elemental ratios for stainless steel and Inconel are (from Reference 9):

	Stainless steel	Inconel
Fe/Cr	3.6	0.35
Fe/Ni	7.6	0.35
Ni/Cr	0.5	2.7
Ni/Mo	--	17.3

the stainless steel components of the core. The Ni/Mo ratios shown in Table 10 suggest that the grid spacers contributed substantially to the formation of the crust because the ratios are similar to those found in the Inconel grid spacers.

3.1.3 Upper Crust Radiochemical Examinations

The radionuclide distribution in the upper crust samples was measured for the samples discussed in Section 3.1.2. Results of the radiochemical analysis of the samples are listed in Appendix H, Tables H1 through H3. To provide information on the characteristic behavior of fission products, they have been categorized by the volatility of the chemical group and element, as shown in Table 11.[13] Possible chemical compounds have been included, and the radionuclides are indicated for which analyses were performed.

The high-volatility fission product groups (I, II, III, and IV.a) are the noble gases, halogens, alkali metals, and heavy chalcogens. They are characterized by boiling points less than 1600 K for the elemental forms as well as for the listed oxide compounds. From this group, measurements were made for ^{129}I and ^{137}Cs.

The medium-volatility fission products are characterized by boiling points less than 3100 K (UO_2 melting). These fission products are from the Group VA metals, alkaline earths, some of the rare earths, and actinides. However, it should be noted that the volatility of these fission products is strongly dependent on the chemical form of the fission product. For example, ruthenium has two highly volatile oxides (i.e., RuO_2 and RuO_4) that either decompose or boil at less than 400 K. Radionuclides from these groups for which measurements were made are ^{125}Sb, ^{90}Sr, ^{154}Eu, and ^{106}Ru.

The low-volatility fission products include elements from the noble metals, the remaining rare earths and actinides, tetravalents, and early transition elements. Generally, the oxides of these elements have low volatilities; however, some (e.g., LaO or CeO) have lower boiling points

TABLE 11. CORE MATERIAL VOLATILITY GROUPS

WASH-1400 Group Number	Chemical Group	Element	Boiling[a] Temperature (K)	Volatility	Possible Compounds	Boiling[a] Temperature (K)	Volatility	Analysis Performed
I	Noble gases	Kr[b]	120	High		--	--	--
		Xe[b]	166	High		--	--	--
II	Halgoens	Br	332	High	CsBr	1573	High	--
		I	458	High	CsI[b]	1553	High	X
					HI	238	High	--
					I_2	457	High	--
III	Alkali metals	Rb[b]	973	High	RbI	1573	High	--
					Rb_2O	--	High	--
					Rb_2O_2	1284	High	--
		Cs[b]	963	High	CsI[b]	1553	High	X
					CsOH	~1350[c]	High	--
					Cs_2O	--	High	--
					Cs_2O_2	923	High	--
					Cs_2UO_4	--	--	--
IV.a	Heavy chalcogens	Se[b]	958	High	SeO_3	453	High	--
					SeO_2	--	--	--
		Te[b]	1663	High	TeO_2	--	--	X
					Te_2O_2	--	--	--
					Silver-telluride	--	--	--
					Iron-telluride	--	--	--
					Zirconium telluride	--	--	--
					Tin-telluride	--	--	--
					Nickel telluride	--	--	--
					Chrome telluride	--	--	--
IV.b	Group VA metals	Sb[b]	1653	Medium	Sb_2O_3	1323	Medium	X
V	Alkaline earths	Sr	1639	Medium	SrO[b]	~3100	Low	X
		Ba	1800	Medium	BaH_2	1673	Medium	--
					BaO[b]	~2273	Medium	--
					BaO_2	1073	High	--
					$Ba(OH)_2$	1053	High	--
VI	Rare earths	Eu	--	Medium	Eu_2O_3[b]	--	--	X
		Sm	2173	Medium	SM_2O_3[b]	--	--	--
		Pm	3400	Low	Pm_2O_3[b]	--	--	--
	Actinides	Am	2873	Medium	AmO_2[b]	--	--	--

TABLE 11. Continued

Periodic Table Group Number	Chemical Group	Element	Boiling[a] Temperature (F)	Volatility	Possible Compounds	Boiling[a] Temperature (F)	Volatility	Analysis Performed
VIII	Noble metals	Pd	2473	Low	PdO	--	--	--
		Rh	5173 (est)	Low	RhO_2	--	--	X
					Rh_2O_3	--	--	--
		Ru	4423	Low	RuO_2	--	X	--
					RuO_4	125	High	--
		Mo	4780	Low	MoO_2	--	--	--
					Mo_2O_5	--	--	--
					MoO_3	--	--	--
		Tc	--	Low		--	--	--
VIII	Rare earths	Y	3260	Low	Y_2O_3[b]	--	--	--
		La	3743	Low	LaO	--	Medium-high	--
					La_2O_3[b]	4473	Low	--
		Ce	2690	Low	CeO_2	--	--	X
					Ce_2O_3[b]	--	--	--
		Pr	3400	Low	PrO_2	--	--	--
					Pr_2O_3[b]	--	--	--
		Nd	3300	Low	Nd_2O_3	--	--	--
	Actinides	Np	--	Low	NpO_2[b]	--	--	--
		Pu	3508	Low	PuO_2[b]	--	Low	--
		Cm	--	Low	CmO_2[b]	--	--	--
	Tetravalents	Zr[c]	>3173	Low	ZrO_2[b]	~5273	Low	--
	Early transition	Nb	~3573	Low	NbO_2	--	Low	--
					Nb_2O_5	--	--	--

a. Boiling temperature at 1 atm., data primarily from CRC Handbook of Chemistry and Physics, 50th Edition.

b. Probable chemical form of the fission product within the fuel.

c. Zirconium is both a fission product and structural material.

than do the elements. The only radionuclide from this group that was measurable during the lower vessel examination program was cerium/praseodymium. In addition, ^{235}U and ^{238}U, which are also low volatile isotopes, were measured to assess uranium content and ^{235}U enrichment.

Table 12 lists the average radionuclide concentrations, the range, and the ratio of high to low values in the upper crust samples. The ratios of high to low concentrations are from 10^1 to 10^3, indicating a relatively wide range of concentrations in the crust; however, the radionuclides with high to low ratios greater than 10^2 are the more volatile species (i.e., ^{134}Cs and ^{137}Cs), the metallic species (^{106}Ru and ^{125}Sb), and the neutron activation product ^{60}Co. Surprisingly, the ^{129}I is relatively evenly distributed in the crust with a high to low ratio of 54.

3.1.3.1 Upper Crust Uranium-235 Enrichment. Measurements were performed to evaluate the concentrations of ^{235}U and ^{238}U in the upper crust and to determine ^{235}U enrichment in the crust. The ^{235}U and ^{238}U concentrations are listed in Appendix H; the ^{235}U enrichments are listed in Table 13. These measurements should be treated with some caution because the measurement technique used is affected by the presence of control materials. For this reason, measured values lower than actual concentration may result for those samples with high control material content. Table 13, which summarizes the ^{235}U and ^{238}U data, indicates a range of enrichments from 1.7 to 2.3 wt%; however, the bulk of the data is in the range from 2.2 to 2.3 wt% and indicates that the upper crust debris samples are mostly a composite of the 1.98% and 2.64% enriched assemblies.[a] A relatively homogeneous distribution of the fuel material from the two assembly enrichments is indicated for the upper crust which suggests that the fuel material had melted and was well mixed prior to formation of the crust.

---

a. Assembly locations K09 and D08 had original enrichments of 1.98%, and G08 had an enrichment of 2.64%.

TABLE 12. UPPER CRUST AVERAGE RADIONUCLIDE CONCENTRATIONS (microcuries/g sample on April 1, 1987)

Radionuclide	Average	Range	High/Low Ratio
^{60}Co	262	5.2 to 1430	275
^{90}Sr	1820	3.6 to 6300	1750
^{106}Ru	360	44[a] to 1510	34
^{125}Sb	336	0.4[a] to 1330	3325
^{129}I	2.2 E-4	1.3E-5[a] to 7.0E-4	54
^{134}Cs	27	0.24[a] to 217	900
^{137}Cs	1220	11 to 9600	872
^{144}Ce	106	12[a] to 204	17
^{154}Eu	26	1.6[a] to 42	26
^{155}Eu	40	13[a] to 60	5

a. Detection limit values not included in the range or the high to low ratios.

TABLE 13. UPPER CRUST URANIUM-235 ENRICHMENT

Sample ID	^{235}U Enrichment[a]
K09-P2-C	
No. 1	--[b]
No. 2	2.2
No. 3	2.2
No. 4	--[b]
G08-P11-B	
No. 1	2.2
No. 2	1.9
No. 3	2.3
G08-P11-E	
No. 1	1.7
No. 2	2.3
No. 3	2.0
D08-P3-A	
No. 1	2.3
No. 2	2.2

a. The core average ^{235}U enrichment is approximately 2.56%, with the peripheral assemblies having an enrichment of 2.98 and the central assemblies having enrichments of 1.98% and 2.64%.

b. Not measured.

c. Large uncertainties associated with result.

3.1.3.2 Comparisons with ORIGEN2. The measured radionuclide concentrations in the upper crust were compared with concentrations predicted by the ORIGEN2 Code in order to assess retention of radionuclides in the ceramic and metallic regions of the upper crust. The ORIGEN2 analysis model used for the TMI-2 core[8,14] contained 1239 core nodes. Analyses were performed for ranges of burnup for each of the three ^{235}U enrichments present (i.e., 1.98%, 2.64%, and 2.98%). Table 14 lists the ORIGEN2 values used for comparison with the core bore data. The original core average values have been adjusted because: (a) the peripheral (2.98% enriched) assemblies did not participate in the accident, and (b) an ORIGEN2 verification study was performed for the TMI-2 core[14] that indicated core specific differences in radionuclide concentrations. This study indicated the correction factors listed in Table 14. The method used to estimate retention is shown below:

$$\frac{\text{Radionuclide concentration (mCi/g)}}{\text{Uranium content (gU/g sample)}} \times \frac{100}{\text{ORIGEN-2 predicted radionuclide concentration (microcuries/g uranium)}} = {}^{235}U \text{ normalized fission product content (retention in \%)} \quad (1)$$

The radionuclide concentrations used were from Appendix H and the uranium content data was from the elemental analysis results in Appendix G. The results of these calculations, the normalized fission product retentions, are listed in Table 15, and a summary of the average retentions for the metallic and ceramic samples is listed in Table 16. A wide range of retentions is indicated for most radionuclides, including the relatively stable low volatiles. The following sections contain discussions of the radionuclide retentions for the low, medium, and high volatility fission products.

3.1.3.3 Low Volatiles. The low volatiles for which radionuclide comparisons were performed are ^{144}Ce and ^{154}Eu. Tables 15 and 16 list the normalized retentions for the upper crust. It should be noted that

TABLE 14. ORIGEN2 PREDICTED RADIONUCLIDE CONCENTRATIONS
(in microcuries/g uranium on April 1, 1987)

Radionuclide	Core[a] Average	Central Core[b] Assemblies	Verification[c] Correction	Adjusted Radionuclide Concentration
^{90}Sr	7540	1.08	0.988	8045
^{106}Ru	168	1.16	0.961	187
^{125}Sb	206	1.13	0.432	101
^{129}I	2.81E-3	1.11	0.867	2.70E-3
^{137}Cs	8680	1.09	1.021	9659
^{144}Ce	215	1.08	1.069	248
^{154}Eu	60	1.21	0.626	45.6
$^{155}5Eu$	125	1.10	0.614	84.4

a. Core average concentration as listed in Reference 8. The data are listed as reference values rather than with the proper number of significant figures and associated uncertainties that are defined in Reference 14.

b. Correction to the core average value to account for the fact that the peripheral 2.98% enriched fuel assemblies did not participate in the accident.

c. Correction for the measured variations from the predicted code values as defined and explained in Reference 14.

TABLE 15. RADIONUCLIDE RETENTION IN THE UPPER CRUST[a]

Sample ID	Radionuclide Retention(%)						
	^{90}Sr	^{106}Ru	^{125}Sb	^{129}I	^{137}Cs	^{144}Ce	^{154}Eu
K09-P2-C							
No. 1[b,c]	0.04	398	1272	26.3	4.21	--[d]	--[d]
No. 2[b]	5.53	466	1715	67.7	14.6	66.8	88.5
No. 3[b]	9.36	1164	1416	34.5	0.27	102	123
No. 4	45.2	--[c]	1.50	0.15	0.41	97.3	143
G08-P11-B							
No. 1	31.5	--[d]	--[d]	0.12	0.41	87.3	135
No. 2	18.1	29.3	509	25.5	13.2	26.8	6.9
No. 3	94.2	5.29	2.32	0.77	0.67	132	151
G08-P11-E							
No. 1[b]	44.8	5360	3880	44.1	93.5	32.2	--[d]
No. 2	121	1.81	0.06	1.20	0.17	113	144
No. 3	16.0	60.5	151	2.36	142	42.6	28.7
D08-P3-A							
No. 1	61.3	176	649	16.4	8.57	47.9	76.9
No. 2	20.6	38.5	63.4	6.07	11.2	92.5	79.6

a. Retention is calculated based on the uranium content of the sample material as determined from the elemental analysis results in Appendix G. Additional figures are shown beyond those statistically appropriate for calculational purposes. The uranium concentrations used for normalization in wt% were:

K09-P2-C - No. 1 - (no measurable U); No. 2 - 32.8; No. 3 - 32.2; No. 4 - 70.5
G08-P11-B - No. 1 - 66.7; No. 2 - 50.7; No. 3 - 62.0
G08-P11-E - No. 1 - 15.1; No. 2 - 64.6; No. 3 - 70.4
D08-P3-A - No. 1 - 60.8; No. 2 - 60.9

b. Contains significant amounts of metallic material (greater than 30%).

c. Sample assumed to be composed of uranium for comparison purposes.

d. Not detected.

TABLE 16. RADIONUCLIDE RETENTION IN METALLIC AND CERAMIC SAMPLES (%)

	Metallic Samples[a]		Ceramic Samples[b]	
Radionuclide	Average	Range	Average	Range
^{90}Sr	15	0.04 - 45	56	20 - 121
^{106}Ru	1490	60 - 5350	50	1.8 - 176
^{125}Sb	1690	151 - 3800	205	2.3 - 649
^{129}I	35	26 - 67	7.2	0.11 - 25
^{137}Cs	28[c]	4.2 - 93	4.9	0.17 -142
^{144}Ce	49	27 - 132	85	32 - 102
^{154}Eu	80	29 - 123	105	6.9 - 150

a. Nominal metallic samples are K09-P2-C No. 1, No. 2, No. 3, and G08-P11-E No. 1.

b. Nominal ceramic samples include all other samples in the upper crust, although there is some metallic material in all samples that may bias the results to some extent.

c. Result biased by the presence of a single high activity sample.

sample K09-P2-C No. 1 contained no measurable uranium and consequently, normalization to the uranium content of the sample is not possible. However, to provide a relative assessment of fission product retention, K09-P2-C was assumed to be composed entirely of uranium. This causes the listed retentions to be artificially lower than the results for those samples containing uranium. Examination of the low volatile ^{144}Ce and ^{154}Eu retention data in Table 15 indicates a range of retentions varying with no apparent correlation with sample location or U content. Losses or releases are indicated for both ^{144}Ce and ^{154}Eu. No explanation is known for this phenomena, which has not been observed in other prior-molten fuel samples from TMI-2. Also, The lack of cerium and uranium content in particle K09-P2-C No. 1 suggests that no partitioning of the lanthanides to the metallic part of the crust occurred, although other more volatile radionuclides partitioned to the metallic melt.

If the average retention data in Table 16 are examined, the data indicate an average retention and standard deviation for the ceramic region of 85 $\pm$ 36%. However, the number of high retentions (i.e., those >100%) suggests that the fuel material forming the upper crust came from a relatively low burnup region of the core. The upper crust, based upon these data, appears to have been primarily formed from fuel material from the periphery of the core or that the losses of low volatiles noted above affected the ^{144}Ce content for all samples of the crust.

3.1.3.4 Medium Volatiles. The fission products that are expected to have a medium volatility are ^{90}Sr, ^{125}Sb, and ^{106}Ru. Strontium-90 is the least volatile and is expected to be retained by the fuel to the greatest extent. The ^{90}Sr data shown in Tables 15 and 16 indicate a range of retentions from 0.04 to 121% and indicate substantial release of this fission product. Examination of the retentions for sample K09-P2-C, which contains no fuel material, indicates little partitioning of ^{90}Sr to the metallic part of the crust. Examination of the metallic sample average retentions in Table 16 indicates lower retentions in these samples. Again little partitioning of ^{90}Sr to the metallic part of crust is indicated.

Substantial retention of ^{90}Sr is indicated for most ceramic fuel samples; however, losses are indicated for some samples (e.g., G08-P11-E No. 3 and D08-P3-A) where retentions are as low as 16%. Release of ^{90}Sr is indicated in the crust where the the less volatile ^{144}Ce is retained.

The medium volatile radionuclides, ^{125}Sb and ^{106}Ru, exhibit a greater range of retentions because they are expected to remain in a metallic state due to the high oxidation potentials required for the oxidation of these elements. An increase in metallic content is generally correlated with increases in ^{125}Sb and ^{106}Ru content for the four metallic samples that have greater than 30 wt% metallic content (Table 15). Samples G08-P11-E No. 1 and K09-P2-C No.1 from near the top of the crust have the highest concentrations of ^{106}Ru and ^{125}Sb in the crust. Sample G08-P11-E contains 54 wt% metallic material and also has the highest normalized retentions of ^{106}Ru (54 times the ORIGEN2 inventory for the fuel present) and ^{125}Sb (39 times the ORIGEN2 inventory). Although the indicated retentions for sample K09-P2-C No. 1 are not as high as the retentions of other samples in the crust, this sample was assumed to be composed of uranium for comparison purposes and, consequently, the retentions are lower. If 1 wt% uranium content had been assumed for K09-P2-C, this sample would have had the highest retentions in the crust. These data suggest accumulation of metallic ^{106}Ru and ^{125}Sb in the metallic material near the top of the upper crust.

3.1.3.5 High Volatiles. The two high volatile radionuclides measurable were ^{137}Cs and ^{129}I. The more volatile ^{129}I was measurable in all samples at retentions lower than those found in intact fuel material. The presence of ^{129}I in sample K09-P2-C No. 1 (26% retention), which does not contain uranium, suggests that ^{129}I is soluble in or reacts with the metallic material causing it to be retained in the crust.

The radionuclide retentions shown in Tables 15 and 16 indicate higher average retentions of ^{129}I and ^{137}Cs for the metallic samples; however, this effect is primarily a result of the low concentrations of uranium in the metallic samples. A comparison of the radionuclide concentrations in

the metallic and ceramic samples indicates similar concentrations for both types of samples. These data again indicate solubility or reactivity of the iodine and cesium in the metallic part of the crust.

3.2 Lower Crust Examination Results

For the lower crust samples, information obtained from the visual and metallurgical examinations is summarized in the following section. Information for this summary was extracted from the visual examinations presented in Appendix C, the density measurements described in Appendix D, the metallographic examinations explained in Appendix E, and the autoradiographic results listed in Appendix F. The bulk elemental and radiochemical analysis results are summarized in Sections 3.2.2. and 3.2.3

3.2.1 Visual and Metallurgical Examinations

Three samples of the lower crust were examined. They included a longitudinal sample at K09, and two samples from the D08 core location. The lower crust sample from K09 was 5.1 cm long, and the combined lengths of samples D08-P1 and D08-P2 resulted in a total estimated crust thickness of 8.9 cm. The densities of these three samples varied from 7.0 to 7.6 g/cm^3.

As described in more detail in Appendix E, all three of these samples consisted of metallic melts surrounding columns of intact fuel pellets. A typical example is shown in the longitudinal metallographic cross section from sample K09-P1 presented in Figure 15. Although not apparent in this figure, small remnants of oxidized ZrO_2 cladding typically surrounded these fuel pellets stacks as shown in Figure 16. These oxidized cladding shells were being dissolved by the metallic melt that flowed down from above. Some fuel dissolution by the zirconium in the metallic melts also occurred, as shown in Figure 17.

An unusual feature observed in samples from the lower crust was the presence of rectangular particles in the metallic melt that were primarily

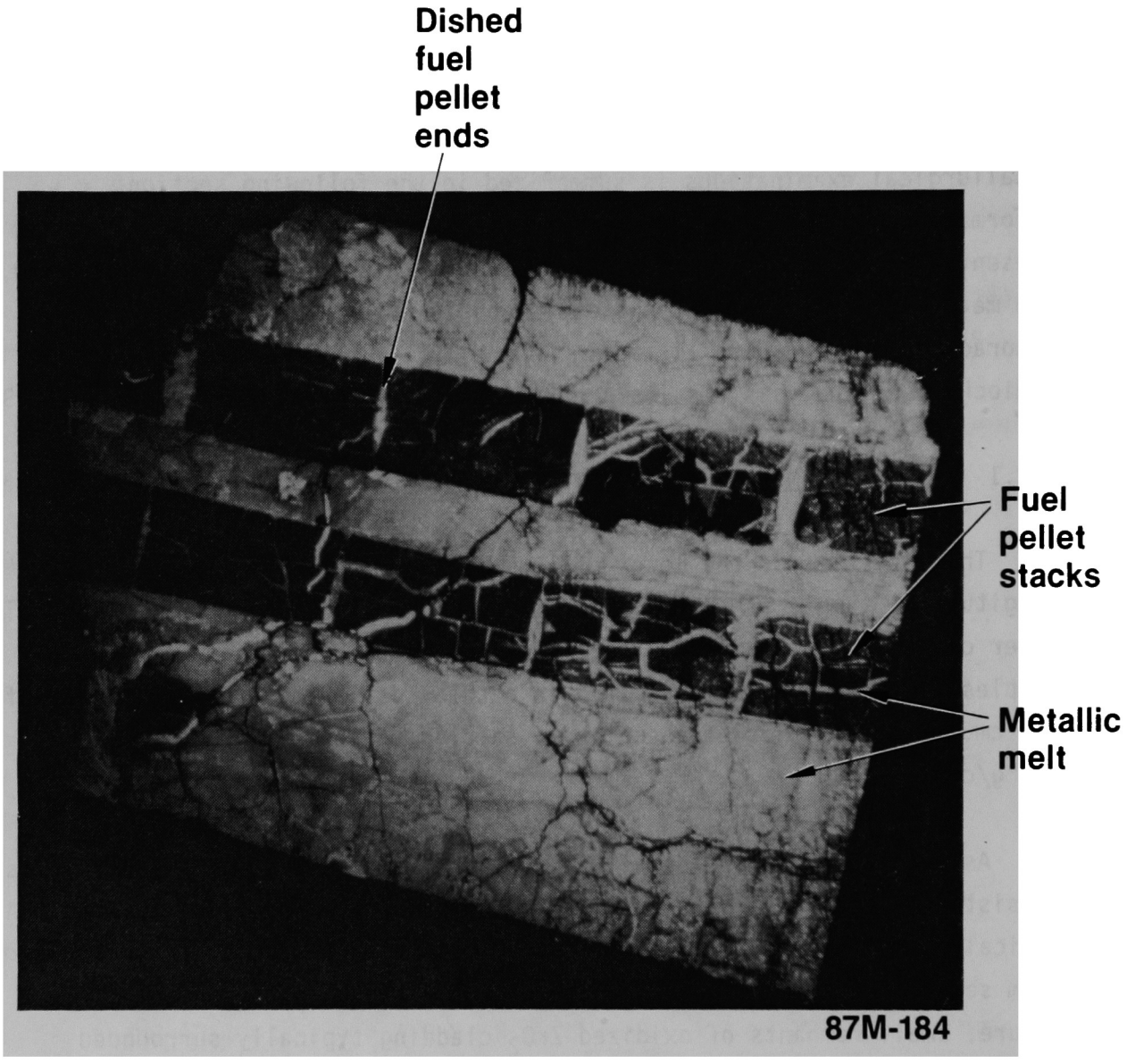

Figure 15. Metallic melt surrounding and penetrating fuel pellet stacks in K09-P1.

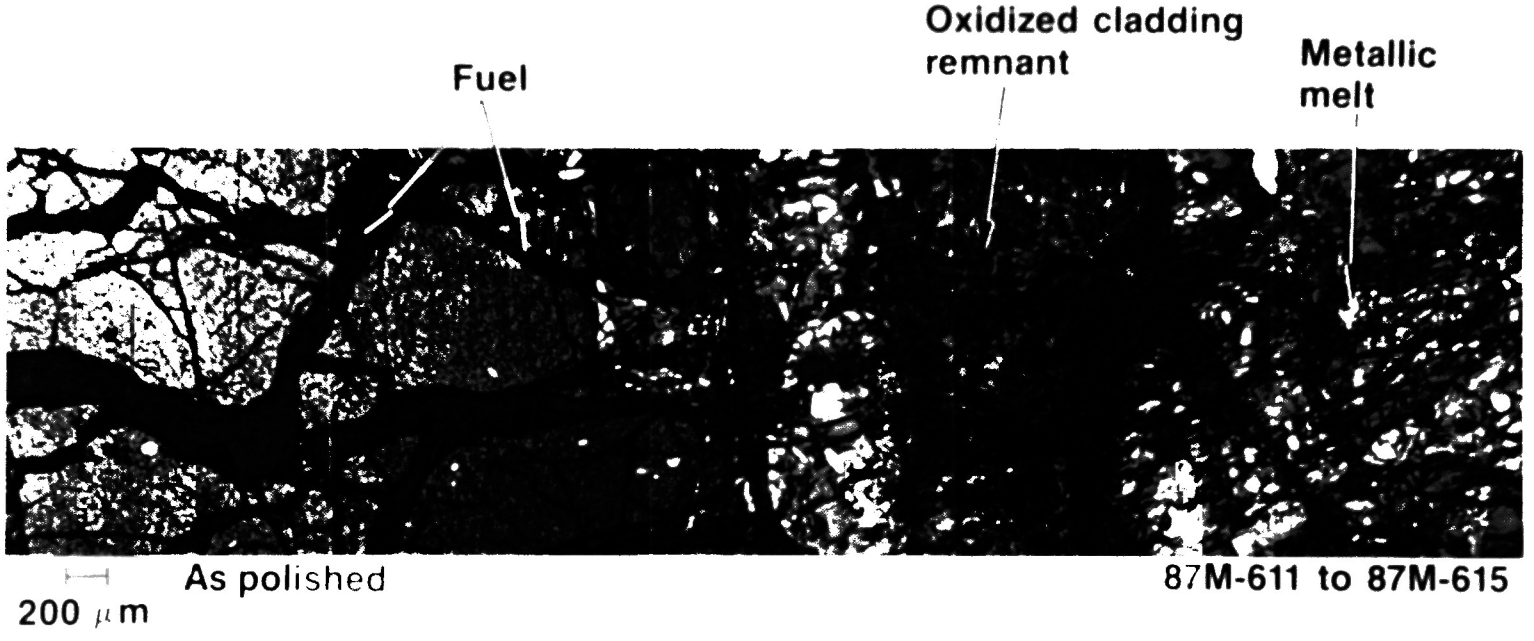

Figure 16. Cladding oxidation and dissolution near fuel pellet in K09-P1.

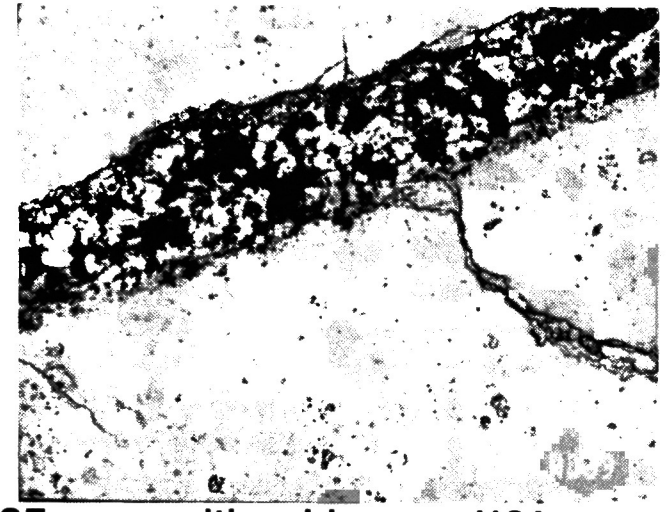

BSE compositional image HCA 87-1220

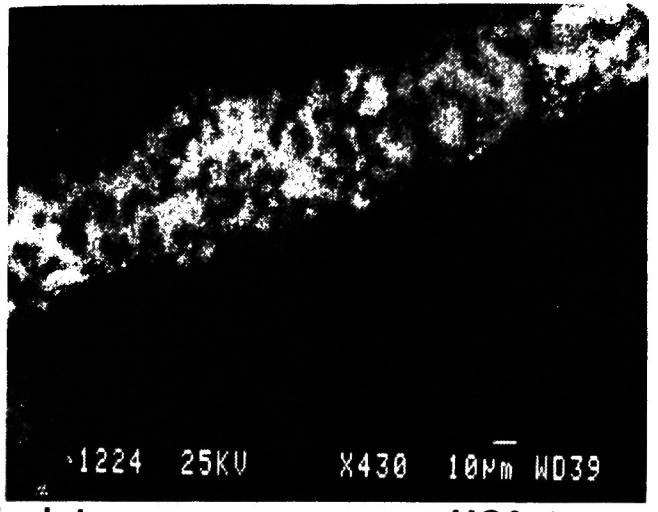

Zr dot map HCA 87-1224

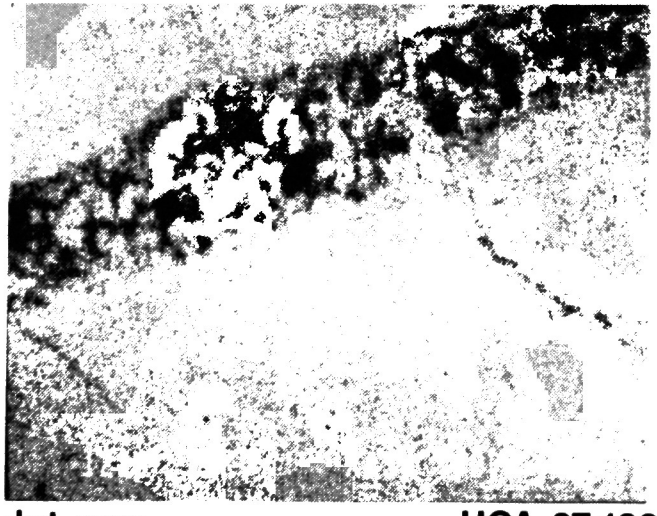

U dot map HCA 87-1226

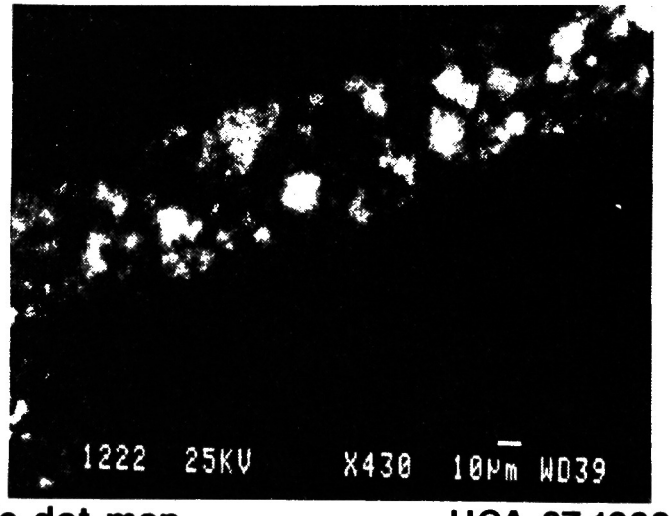

Fe dot map HCA 87-1222

Figure 17. SEM analysis of fuel dissolution in metallic melt (K09-P1).

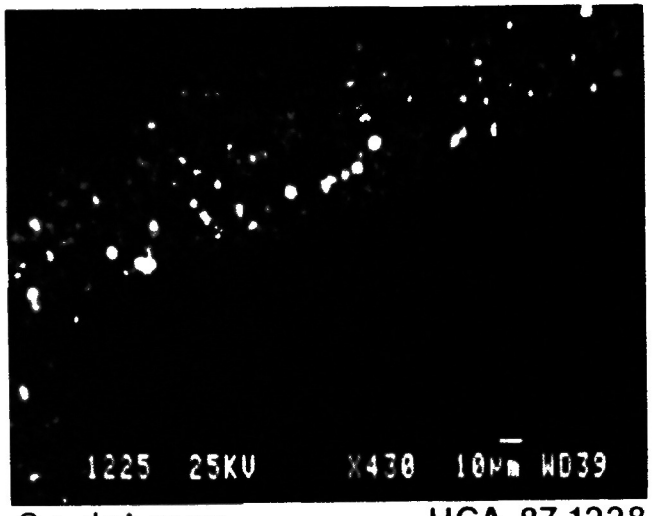

Sn dot map HCA 87-1228

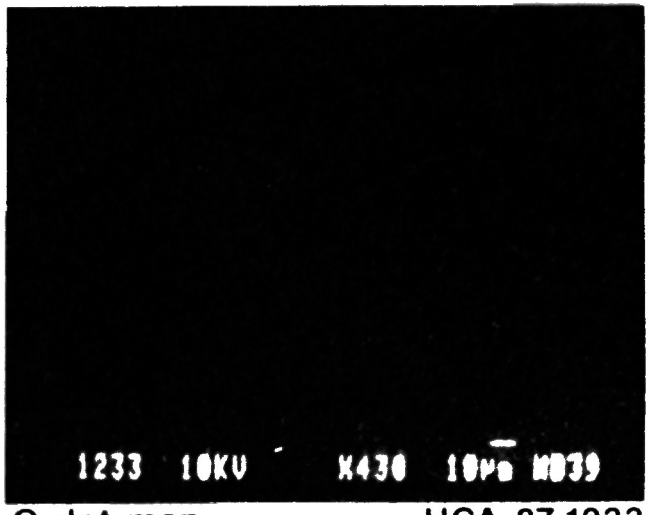

O dot map HCA 87-1233

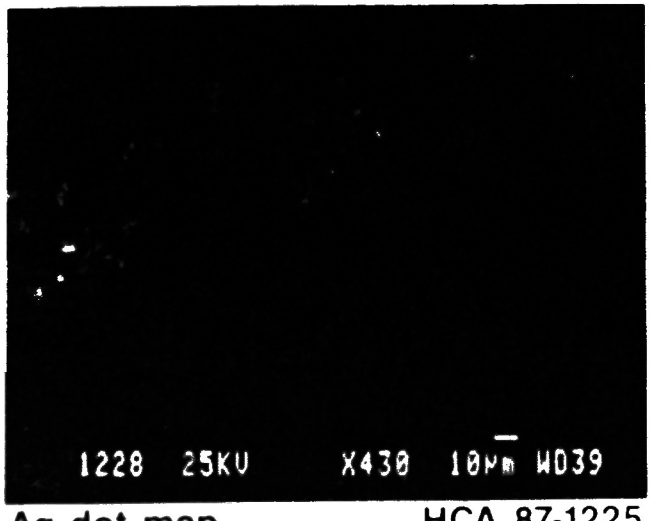

Ag dot map HCA 87-1225

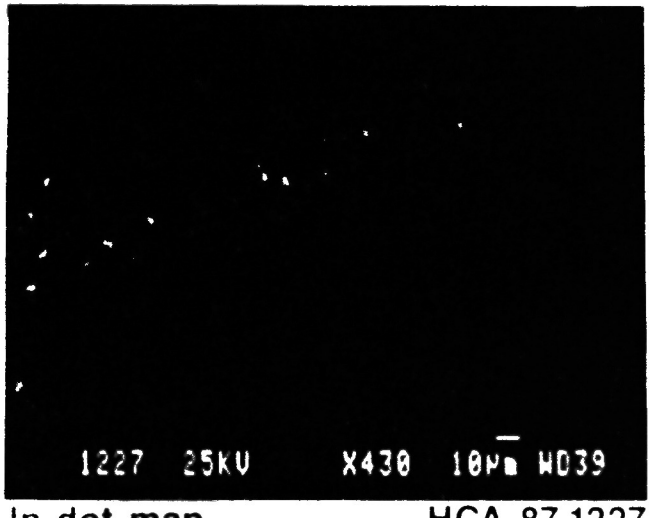

In dot map HCA 87-1227

Figure 17. (Continued)

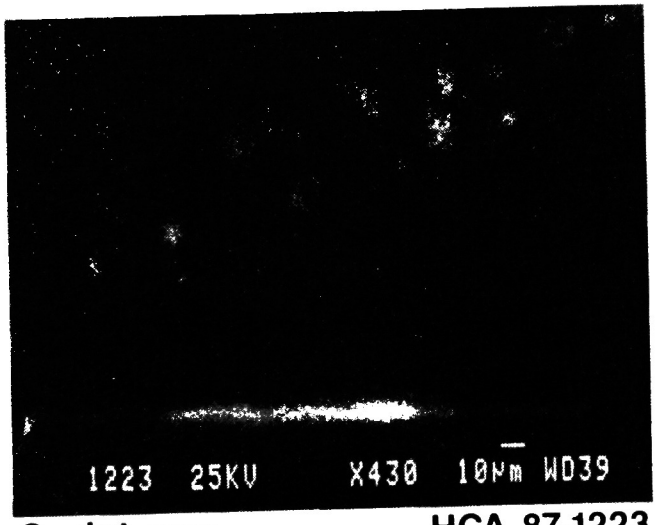

Cr dot map HCA 87-1223

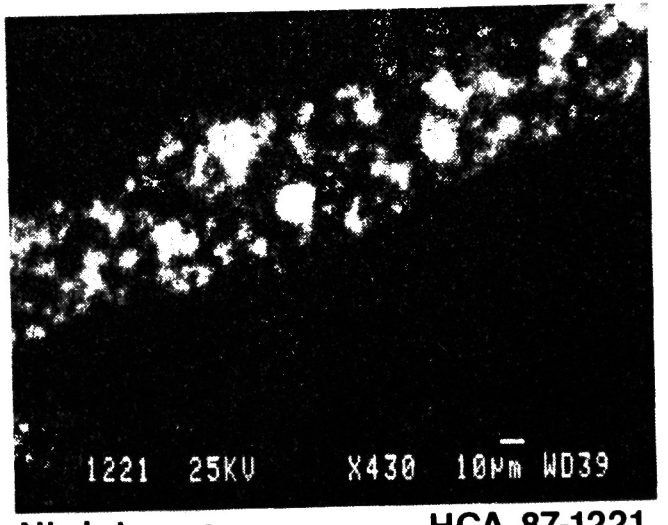

Ni dot map HCA 87-1221

Figure 17. (Continued)

composed of UO_2, with small amounts of ZrO_2 precipitates dispersed within the fuel. An example of these particles is shown in Figure 18, and in more detail in Figure 19. A backscattered electron image of these particles is also shown in Figure 20, and additional SEM images and dot maps are presented in Figures 21. These UO_2 particles precipitated from the metallic melt.

These data suggest that the lower crust was formed by the relocation of metallic melts from the upper regions of the core to cooler areas near the water level. The minimum peak temperature of the metallic melt is approximately 1220 K, based upon the formation of a zirconium-rich eutectic with iron and nickel. However, this minimum peak temperature is for a unique composition, and with the multitude of metallic phases that are present, it is very possible that temperatures were generally above this minimum temperature. Based upon the Zr-Ni, Zr-Fe, Zr-Cr, and Fe-Cr phase diagrams, it is reasonable to assume that many regions of the metallic melt solidified at temperatures up to several hundred degrees above the 1220 K minimum peak temperature, probably in the range of 1300-1500 K. The lack of any significant dissolution of the intact fuel pellet stacks by the zirconium in the metallic melts suggests that peak temperatures were generally below 2200 K. The lack of any unoxidized zircaloy is probably due to interactions between the zircaloy and silver, nickel, and iron in the metallic melts. These reactions can proceed at minimum temperatures of approximately 1200 K, but they are much more rapid. In the case of silver much more zircaloy can be dissolved when temperatures are above approximately 1400 K. Based upon these observations, a best estimate of the temperatures in the lower crust would be approximately 1300-1500 K.

3.2.2 Lower Crust Bulk Composition

Elemental analyses were performed on dissolved microcores from sample locations in the lower crust. Analyses were performed for 17 elements that constitute the principal components of the TMI-2 core. For comparison purposes, Table 1 lists the average core composition of each of the core constituents and the average core composition of the TMI-2 core, including

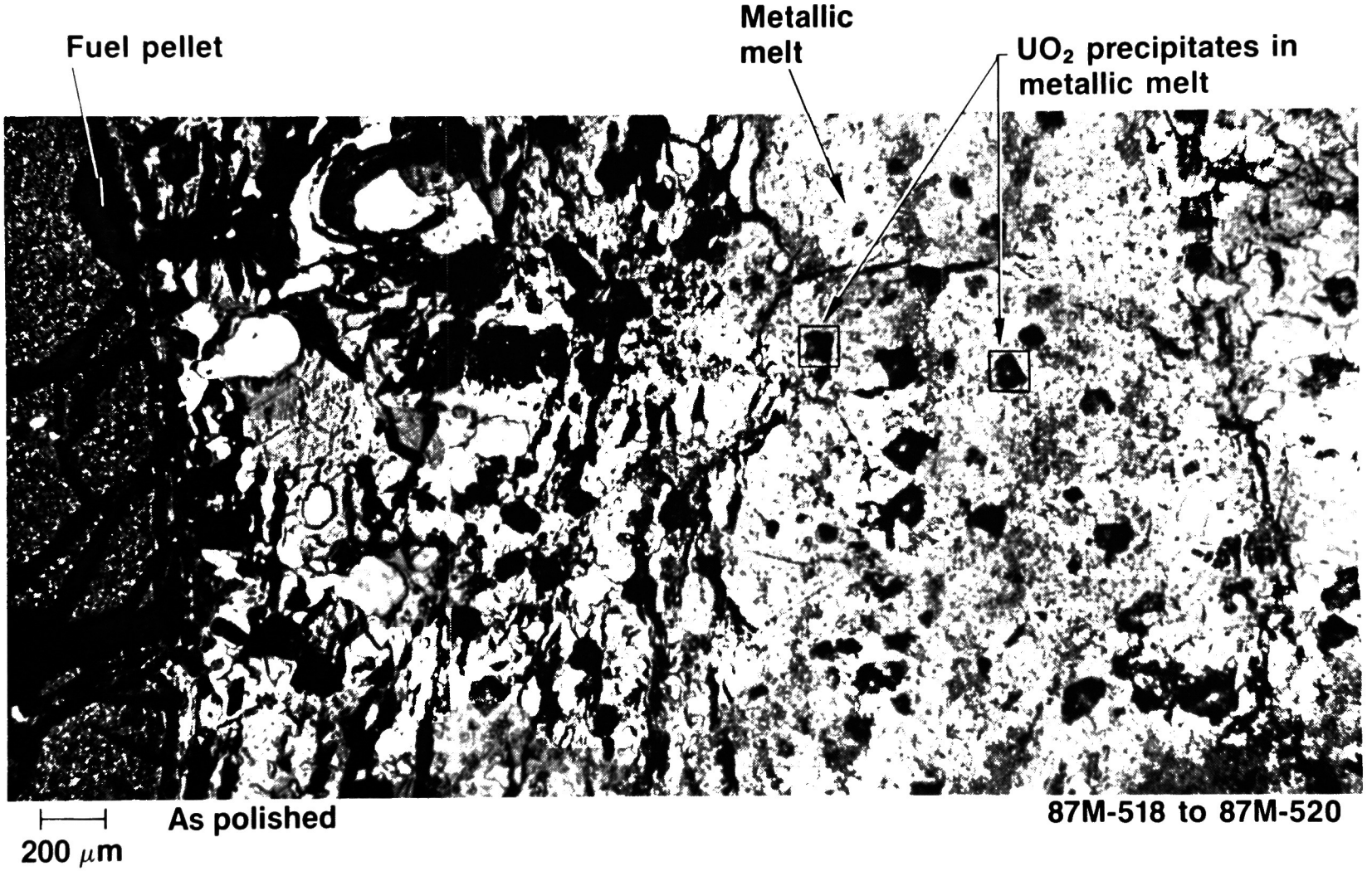

Figure 18. UO_2 precipitates in metallic melt in lower crust (K09-P1).

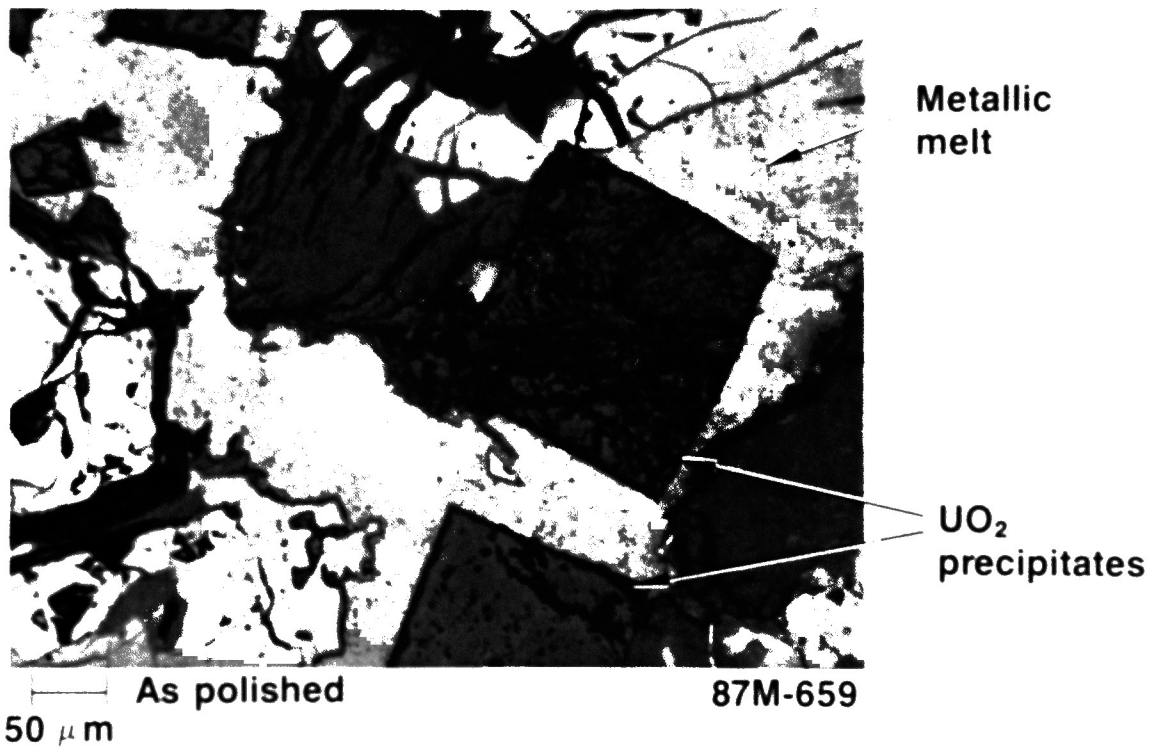

Figure 19. UO_2 precipitates in metallic melt in lower crust (K09-P1).

Figure 20. Backscattered electron image of UO_2 precipitates in metallic melt (K09-P1).

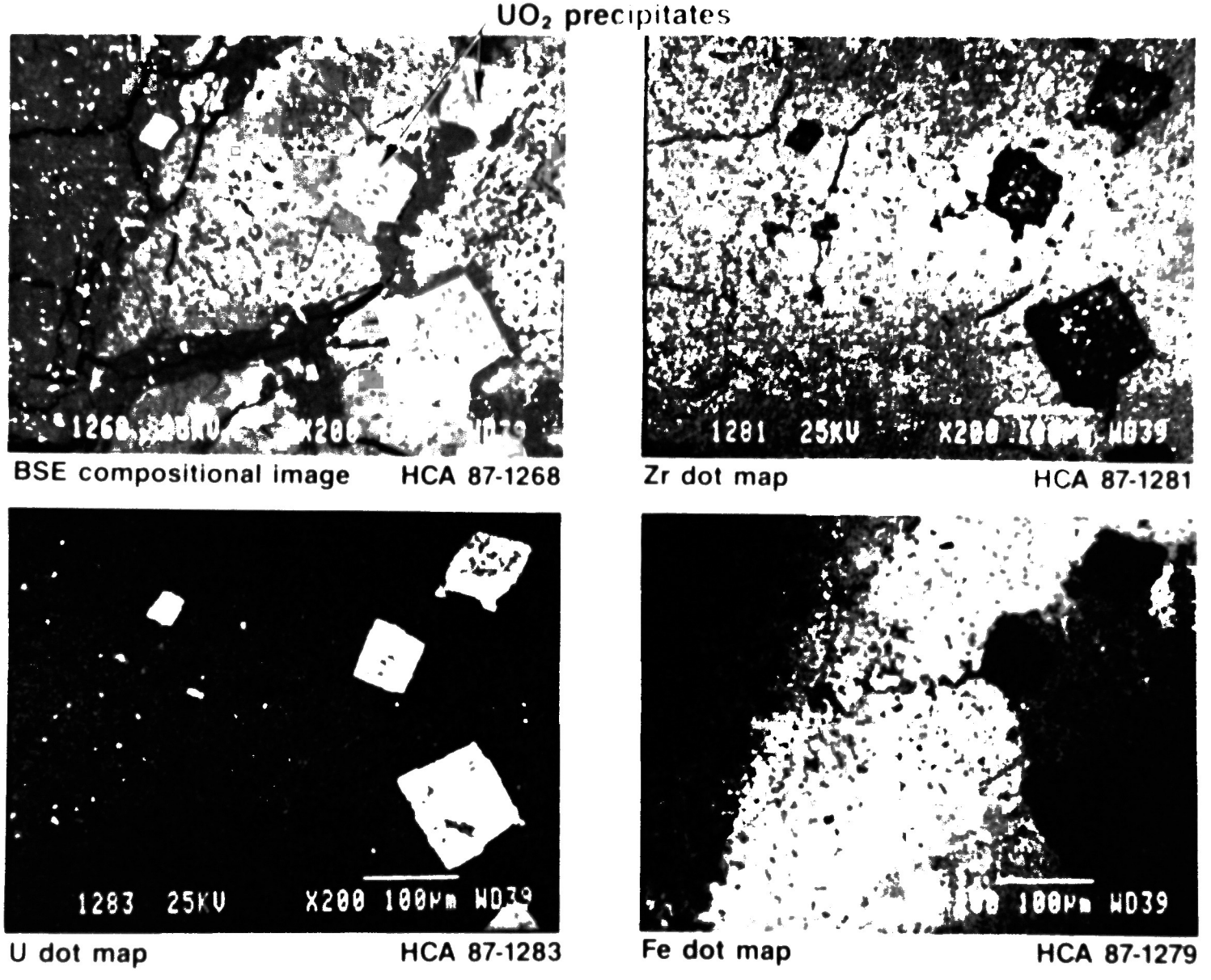

Figure 21. SEM analysis of UO_2 precipitates in metallic melt (K09-P1).

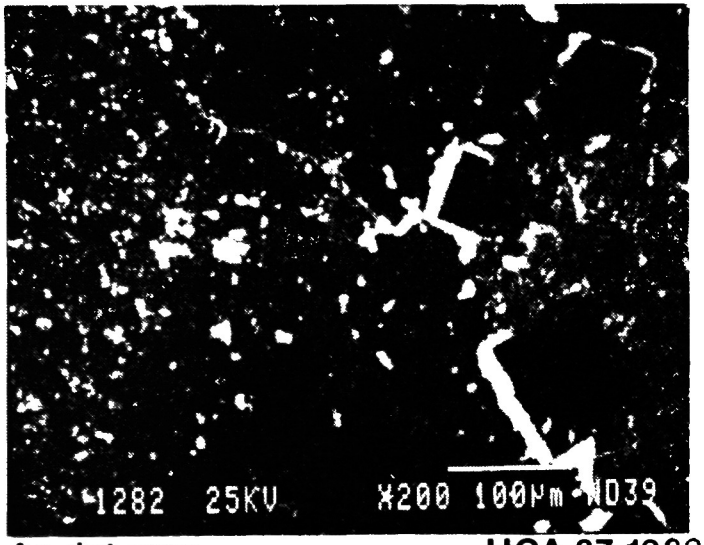

Ag dot map HCA 87-1282

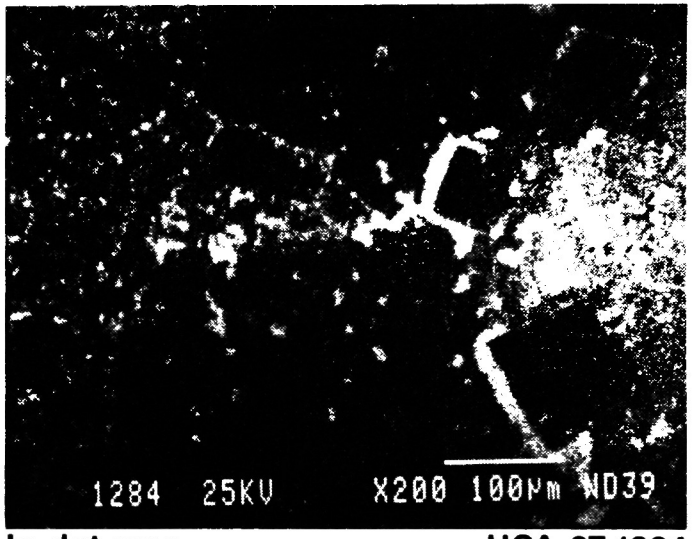

In dot map HCA 87-1284

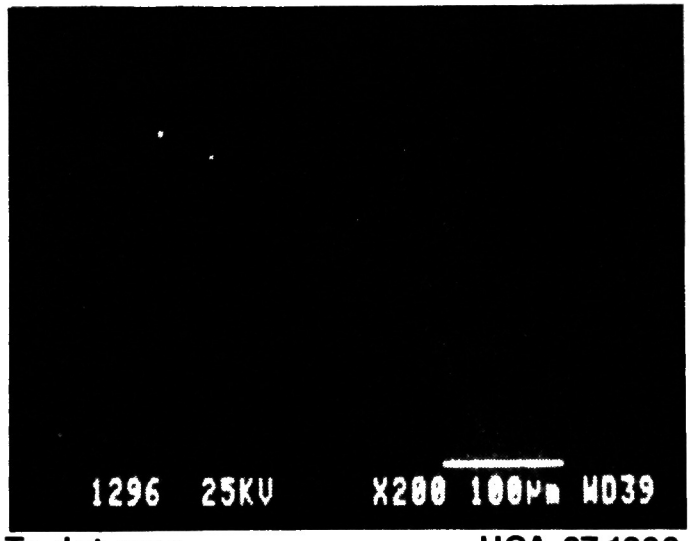

Tc dot map HCA 87-1296

Figure 21. (Continued)

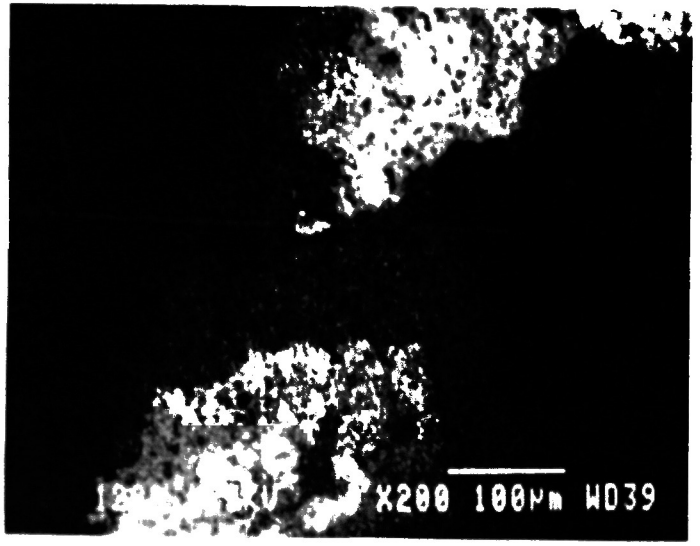

Cr dot map HCA 87-1280

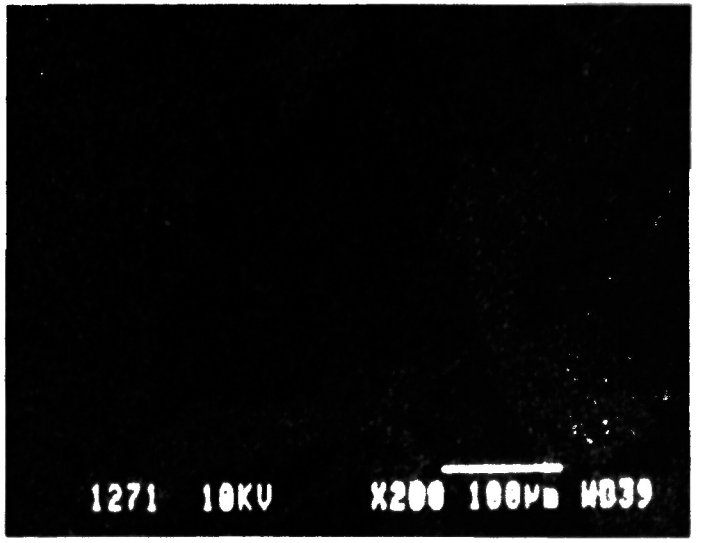

O dot map HCA 87-1271

Ni dot map HCA 87-1278

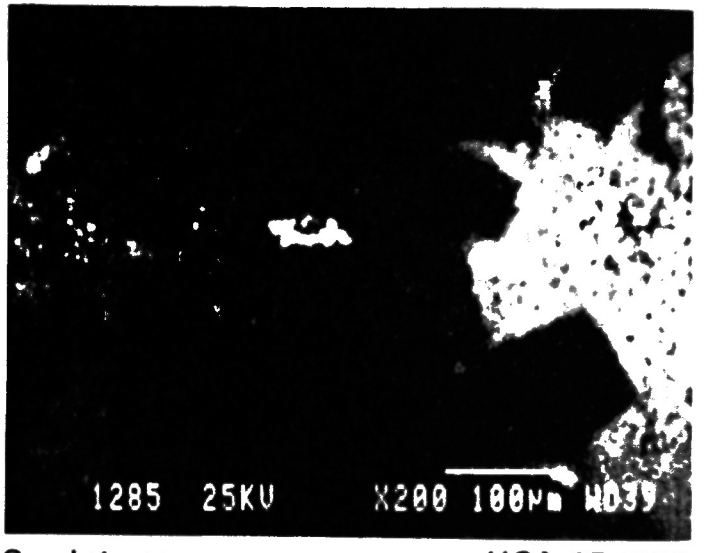

Sn dot map HCA 87-1285

Figure 21. (Continued)

the oxygen content of the uranium, but excluding the oxygen present from the oxidation of zircaloy and structural materials. Lower crust samples from two core locations (K09 and D08) were examined. The elemental data for these samples are listed in Appendix G, Tables G5 to G7.

K09-P1-C, a longitudinal cross section adjacent to the metallurgical sample, was obtained from the lower crust near the center of the core. Figure 22 shows the cross section and the locations sampled. Sample location No. 1 is located in the metallic region closer to the top of the crust, and sample locations No. 3 and No. 4 are located in the metallic material near the bottom crust. Sample location No. 2 is from a relatively intact fuel column that was surrounded by the metallic material. Examination of Table G5 indicates that the metallic region is composed principally of zirconium (37 to 44 wt%) with significant amounts of uranium (7 to 17 wt%), iron (5 to 10 wt%), nickel (4 to 5 wt%), silver (2 to 4 wt%), and smaller amounts of chromium, indium, and tin. The No. 2 location is composed of relatively intact fuel material (approximately 65% uranium) with zirconium (10 wt%), silver (2.3 wt%) and iron (1.8 wt%).

At the D08 core location, two samples of the lower crust were examined: D08-P1-C is a heterogeneous, longitudinal section adjacent to the metallurgical cross section, and D08-P2-A is a relatively homogeneous, longitudinal section. D08-P1-C is shown in Figure 23 and appears to be similar to K09-P1 with fuel rod sections surrounded by prior-molten metallic material. The elemental analysis data indicate that locations No. 1 and No. 3 in the metallic region are relatively homogeneous, and are composed principally of iron (28 to 34 wt%), nickel (13 to 14 wt%), and silver (6 to 10 wt%) with lesser concentrations of other constituents. This sample also contains zirconium at lower concentrations than K09-P1.

In the other longitudinal cross section, D08-P2-A (Figure 24), two samples were obtained: the center of the crust (No. 1) and near the lower periphery of the crust (No. 2). The composition is similar in both cases with the principal components being uranium (52 to 60 wt%) and zirconium

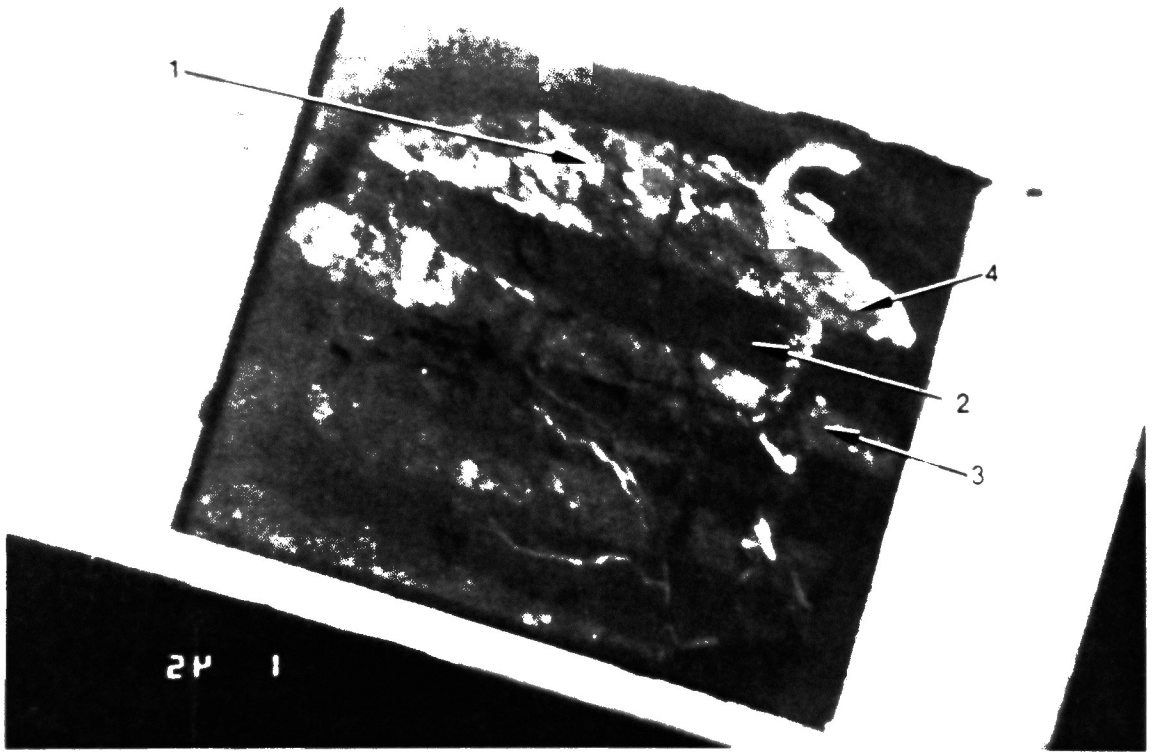

Figure 22. K09-P1-C sampling locations.

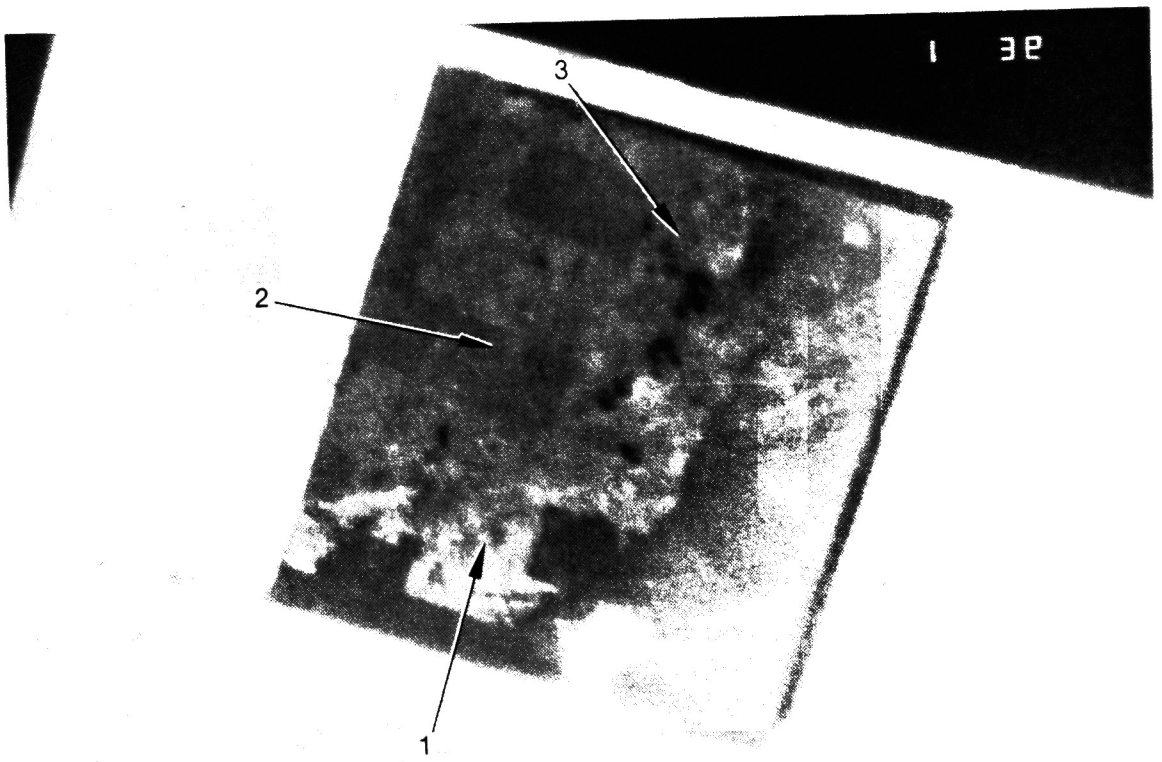

Figure 23. D08-P1-C sampling locations.

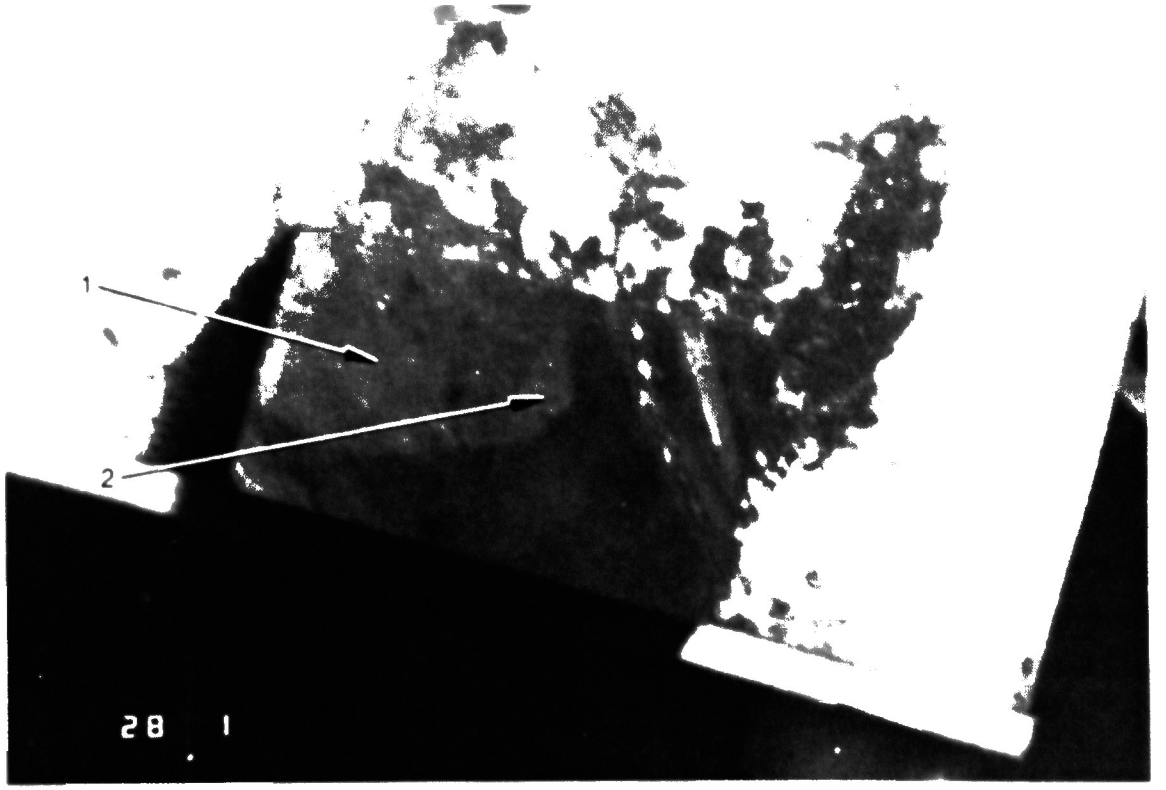

86-614-2-33

Figure 24. D08-P2-A sampling locations.

(8.6 to 18 wt%) with lesser amounts of silver (1.1 to 5 wt%) and iron (2.2 to 2.9 wt%). The data indicate significant differences between this crust sample and D08-P1-C; however, there are significant amounts of control material located in both crust samples.

Table 17 lists the average composition and range of compositions for the lower crust samples. The average uranium content is biased high by the samples of intact fuel columns. The lower crust based upon these data can be considered to be principally zirconium and structural materials with some uranium surrounding relatively intact fuel columns. These data should be treated cautiously due to the high degree of heterogeneity between the metallic and ceramic phases.

3.2.2.1 Uranium Fuel and Zircaloy Cladding. The fuel material (uranium) concentrations in the lower crust have a range from 2.6 to 88 wt%, as indicated in Table 17. However, if the samples from the fuel column locations (i.e., K09-P1 No. 2, D08-P1-C No. 2, and D08-P2-A No. 1 and No. 2) are excluded, the range is 2.5 to 17 wt%. For zirconium, the data from the crust region range from 9 to 44 wt%, and the average is 22 wt%, which indicates that zirconium is enhanced in the lower crust relative to the core average concentration of 18. If only the samples from the melt surrounding K-09 are considered, the average zirconium content is 40 wt%, which would indicate that zirconium is the major constituent of the melt. The remaining constituents of the material that flowed down from the lower crust are primarily iron, nickel, indium, chromium, and silver. These data suggest that metallic zirconium formed low melting alloys with other structural materials and relocated downward before finally cooling at locations in the lower crust.

Table 18 lists the U/Zr and Zr/Sn ratios in the lower crust samples. In the metallic region samples, the U/Zr ratios range from 0.19 to 0.47, which indicates a factor of 10 higher concentrations of zirconium relative to the uranium present.

TABLE 17. LOWER CRUST AVERAGE COMPOSITION[a]
(wt%)

Element	Average Composition[b]	Range[c]
Ag	4.5	1.13 - 10.4
Al	1.1	0.14 - 6.4
B	0.10	0.05 - 0.26
Cd	0.07	0.01 - 0.12
Cr	1.6	0.31 - 4.1
Cu	0.11	0.05 - 0.25
Fe	11	1.76 - 34
Gd	0.40	0.02 - 2.92
In	1.1	0.28 - 13.7
Mn	0.04	0.01 - 0.07
Mo	0.34	0.06 - 1.14
Nb	0.14	0.05 - 0.21
Ni	5.5	0.52 - 13.7
Si	0.42	0.09 - 1.11
Sn	1.5	0.25 - 3.1
Te	0.05	0.11 - 0.07
U	34.0	2.6 - 87.9
Zr	22.0	8.6 - 44.5

a. This table represents the average of the examination results obtained from the lower crust; however, due to the heterogeneity of the material and the small number of samples examined, these data must be used with caution.

b. The average concentration is calculated using only real values and is averaged without zero values.

c. Values below analytical detection limit not included in range.

TABLE 18. LOWER CRUST FUEL MATERIAL (U, Zr, Sn) WEIGHT RATIOS

Sample ID	U/Zr Ratio[a]	Zr/Sn Ratio[b]
K09-P1-C		
No. 1[c]	0.39	31
No. 2	6.0	41
No. 3[c]	0.19	24
No. 4[c]	0.35	22
D08-P1-C		
No. 1[c]	0.23	3.7
No. 2	6.4	19
No. 3[c]	0.47	4.7
D08-P2-A		
No. 1	2.9	12
No. 2	6.9	28

a. The core average U/Zr ratio is 3.7, and the ratio for a fuel rod is 4.0.

b. The average Zr/Sn ratio in zircaloy cladding is 61.

c. Principally metallic samples (<20 wt% U).

In both the metallic samples, there are significant amounts of both zirconium and tin (constituents of the fuel cladding). The Zr/Sn ratios at all sample locations in the melt are less than the core average ratio which suggests the accumulation of tin in these sample locations relative to zirconium and particularly at the two D08-P1-C locations. These data suggest that tin is not transported with the zirconium and that it may tend to form accumulations separate from the zirconium. The SEM examinations support this hypothesis in which tin accumulation is localized in a region containing indium.

3.3.2.2 Control Rod Materials. Control rod materials, including the relatively volatile cadmium, were measurable in most of the lower crust samples. Examination of the data in Tables G5 to G7 and I7 indicates that the least volatile control material, silver, was measurable in all samples at an average concentration of about 4.5 wt%, with a range of concentrations from 1.1 to 10.4 wt%. Although some silver may have precipitated during the analysis, given the sum of the weight percents of the constituents in Tables G5 to G7 and oxidation of the uranium and other probable oxides, the silver content could not increase more than approximately 10 - 15 wt%. These concentrations are all greater than the core average concentration of silver (1.9 wt%), which indicates that this element accumulated in the lower crust.

Indium was measurable in all samples at concentrations averaging 1.1 wt% with the bulk of data ranging from 0.3 to 1.9 wt%. The core average concentration of indium is 0.3 wt%, which indicates that this element is found in the lower crust at concentrations up to 6 times the core average concentrations.

Cadmium was measurable in eight of the nine samples obtained from the lower crust. The concentrations ranged from 0.01 to 0.12 wt%, with an average concentration of about 0.07 wt%. This concentration is less than the core average concentration of 0.12 wt%. The presence of cadmium (boiling point 1040 F) in these samples suggests that the cadmium could

not be volatilized, but was retained to a large extent due to alloying and relocation to cooler portions of the core.

Table 19 presents the ratios among the control rod materials measured in the lower crust samples. The Ag/In ratio ranged from 2 to 6 wt% for both metallic and ceramic samples with the exception of D08-P2-A No. 1, which is a factor of 3 higher than the intact control rod value of 5.3. The average of the Ag/In ratios (excluding D08-P2-A No. 2) is 3.6, which indicates that indium is concentrated in the lower crust relative to silver, although this may be an artifact of the precipitation of silver during the analysis. These data are relatively consistent for all samples and a wide range of concentrations.

The Ag/Cd ratios vary over a range of a factor of 5. The ratios are greater than those found in intact control rods by factors greater than 2, indicating that the cadmium has been partially lost from the debris relative to silver. This is particularly apparent for sample D08-P2-A No. 1, where the ratio is 390. The data for In/Cd are consistent with the Ag/Cd data and again indicate loss of the cadmium in the debris relative to indium.

3.2.2.3 Poison Rod Materials. Poison rod materials measurable in the lower crust included aluminum, boron, and gadolinium. Aluminum was measurable in all samples at concentrations averaging 1.1 wt%, which is greater than the core average concentration of 0.2 wt%. However, this average is biased by sample D08-P1-C No. 1, which has an aluminum concentration of 6.4 wt%. Excluding this sample, the average is 0.4 wt%, which is much nearer the core average concentration of 0.2 wt%. The high concentration in D08-P1-C suggests that this sample came from a poison assembly.

Boron from the poison rods and reactor coolant is present in most samples at concentrations between 0.05 and 0.26 wt%. Gadolinium is also present in the lower crust in a range of concentrations from 0.02 to

TABLE 19. LOWER CRUST CONTROL MATERIAL (Ag, In, Cd) WEIGHT RATIOS

Sample ID	Ag/In Ratio[a]	Ag/Cd Ratio[b]	In/Cd Ratio[c]
K09-P1-C			
No. 1[d]	2.0	57	29
No. 2[d]	3.0	115	38
No. 3	3.6	37	10
No. 4[d]	2.6	26	10
D08-P1-C			
No. 1[d]	6.0	88	15
No. 2	4.1	52	13
No. 3[d]	3.3	76	23
D08-P2-A			
No. 1	18	390	21
No. 2	3.9	--[e]	--[e]

a. The average Ag/In ratio is in a control rod is 5.3.

b. The average Ag/Cd ratio in a control rod is 16.

c. The average In/Cd ratio in a control rod is 3.0.

d. Principally metallic samples.

e. A component of the comparison was below the detection limit of the analysis method.

2.9 wt% with an average of 0.4 wt%. This concentration is greater than the average concentration of 0.01 wt%, which suggests significant accumulation of gadolinium in the lower crust. The principal source of this high average concentration is sample D08-P2-C with a high gadolinium concentration of 2.9 wt%. The presence of relatively intact poison materials is indicated at the D08 core location, a control rod assembly location in the original core configuration.

3.2.2.4 Structural Materials. Measurements were made for all structural material constituents in the core (i.e., iron, chromium, nickel, manganese, niobium, and molybdenum). The average concentration data in Table 17 indicates that iron is the principal structural material present (average 11 wt%), and that it ranges up to 34 wt% in the metallic regions of the crust. Lesser concentrations of nickel (average - 5.5 wt%) and chromium (average - 1.6 wt%) are also present. All these elements have accumulated in the lower crust in concentrations exceeding the core average.

Examination of the ratio data for the principal components of the metallic crust (Table 20) indicates that Fe/Cr ratios are greater than those found in stainless steel and Inconel, and that the Fe/Ni ratios are between the stainless steel and Inconel ratios. The presence of significant amounts of molybdenum in the lower crust at ratios approximately 0.75 times those for Inconel suggests that the crust was formed to a significant extent from the Inconel grid spacers as well as some stainless steel components.

3.2.3 Lower Crust Radiochemical Examinations

The radionuclide distribution in the lower crust was determined for the samples discussed in Section 3.2.2. Results of the radiochemical analysis of the samples are listed in Appendix H, Tables H1 and H3. To provide information on the characteristic behavior of fission products, they have been categorized by the volatility of the chemical group and element, as discussed in Section 3.1.3.

TABLE 20. LOWER CRUST METALLIC MATERIAL (Fe, Cr, and Ni) WEIGHT RATIOS[a]

Sample ID	Fe/Cr Ratio	Fe/Ni Ratio	Ni/Cr Ratio	Ni/Mo Ratio
K09-P1-C				
No. 1	5.0	2.1	2.4	13
No. 2	5.7	1.7	3.4	12
No. 3	5.0	1.5	3.3	21
No. 4	4.9	2.0	2.4	13
D08-P1-C				
No. 1	8.4	2.5	3.4	--[b]
No. 2	8.1	2.5	3.2	10
No. 3	8.7	2.2	4.0	11
D08-P2-A				
No. 1	6.3	0.50	12	--[b]
No. 2	5.1	4.2	1.2	9.0

a. The elemental ratios for stainless steel and Inconel are:

	Stainless Steel	Inconel
Fe/Cr	3.6	0.35
Fe/Ni	7.6	0.35
Ni/Cr	0.5	2.7
Ni/Mo	--	17.3

b. Component not detected.

Table 21 lists the average radionuclide concentrations, the range of values, and the ratio of the high and low concentrations. The ratios of high to low concentrations are from 10^1 to 10^3, indicating a relatively wide range of radionuclide concentrations; however, the radionuclides with high/low concentration ratios greater than 10^2 are the more volatile species (i.e., ^{129}I and ^{137}Cs), the metallic species (^{106}Ru), and surprisingly, the relatively stable ^{90}Sr. The large range of concentrations is partially due to the differing compositions of the two regions in the crust and the apparent segregation of some fission products in the crust, as will be discussed in a following section.

3.2.3.1 Lower Crust Uranium-235 Enrichment. Measurements were performed to evaluate the concentrations of ^{235}U and ^{238}U in the lower crust and to determine ^{235}U enrichment in the crust. The ^{235}U and ^{238}U concentrations are listed in Appendix H and the ^{235}U enrichments are listed in Table 22. These measurements should be treated with some caution, as the technique used for the measurements is affected by the presence of control materials, which may result in measured concentrations lower than actual for those samples with high control material content. Table 22, which summarizes the ^{235}U data, indicates a range of enrichments from 1.8 to 2.4. However, the bulk of the data is in the range from 1.8 to 2.0, suggesting that the lower crust debris samples are mostly composed of the 1.98% enriched assemblies (assembly locations K09 and D08 had original enrichments of 1.98%). The data from the samples identified in Table 22 would suggest that uranium present in the 1.98% enriched assemblies remained at those locations in the reactor core and mixed with metallic structural and control materials before relocating to form the lower crust.

3.2.3.2 Comparisons with ORIGEN2. The measured radionuclide concentrations in the lower crust were compared with concentrations predicted by the ORIGEN2 code in order to assess retention of radionuclides in the ceramic and metallic regions of the lower crust. The ORIGEN2 data and analysis methods are discussed in Section 3.1.3, and Table 14 lists the ORIGEN2 values used for comparison with the analysis results.

TABLE 21. LOWER CRUST AVERAGE RADIONUCLIDE CONCENTRATIONS
(microcuries/g sample on April 1, 1987)

Radionuclide	Average	Range	High/Low Ratio[b]
^{60}Co	553	34 to 1871	55
^{90}Sr	3100	14 to 7040	500
^{106}Ru	609	72 to 1744	24
^{125}Sb	495	0.3 to 1330	4400
^{129}I	8.00 E-4	3.4 E-5 to 4.6 E-3	135
^{134}Cs	32	1.6[a] to 123	77
^{137}Cs	1150	15 to 5300	353
^{144}Ce	127	11[a] to 238	22
^{154}Eu	28	2.7[a] to 50	18
^{155}Eu	37	3.6[a] to 64	18

a. Detection limit value not included in range.

b. High value divided by the low.

TABLE 22. LOWER CRUST URANIUM-235 ENRICHMENT

Sample ID	^{235}U Enrichment[a]
K09-P1-C	
No. 1[b]	2.4
No. 2	3.4[c]
No. 3[b]	1.8
No. 4[b]	--[d]
D08-P1-C	
No. 1[b]	--[d]
No. 2	1.8
No. 3[b]	1.8
D08-P2-A	
No. 1	--[d]
No. 2	2.0

a. The core average ^{235}U enrichment is approximately 2.56% with the peripheral assemblies having an enrichment of 2.98 and the central assemblies having enrichments of 1.98% and 2.64%.

b. Less than 30% U content.

c. Large uncertainty (>50%) associated with value.

d. Not measured or not detected.

A summary of the measured radionuclide retentions (based on uranium content) in the lower crust is provided in Table 23. These data indicate a wide range of retentions, principally for the more volatile or metallic radionuclides. The low volatile radionuclides (^{144}Ce and ^{154}Eu) generally have similar retentions from 130 to 202%, which suggests that much of the lower crust was formed from fuel material from a relatively high burnup region closer to the center of the reactor core. The following sections discuss the radionuclide distributions for the principal low, medium, and high volatility radionuclides.

3.2.3.3 Low Volatiles. The low volatiles for which radionuclide comparisons were performed are ^{144}Ce and ^{154}Eu. The average retentions for the ceramic and metallic regions are between 130 and 134%, and the high concentrations (i.e., >100% retentions) indicate that the fuel material forming the lower crust has a relatively high burnup. Comparisons with the fuel column samples (e.g., K09-P1-C No. 2) indicates similar burnup for all of the high burnup samples. The lower cerium and europium retentions (i.e., samples K09-P1-C No. 1 and D08-P1-C No. 1) are from samples with low uranium content, 17.4% and 2.65%, respectively. Apparently, some low volatile release occurred from these samples that had a large metallic constituent. Why the apparent release occurred from these samples is not known.

3.2.3.4 Medium Volatiles. The fission products that are expected to have a medium volatility are ^{90}Sr, ^{125}Sb, and ^{106}Ru. The ^{90}Sr data shown in Tables 23 and 24 indicate a wide range of concentrations, especially for the principally metallic samples. The data in Table 24 indicate similar average ^{90}Sr retentions for both the metallic and ceramic samples. The bulk of the ^{90}Sr was apparently retained in the ceramic samples with some relocation to the metallic regions.

Both ^{125}Sb and ^{105}Ru have accumulated in the metallic samples at concentrations ranging up to 40 and 54 times the core average concentrations for ^{125}Sb and ^{106}Ru, respectively. The sample with the highest metallic

TABLE 23. RADIONUCLIDE RETENTION IN THE LOWER CRUST[a]

Sample ID	Radionuclide Retention(%)						
	^{90}Sr	^{106}Ru	^{125}Sb	^{129}I	^{137}Cs	^{144}Ce	^{154}Eu
K09-P1-C							
No. 1[b]	10.0	226	141	23.4	1.46	25.1	33.6
No. 2	145	18.4	14.9	282	91.0	159	183
No. 3[b]	133	93.9	347	17.5	56.4	--[c]	--[c]
No. 4[b]	287	541	925	6.94	14.0	202	228
D08-P1-C							
No. 1[b]	38.4	5400	3970	321	14.8	57.1	--[c]
No. 2	77.4	27.8	0.032	42.1	47.6	173	121
No. 3[b]	2.57	2480	1390	95.8	48.4	170	203
D08-P11-A							
No. 1	109	67.7	88.8	10.6	0.30	170	146
No. 2	134	20.1	13.1	55.9	1.15	133	146

a. Retention is calculated based on the uranium content of the sample material as determined from the elemental analysis results in Appendix G. Additional figures are shown beyond those statistically appropriate for calculational purposes. The uranium concentrations used for normalization in wt% were:

K09-P1-C -- No. 1 - 17.4; No. 2 - 60.3; No. 3 - 7.2; No. 4 - 14.2
D08-P1-C -- No. 1 - 2.65; No. 2 - 87.9; No. 3 - 6.57
D08-P2-A -- No. 1 - 52.5; No. 2 - 59.6

b. Contains significant amounts of metallic material (>30%).

c. Not detected.

TABLE 24. RADIONUCLIDE RETENTION IN METALLIC AND CERAMIC SAMPLES

Radionuclide	Metallic Samples[a] Average	Metallic Samples[a] Low/High	Ceramic Samples[b] Average	Ceramic Samples[b] Low/High
^{90}Sr	94	2.6 - 290	117	77 - 145
^{106}Ru	1750	93 - 5410	34	18 - 68
^{125}Sb	1360	41 - 3970	29	0.03 - 88
^{129}I	93	6.9 - 321	98	11 - 283
^{137}Cs	27	1.4 - 56	35	0.3 - 91
^{144}Ce	134	25 - 203	130	57 - 170
^{154}Eu	131	33 - 228	149	121 - 184

a. Nominal metallic samples are K09-P2-C No. 1, No. 2, No. 3, and G08-P11-E No. 1.

b. Nominal ceramic samples include all other samples in the upper crust, although there is some metallic material in all samples that may bias the results.

material content was sample D08-P1-C No. 1 at approximately 70% metallic. The normalized retention for this mostly metallic sample is by far the highest in the lower crust. The measurement data indicate significantly lower concentrations of ^{125}Sb in the ceramic region. The correlation between metallic constituents of the sample material and ^{125}Sb concentrations are discussed in Section 4.

3.2.3.5 High Volatiles. The two high volatile radionuclides measurable were ^{137}Cs and ^{129}I. Iodine-129 was measurable in most samples at concentrations lower than those found in intact fuel material. Comparison of the ^{144}Ce retention data (159%) for K09-P1-C No. 2 with the iodine retention data (282%) suggests that radioiodine may have been retained or trapped to a slight extent in the cooler portion of the molten pool.

The D08-P1-C metallic samples have iodine retentions at higher levels than those expected based on the ^{144}Ce content of the material. Sample No. 1, the highest retention, was obtained from near the bottom of the crust with high retentions for prior molten fuel at all sample locations. No explanation is apparent for the retention of these relatively low concentrations of iodine in the crust.

The ^{137}Cs concentrations shown in Tables 23 and 24 indicate lower relative retentions than those of ^{129}I for both the metallic and ceramic samples, and no apparent correlation between the retentions of the two radionuclides. The data for the ceramic sections suggests only limited retention of cesium at any location in the crust and at significantly lower concentrations than ^{129}I in the primarily metallic samples.

3.3 Peripheral Crust Examination Results

The peripheral crust was identified as a part of the top crust from mid-radius to near the edge of the core. The peripheral crust had different characteristics than the upper crust, which was characterized by the materials behavior near the center of the core. For the peripheral crust samples, information obtained from the visual and metallurgical examinations is summarized in the following section. This summary was extracted from the visual examinations presented in Appendix C, the density measurements described in Appendix D, the metallographic examinations explained in Appendix E, and the autoradiographic results listed in Appendix F. The bulk elemental and radiochemical analysis results are summarized in Sections 3.3.2. and 3.3.3.

3.3.1 Visual and Metallurgical Examinations

Two samples were obtained from the peripheral crust regions at core bore locations G12 and 007. Samples G12-P1 and 007-P4 were both 5.1 cm long and ranged in density from 7.6 to 8.8 g/cm^3. Typical microstructures in the G12 peripheral crust region are shown in Figures 25 and 26. These photomicrographs display a $(U,Zr)O_2$ matrix containing extensive porosity and a eutectic phase with a mottled appearance. SEM dot maps of this mottled phase, described in detail in Appendix E, identified it as being primarily composed of iron, chromium, nickel, and oxygen.

Figure 27 shows a cross section through sample 007-P4. This sample contained relatively large amounts of metallic melts, and metallographic examinations detailed in Appendix E revealed that these metallic melts were largely composed of immiscible Ag In and Fe-Cr-Ni melts.

These examinations indicate a relatively thin crust composed of a mixture of ceramic $(U,Zr)O_2$ melt and immiscible metallic melts, similar to samples from the upper crust. The density and thickness of this material were also comparable to that found in the upper crust.

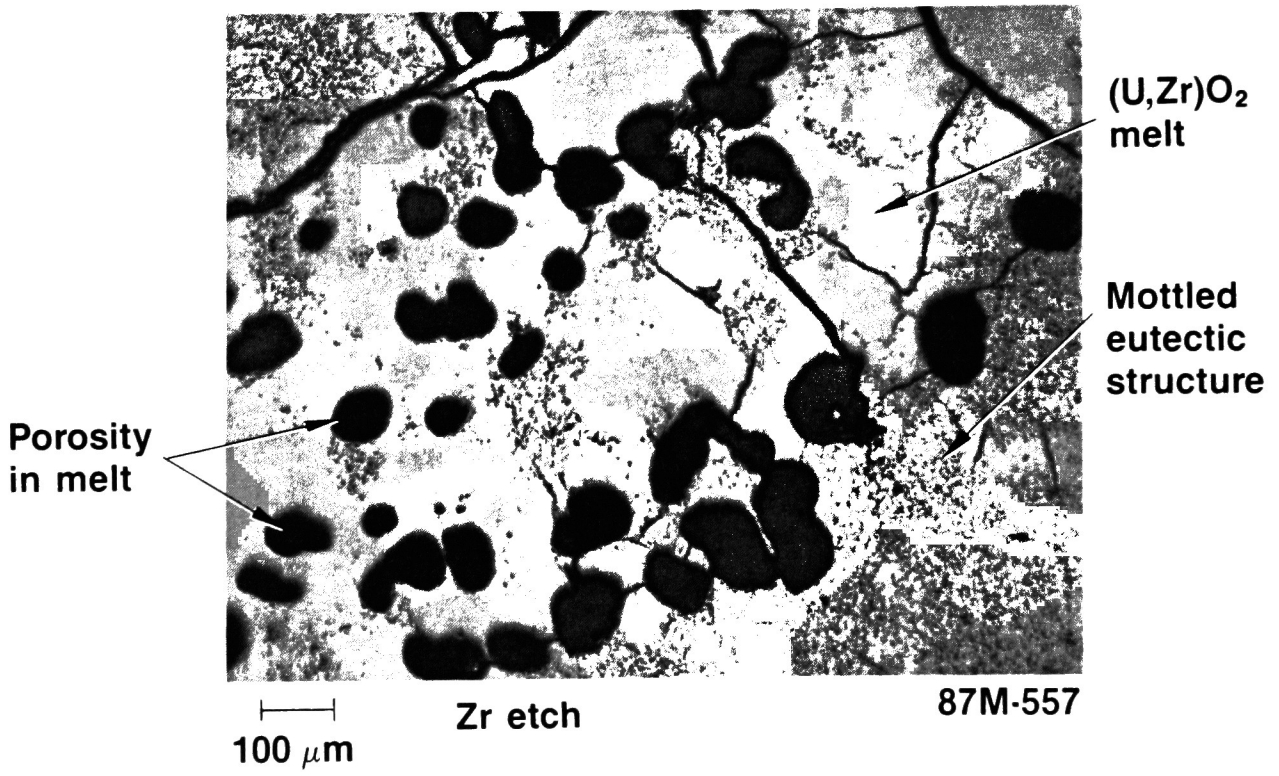

Figure 25. Morphology of ceramic melt in peripheral crust (G12-P1).

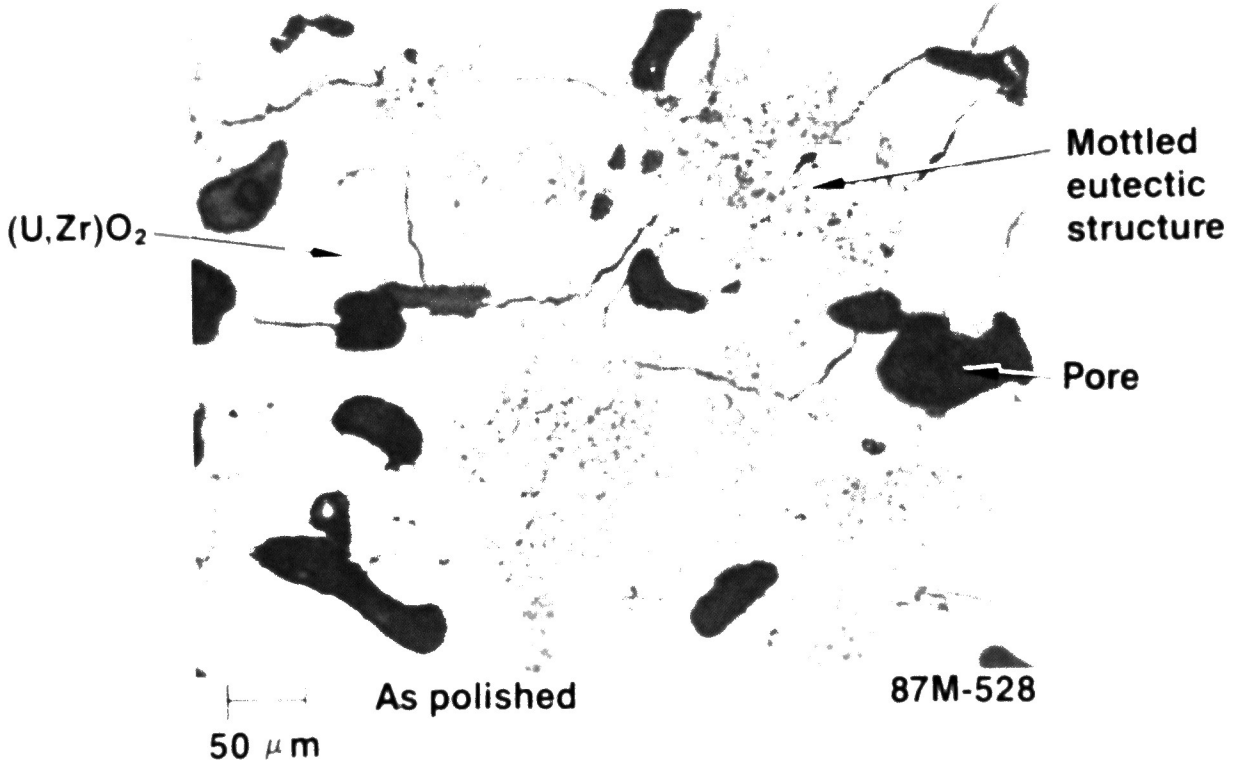

Figure 26. Mottled structure in ceramic melt of peripheral crust (G12-P1).

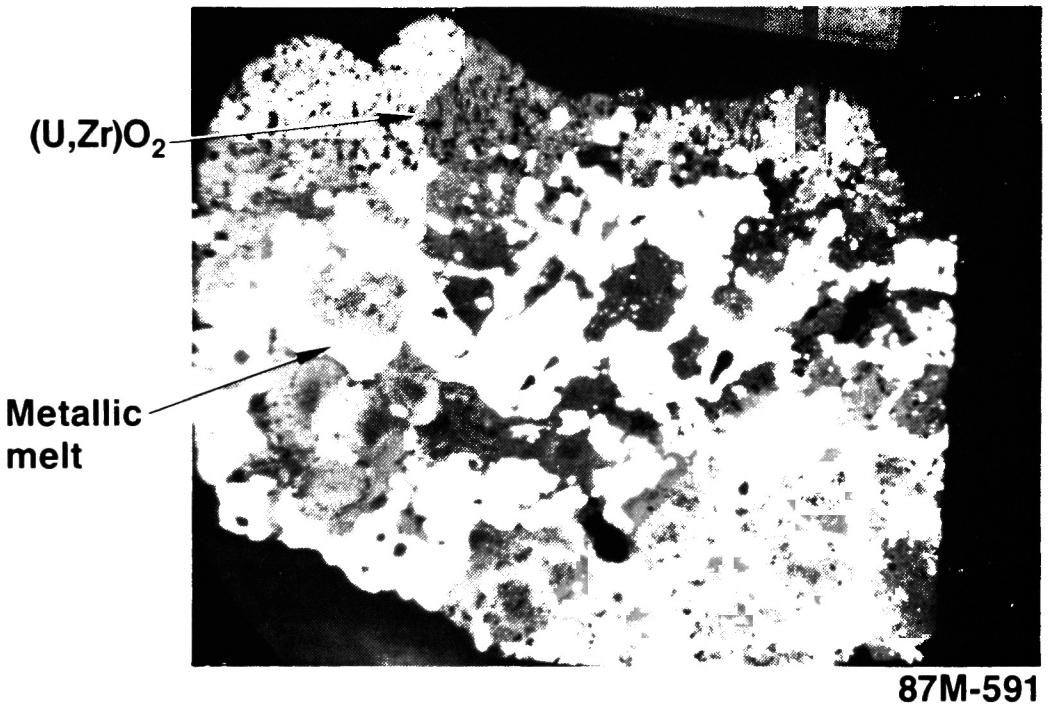

Figure 27. Longitudinal cross section through peripheral crust sample 007-P4.

3.3.2 Peripheral Crust Bulk Composition

Elemental analyses were performed on dissolved microcores from sample locations in the side or peripheral crust. Analyses were performed for 17 elements that constitute the principal components of the TMI-2 core. For comparison purposes, Table 1 lists the average core composition of each of the core constituents and the average core composition of the TMI-2 core. Two core locations in the peripheral crust (007 and G12) were examined. The elemental data for these samples are listed in Appendix G, Tables G8 to G10. Sample 007-P4-C is a longitudinal cross section, and the locations sampled are shown in Figure 28. Samples No. 1 and No. 2 are located in the metallic and ceramic regions close to the top of the crust, respectively. Samples No. 3 and No. 4 are, respectively, from ceramic regions near the midpoint and bottom of the crust. Examination of Table G8 indicates that the metallic region (Sample No. 1) is composed principally of iron (29 wt%) and zirconium (17 wt%) with nickel (13 wt%), silver (6.9 wt %), and other structural materials. Location Nos. 2, 3, and 4 are composed principally of uranium (53 to 66 wt%) and zirconium (4 to 17 wt%) with lesser amounts of structural materials and silver (1.9 to 5.4 wt%).

At the G12 core location, two samples of the upper crust were examined: G12-P1-E is a heterogeneous, longitudinal section and G12-P1-D2 is a relatively homogeneous, transverse, partial disk section. Sample G12-P1-E had samples removed from near the top of the crust (No. 2), at midpoint (No. 3), and from near the bottom of the crust (No. 4). The elemental analysis data indicate that location No. 2 in the metallic region is composed principally of zirconium (23 wt%) and iron (18 wt%) with lesser amounts of uranium (14 wt%) and silver (7.4 wt%), similar to the metallic part of 007. The ceramic sample locations (Nos. 3 and 4) are composed principally of uranium (49 to 54 wt%) and zirconium (18 to 19 wt%), and insignificant quantities of other constituents.

In the transverse cross section, G12-P1-D2 (Figure 29), two samples were obtained: the center of the crust (No. 1) and near the lower periphery of the sample (No. 2). There appears to be a greater degree of porosity at

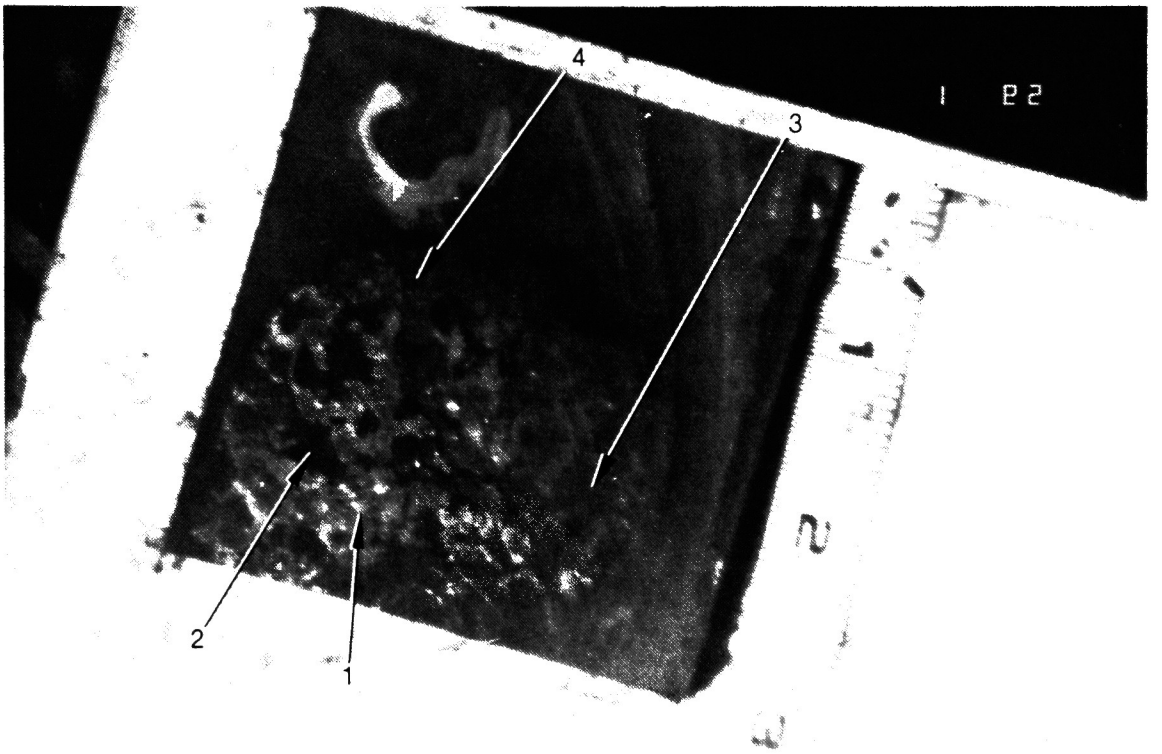

86-614-2-13

Figure 28. 007-P4-C sampling locations.

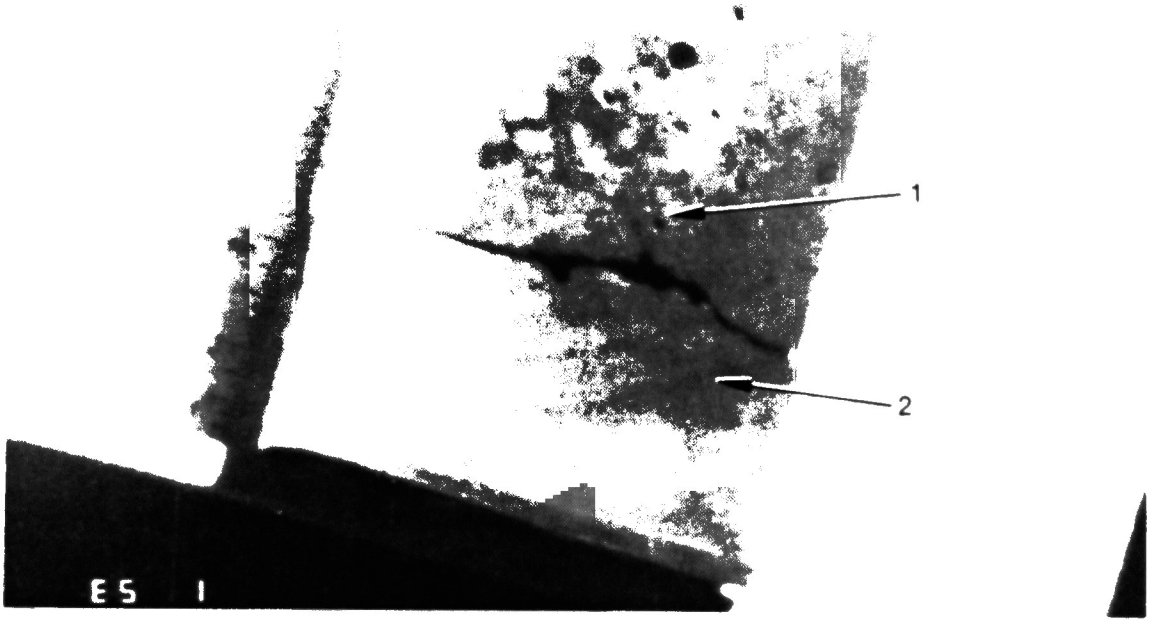

Figure 29. G12-P1-D2 sampling locations.

the No. 1 location; however, the composition is similar in both cases with the principal components being uranium (55 and 63 wt%) and zirconium (20 and 22 wt%) with lesser amounts of silver (0.18 and 0.21 wt%) and iron (1.1 and 1.6 wt%).

Table 25 lists the average composition and range of compositions for the peripheral crust samples. These data should be treated cautiously because of the high degree of heterogeneity between the metallic and ceramic phases. In the following sections, each region is treated separately due the substantial differences in composition.

3.3.2.1 Uranium Fuel and Zircaloy Cladding. The fuel material (uranium) concentrations in the peripheral crust have a range from 3.2 to 66 wt%. However, if only the samples from the fuel material sample locations (i.e., all samples except 007-P4-C No. 1 and G12-P1-E No. 2) are considered, the range is 49 to 66 wt%. For zirconium, the data from these samples range from 4.4 to 23 wt%, and the average is 16 wt%.

Table 26 lists the U/Zr and Zr/Sn ratios in the peripheral crust samples. The core average U/Zr ratio is 3.7, which is less than the average ratio for the ceramic samples (5.2); however, these data are biased by the data from 007-P4-C, which has higher U/Zr ratios and consequently, lesser relative amounts of zirconium. The U/Zr component of the peripheral crust appears to be depleted in zirconium content at 007-P4 and enriched at the G12 location. In the metallic phase, the U/Zr ratios range from 0.19 to 0.6, which indicates a factor of 10 higher concentrations of zirconium relative to the uranium present. These data suggest differences in behavior at the two side crust locations and that one location (007) is similar in composition to the upper crust and one (G12) is similar to the lower crust.

In both the metallic and ceramic samples of the peripheral crust, there are significant amounts of zirconium and tin (constituents of the fuel cladding). The ratio data indicate greater relative concentrations of tin in some metallic and ceramic samples, and less than the core average in the

TABLE 25. PERIPHERAL CRUST AVERAGE COMPOSITION[a] (wt%)

Element	Average Concentration[b]	Low/High ratio[c]
Ag	2.9	0.04 - 7.4
Al	0.29	0.07 - 0.63
B	0.08	0.03 - 0.19
Cd	0.14	0.008 - 0.42
Cr	1.7	0.11 - 3.9
Cu	0.09	0.09 - 0.14
Fe	6.4	0.84 - 29
Gd	0.06	0.02 - 0.09
In	1.3	0.18 - 2.9
Mn	0.10	0.03 - 0.40
Mo	0.25	0.02 - 0.17
Nb	0.13	0.08 - 0.17
Ni	2.7	0.17 - 12.6
Si	0.52	0.10 - 1.51
Sn	1.3	0.12 - 2.9
Te	0.06	0.02 - 0.12
U	46.0	3.2 - 66.3
Zr	16.2	4.4 - 23.2

a. This table presents the average of the examination results obtained from the side crust; however, because of the heterogeneity of the material and the small number of samples examined, these data must be used with caution.

b. The average concentration is calculated using only real values and is averaged without zero values.

c. Values below analytical detection limit not included in range.

TABLE 26. PERIPHERAL CRUST FUEL MATERIAL (U, Zr, Sn) WEIGHT RATIOS

Sample ID	U/Zr Ratio[a]	Zr/Sn Ratio[b]
007-P4-C		
No. 1[c]	0.19	5.7
No. 2	12	1.6
No. 3	9.4	6.7
No. 4	3.9	76
G12-P1-E		
No. 2[c]	0.6	11.0
No. 3	2.8	120
No. 4	2.8	--[d]
G12-P1-D2		
No. 1	2.9	--[d]
No. 2	2.8	158

a. The core average U/Zr ratio is 3.7, assuming oxidation of the zircaloy.

b. The average Zr/Sn ration in zircaloy cladding is 61.

c. Principally metallic samples (<20 wt% U).

d. A component of the ratio was not measurable.

G12 samples. The relative accumulation of tin, as compared with zirconium in some samples, is suggested.

3.3.2.2 Control Rod Materials. Control rod materials, including the relatively volatile cadmium, were measurable in most of the peripheral crust samples. Examination of the data in Tables G8 to G10 and 25 indicate that the least volatile control material, silver, was measurable in both metallic and ceramic material samples at an average concentration of about 2.9 wt%, with a range of concentrations from 0.04 to 7.4 wt%. This is greater than the expected core average concentration of silver (1.8 wt%); however, inspection of the data indicates accumulations of this element in both metallic and ceramic regions in this part of the reactor core. Lower concentrations are present in the more ceramic samples.

Indium was measurable in all samples at concentrations averaging 1.3 wt%, with the bulk of data ranging from 0.2 to 2.9 wt%. The core average concentration of this element is 0.3 wt%, which indicates that indium is concentrated in the peripheral crust.

Cadmium was measurable in six of the nine samples obtained from the peripheral crust. The concentrations ranged from 0.01 to 0.42 wt%, with an average concentration of about 0.14 wt%. This concentration is greater than the core average concentration of 0.12 wt%; however, the bulk of the element is located in the metallic regions.

Table 27 presents ratios among silver, indium and cadmium for the lower crust samples. The Ag/In data indicate a ratio range from 0.1 to 10, with the bulk of the data below the average ratio (5.3) for intact control rods. These data indicate that indium is present at greater relative concentrations in this part of the crust than silver, with the exception of 007-P4-C No. 4, where the ratio is greater than the core average. These data suggest that indium is accumulating at the peripheral portion of the core relative to silver. This is similar to the behavior observed in the lower crust.

TABLE 27. PERIPHERAL CRUST CONTROL MATERIAL (Ag, In, Cd) WEIGHT RATIOS

Sample ID	Ag/In Ratio[a]	Ag/Cd Ratio[b]	In/Cd Ratio[c]
007-P4-C			
No. 1[d]	2.5	16	6.5
No. 2	1.8	24	13
No. 3	3.5	51	14
No. 4	10	124	12
G12-P1-E			
No. 2[d]	3.6	104	29
No. 3	0.1	--[e]	--[e]
No. 4	0.14	6.0	43
G12-P1-D2			
No. 1	--[e]	--[e]	--[e]
No. 2	1.2	--[e]	--[e]

a. The core average Ag/In ratio is 5.3.

b. The average Ag/Cd ratio is 16.

c. The average In/Cd ratio is 3.0.

d. Principally metallic samples.

e. A component of the comparison was below the detection limit of the analysis method.

The Ag/Cd ratios vary over a factor of 10, and the cadmium was not measurable at three locations. The measured ratios are greater than those found in intact control rods by factors greater than 2, indicating that the cadmium has been partially depleted in the debris relative to silver, similar to the upper and lower crust data. This is particularly apparent for sample 007-P4-C, where there is a variation in the Ag/Cd ratio from near the intact control rod ratio at the top of the crust to significantly greater near the bottom of the crust. The data for In/Cd are consistent with the Ag/Cd data and again indicate relatively less cadmium in the debris.

3.3.2.3 Poison Rod Materials. Poison rod materials measurable in the peripheral crust included aluminium, boron, and gadolinium. Aluminium was measurable in all samples at concentrations averaging 0.3 wt%, which is similar to the core average concentration of 0.2 wt%. Boron from the poison rods and reactor coolant is present in most samples at concentrations between 0.03 and 0.19 wt%. Gadolinium is also present in the peripheral crust in a range of concentrations from 0.02 to 0.09 wt%, with an average of 0.06 wt%. This concentration is greater than the average concentration of 0.01 wt%, which suggests accumulation of this element in the peripheral crust.

3.3.2.4 Structural Materials. Measurements were made for all structural material constituents in the core (i.e., iron, chromium, nickel, manganese, niobium and molybdenum). The average concentration data in Table 25 indicates that iron is the principal structural material present (average 6.4 wt%), and that it ranges up to 29 wt% in the metallic regions of the crust. Lesser concentrations of nickel (average - 2.7 wt%) and chromium (average - 1.7 wt%) are also present. Examination of the ratio data for the principal components of the metallic crust (Table 28) indicates that Fe/Cr and Fe/Ni and Ni/Cr ratios tend to be between those found in stainless steel and Inconel, but appear to be closer to stainless steel. The presence of molybdenum in the peripheral crust suggests again that the Inconel grid spacers were contributors to the formation of the crust. The

TABLE 28. PERIPHERAL CRUST STRUCTURAL MATERIAL (Fe, Cr, and Ni) WEIGHT RATIOS[a]

Sample ID	Fe/Cr Ratio	Fe/Ni Ratio	Ni/Cr Ratio	Ni/Mo Ratio
007-P4-C				
No. 1	7.7	2.3	3.4	11
No. 2	1.2	2.2	0.5	11
No. 3	1.2	6.4	0.2	0.6
No. 4	2.1	3.4	0.6	18
G12-P1-E				
No. 2	4.5	2.0	2.2	27
No. 3	2.2	4.4	0.5	5.0
No. 4	2.0	4.1	0.5	--[b]
G12-P1-D2				
No. 1	2.4	6.2	0.4	--[b]
No. 2	1.5	4.3	0.3	24

a. The elemental ratios for stainless steel and Inconel are:

	Stainless Steel	Inconel
Fe/Cr	3.6	0.35
Fe/Ni	7.6	0.35
Ni/Cr	0.5	2.7
Ni/Mo	--	17.3

b. Component not detected.

Ni/Mo ratios shown in Table 28 indicate that some stainless steel has contributed to the formation of the crust.

3.3.3 Peripheral Crust Radiochemical Examinations

The radionuclide distribution in the peripheral crust was determined for the samples discussed in Section 3.3.2. Results of the radiochemical analysis of the samples are listed in Appendix H, Tables H4 and H5. To provide information on the characteristic behavior of fission products, they have been categorized by the volatility of the chemical group and element as discussed in Section 3.1.3.

Table 29 lists the average radionuclide concentrations, the range of concentrations, and the ratio of high to low values. The ranges of concentrations are from 10^0 to 10^3, indicating a relatively wide range of radionuclide concentrations; however, the only radionuclides with concentration ranges greater than 10^2 are the metallic species (^{106}Ru and ^{125}Sb) that accumulate in the metallic portions of the crust.

3.3.3.1 Peripheral Crust Uranium-235 Enrichment. Measurements were performed to evaluate the concentrations of ^{235}U and ^{238}U in the peripheral crust and to determine ^{235}U enrichment in the crust. The ^{235}U and ^{238}U concentrations are listed in Appendix H and the ^{235}U enrichments are listed in Table 30. These measurements should be treated with some caution as the technique used for the measurements is affected by the presence of control materials that may result in measured concentrations lower than actual for those samples with high control material content. Table 30, which summarizes the ^{235}U and ^{238}U data, indicates a range of enrichments from 1.8 to 3.5; however, the bulk of the data is in the range from 2.2 to 2.4, which suggests that the peripheral crust debris samples are mostly a composite of the 1.98% and 2.64% enriched assemblies. Assembly location 007 had an original enrichment of 1.98%, and G12 had an enrichment of 2.64%. These data suggest that uranium present in the 1.98% enriched assemblies was mixed with the adjacent 2.64% assemblies to form the peripheral crust.

TABLE 29. PERIPHERAL CRUST AVERAGE RADIONUCLIDE CONCENTRATIONS (microcuries/g sample on April 1, 1987)

Radionuclide	Average	Range	High/Low ratio
^{60}Co	172	12 to 887	74
^{90}Sr	1120	152 to 2460	16
^{106}Ru	181	2.4[a] to 500	210
^{125}Sb	218	0.1 to 844	8400
^{129}I	7.7 E-5	3.9 E-6 to 3.0 E-4	77
^{134}Cs	6.3	0.5[a] to 23	46
^{137}Cs	261	13 to 1050	81
^{144}Ce	125	21[a] to 188	17
^{154}Eu	26	19[a] to 43	2.1
^{155}Eu	33	2.0 to 56	18

a. Detection limit value not included in range.

TABLE 30. PERIPHERAL CRUST URANIUM-235 ENRICHMENT

Sample ID	^{235}U Enrichment[a]
007-P4-C	
No. 1[b]	3.5[c]
No. 2	2.1
No. 3	1.8
No. 4	2.2
G12-P1-E	
No. 2[b]	2.2
No. 3	2.4
No. 4	2.6
G12-P1-D2	
No. 1	2.2
No. 2	2.3

a. The core average ^{235}U enrichment is approximately 2.56% with the peripheral assemblies having an enrichment of 2.98 and the central assemblies having enrichments of 1.98% and 2.64%.

b. Less than 30% U content.

c. Large uncertainty (>50%) associated with value.

d. Not measured or not detected.

3.3.3.2 Comparisons with ORIGEN2. The measured radionuclide concentrations in the peripheral crust were compared with concentrations predicted by the ORIGEN2 Code in order to assess retention of radionuclides in the ceramic and metallic regions of the peripheral crust. The ORIGEN2 data and analysis methods are discussed in Section 3.1.3, and Table 14 lists the ORIGEN2 values used for comparison with the core bore data.

A summary of the measured radionuclide retentions (based on uranium content) in the lower crust is provided in Table 31. The data listed in Table 31 indicate a wide range of retentions. Greater inaccuracies would be expected from those samples with low uranium contents (indicated in Table 31). However, this method provides a means of normalizing fission product concentrations to a standard value for comparison purposes. The following sections discuss the radionuclide distributions for the low, medium, and high volatility radionuclides.

3.3.3.3 Low Volatiles. The low volatiles for which radionuclide comparisons were performed are ^{144}Ce and ^{154}Eu. Tables 31 and 32 indicate a range for ^{144}Ce from 50 to 153%. The average ^{144}Ce retention in ceramic samples is 91%, and that for ^{154}Eu is 105%, as shown in Table 32. The relatively low volatiles ^{144}Ce and ^{154}Eu have been retained, within the uncertainty associated with analysis, entirely in the fuel material. The high retentions (i.e., >100%) suggest that some of the fuel material forming the peripheral crust came from high burnup material.

3.3.3.4 Medium Volatiles. The fission products that are expected to have a medium volatility are ^{90}Sr, ^{125}Sb, and ^{106}Ru. Strontium-90 is expected to be the least volatile because it is likely to be in the relatively non-volatile oxide chemical form. The ^{90}Sr data shown in Tables 31 and 32 indicate a range of concentrations with the lowest retention (6.4%) in 007-P4-C No. 4, a ceramic sample. The data in Table 32 indicate low average ^{90}Sr retentions for both the metallic and ceramic samples. The data generally indicate that some relocation of the ^{90}Sr has occurred, but that approximately half was retained in the debris.

TABLE 31. RADIONUCLIDE RETENTION IN THE PERIPHERAL CRUST[a]

Sample ID	Radionuclide Retention(%)						
	^{90}Sr	^{106}Ru	^{125}Sb	^{129}I	^{137}Cs	^{144}Ce	^{154}Eu
007-P4-C							
No. 1[b]	60.0	8360	26100	25.5	4.33	--[c]	--[c]
No. 2	32.7	268	0.24	8.35	3.45	74.9	78.5
No. 3	16.6	50.5	457	9.78	23.2	102	101
No. 4	6.54	7.16	94.3	4.08	5.18	50.3	39.8
G12-P1-E							
No. 2[b]	56.1	966	966	78.8	77.0	59.0	82.4
No. 3	45.7	--[c]	0.032	0.27	0.49	128	169
No. 4	37.6	--[c]	1390	0.63	0.62	153	192
G12-P1-D2							
No. 1	16.2	--[c]	--[c]	0.39	0.35	119	146
No. 2	55.5	2.3	2.6	0.66	0.60	78.4	84.4

a. Retention is calculated based on the uranium content of the sample material as determined from the elemental analysis results in Appendix G. Additional figures are shown beyond those statistically appropriate for calculational purposes. The uranium concentrations used for normalization in wt% were:

007-P4-C--No. 1 - 3.2; No. 2 - 53.2; No. 3 - 56.8; No. 4 - 66.3
G12-P1-E--No. 2 - 14.1; No. 3 - 53.8; No. 4 - 49.5
G12-P1-D2--No. 1 - 63.2; No. 2 - 55.1

b. Contains significant amounts of metallic material (greater than 30%).

c. Not detected.

TABLE 32. AVERAGE RADIONUCLIDE RETENTION IN METALLIC AND CERAMIC SAMPLES

	Metallic Samples[a]		Ceramic Samples[b]	
Radionuclide	Average	Range	Average	Range
^{90}Sr	58	56 to 62	31	6.5 to 56
^{106}Ru	4660	966 to 8360	47	2.3 to 268
^{125}Sb	15100	4000 to 26100	80	0.24 to 457
^{129}I	52	26 to 78	3.5	0.27 to 9.8
^{137}Cs	41	4.3 to 77	3.2	0.5 to 12
^{144}Ce	59[c]	0 to 59	91	50 to 153
154Eu	82[c]	0 to 82	105	40 to 192

a. Nominal metallic samples are 007-P4-C No. 1 and G8-P11-E No. 1.

b. Nominal ceramic samples include all other samples in the side crust, although there is some metallic material in all samples that may bias the results to some extent.

c. Single analysis result.

The ^{125}Sb and ^{106}Ru radionuclides are expected to exhibit a greater range of concentrations in the peripheral crust because they had a substantial range of concentrations in both the upper and lower vessel debris,[15,16] suggesting significant mobility for these radionuclides. For ^{125}Sb, comparisons were performed with the concentrations of elemental constituents of the crust; no correlations were observed with the exception that a general increase in metallic content generally correlated with an increase in ^{125}Sb content. The sample with the highest metallic material content was sample 007-P4-C No. 1 at approximately 77 wt% metallic. The normalized retention for ^{125}Sb in this sample is by far the highest in the peripheral crust and in the entire core. The high concentrations of ^{125}Sb in samples 007-P4-C No. 3 and G12-P1-E No. 4 are anomalous, as both samples are principally composed of uranium and zirconium with small amounts of the metallic constituents. These data suggest that the ^{125}Sb is heavily concentrated in the metallic portion of the two samples.

Ruthenium-106 was measurable in most samples; however, there was a wide range of concentrations in the metallic and ceramic samples, and there is no apparent correlation with the distribution of the ^{125}Sb. These data indicate significant accumulation of ^{106}Ru in the metallic layers at concentrations up to 83 times the core average concentration for uranium; and in the ceramic layers, accumulations up to 3 times the ORIGEN2 calculated concentration.

3.3.3.4 High Volatiles. The two high volatile radionuclides measurable were ^{137}Cs and ^{129}I. The more volatile ^{129}I was measurable in most samples at retentions lower than those found in intact fuel material. The presence of ^{129}I in the metallic samples at relatively high retentions is somewhat misleading, as the data has been adjusted for uranium content. The actual concentrations are similar or less than those measured in the ceramic samples. The data suggest relatively low retention of ^{129}I in the peripheral crust at retentions averaging 3.5% in the ceramic samples.

The ^{137}Cs retentions shown in Tables 31 and 32 indicate similar relative retentions to those of ^{129}I for both the metallic and ceramic

samples, and no apparent correlation between the retentions of the two radionuclides. The data for the ceramic sections suggests only limited retention of cesium at any location in the crust.

3.4 Central Core Consolidated Region Examination Results

The central consolidated region represents the largest fraction of the material in the lower reactor core (approximately 20% of the total core). The samples obtained from this part of the lower core are quite heterogeneous; many samples are either metallic or ceramic, and some samples are a mixture of the two types of material. For the central core region, information obtained from the visual and metallurgical examinations is summarized in the following section. This summary was extracted from the visual examinations presented in Appendix C, the density measurements described in Appendix D, the metallographic examinations described in Appendix E, and the autoradiographic results listed in Appendix F. The bulk elemental and radiochemical analysis results are summarized in Sections 3.4.2. and 3.4.3

3.4.1 Visual and Metallurgical Examinations

The initial visual examinations performed on particles of debris from this region indicated a wide variation in the composition of these particles. As a result, various rocks from this region were characterized as being primarily ceramic, metallic, or a mixture of ceramic and metallic phases.

The density of particles which were characterized as being primarily metallic varied between 5.5 and 8.8 g/cm^3. These particles were generally found in the peripheral core bores in locations D04, 007, and 009. Most of these particles consisted of an iron-nickel alloy with small amounts of chromium and silver-indium inclusions in the matrix. A typical example of these metallic melts is shown in Figure 30. As described in detail in Appendix E, previously molten droplets of Cr_2O_3 were identified in some

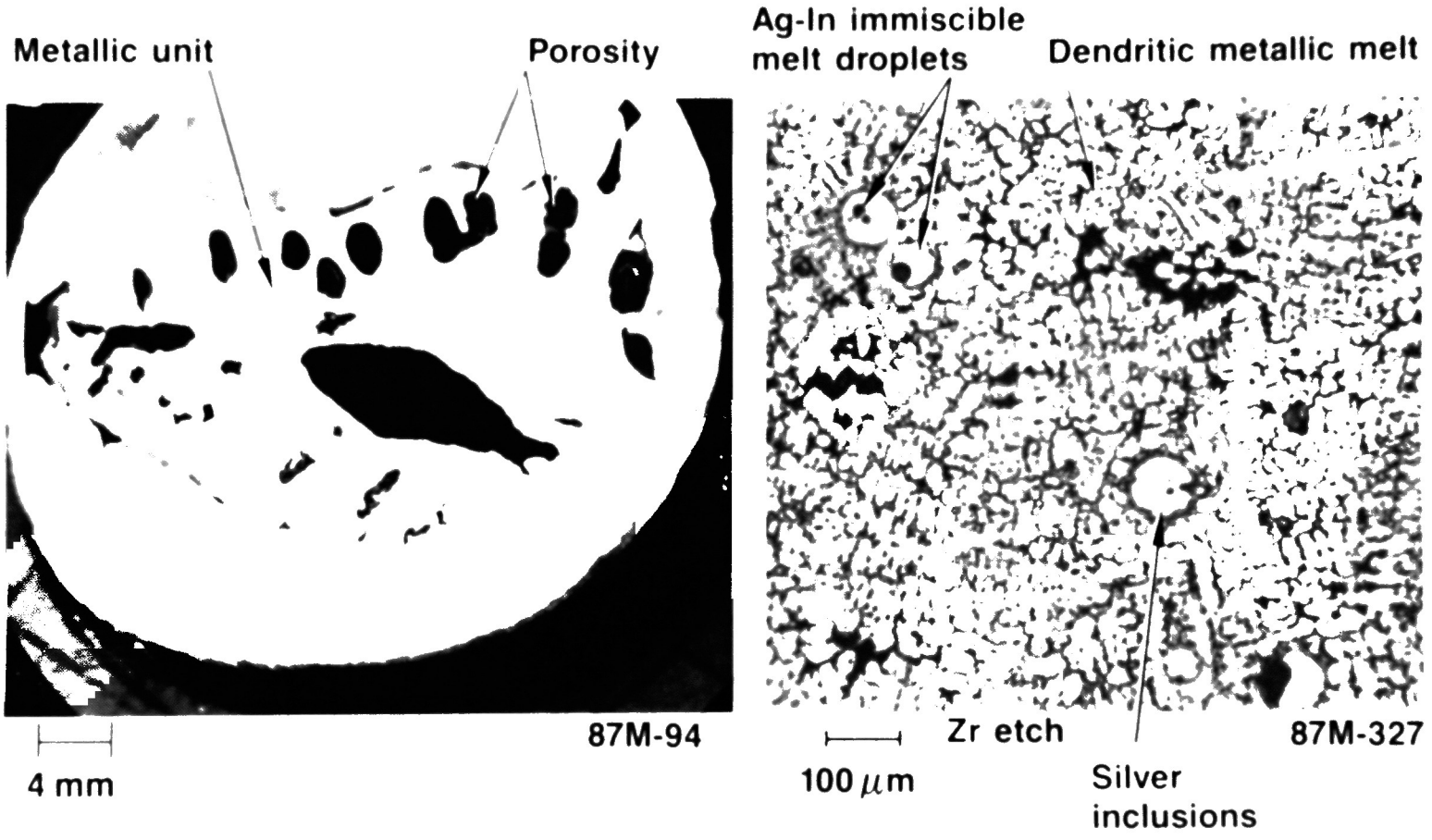

Figure 30. Metallic melt particle from central core region (009-P1).

of these metallic particles, which indicates temperatures in excess of 2266 K.

Fifteen particles of ceramic material from core locations D08, G08, G12, and K09 were examined. The details of these examinations are described in Appendix E. The density of these samples ranged from 6.9 to 8.8 g/cm^3. These samples consisted primarily of a $(U,Zr)O_2$ ceramic melt with structural elements dispersed in the melt. Figure 31 shows the $(U,Zr)O_2$ ceramic melt surrounding fuel pellet remnants which were in the process of being liquefied. Large pores formed within the fuel pellet matrix, which indicates localized temperatures in excess of the 3100 K melting point of the fuel. This area is shown in more detail in Figure 32.

Five particles which were characterized as being a mixture of ceramic and metallic phases were examined. These samples were obtained from core locations G08, G12, and N05, and their densities ranged from 7.6 to 9.1 g/cm^3. Areas of this ceramic melt region had a mottled structure, similar to other ceramic melt regions, which resulted from the segregation of structural oxides. Typical examples are provided in Figures 33, 34, and 35. Immiscible metallic melts were also distributed throughout these samples, as described in detail in Appendix E. These structures were very similar to those observed in the upper and peripheral crust regions. However a somewhat unusual feature, observed in samples from core bore location G12, is shown in Figure 36, and in more detail in Figure 37. These SEM images show the presence of UO_2 crystals within pores in the ceramic matrix.

These metallographic and SEM examinations indicate structures very similar to those found in other regions of the crust. Immiscible metallic melts consisting primarily of structural components and control rod material alloy were dispersed throughout the ceramic matrix. The ceramic phase was primarily composed of molten $(U,Zr)O_2$ with temperatures in excess of 2810 K, with localized temperatures exceeding the 3120 K melting point of the fuel.

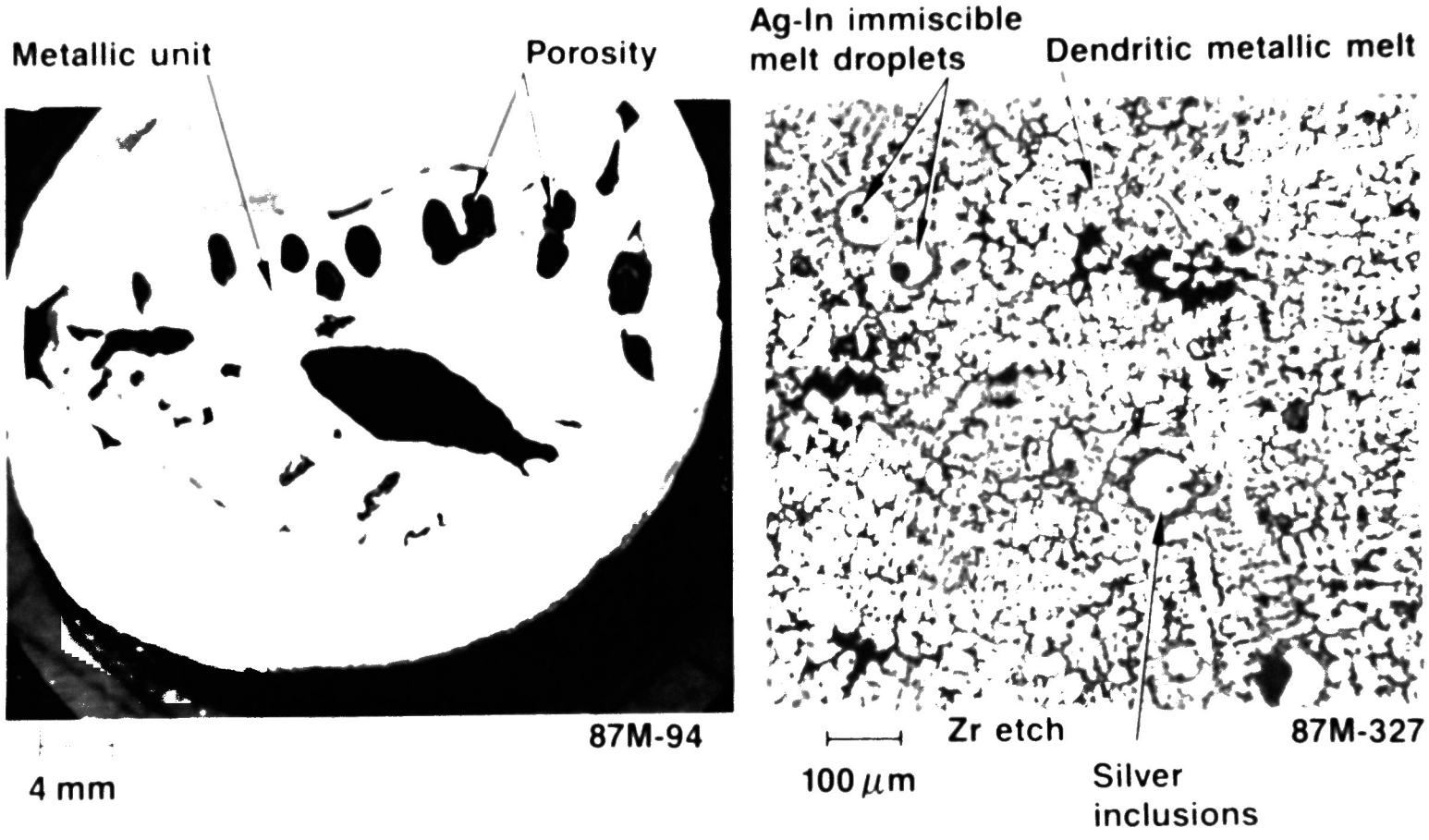

Figure 30. Metallic melt particle from central core region (009-P1).

of these metallic particles, which indicates temperatures in excess of 2266 K.

Fifteen particles of ceramic material from core locations D08, G08, G12, and K09 were examined. The details of these examinations are described in Appendix E. The density of these samples ranged from 6.9 to 8.8 g/cm^3. These samples consisted primarily of a $(U,Zr)O_2$ ceramic melt with structural elements dispersed in the melt. Figure 31 shows the $(U,Zr)O_2$ ceramic melt surrounding fuel pellet remnants which were in the process of being liquefied. Large pores formed within the fuel pellet matrix, which indicates localized temperatures in excess of the 3100 K melting point of the fuel. This area is shown in more detail in Figure 32.

Five particles which were characterized as being a mixture of ceramic and metallic phases were examined. These samples were obtained from core locations G08, G12, and N05, and their densities ranged from 7.6 to 9.1 g/cm^3. Areas of this ceramic melt region had a mottled structure, similar to other ceramic melt regions, which resulted from the segregation of structural oxides. Typical examples are provided in Figures 33, 34, and 35. Immiscible metallic melts were also distributed throughout these samples, as described in detail in Appendix E. These structures were very similar to those observed in the upper and peripheral crust regions. However a somewhat unusual feature, observed in samples from core bore location G12, is shown in Figure 36, and in more detail in Figure 37. These SEM images show the presence of UO_2 crystals within pores in the ceramic matrix.

These metallo[illegible]hic and SEM examinations indicate structures very similar to those found in other regions of the crust. Immiscible metallic melts consisting primarily of structural components and control rod material alloy were dispersed throughout the ceramic matrix. The ceramic phase was primarily composed of molten $(U,Zr)O_2$ with temperatures in excess of 2810 K, with localized temperatures exceeding the 3120 K melting point of the fuel.

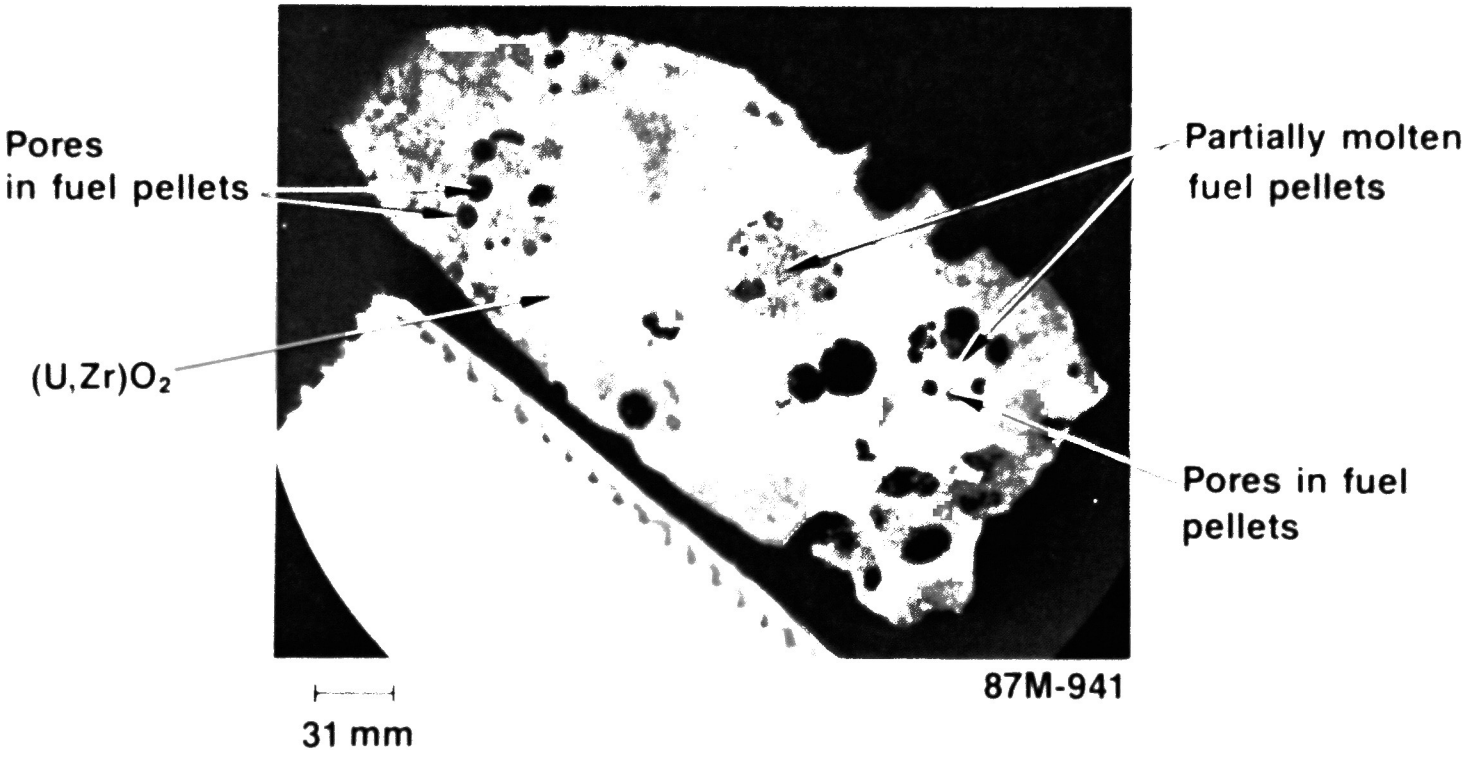

Figure 31. Partially molten fuel pellets in central core region (G12-P4).

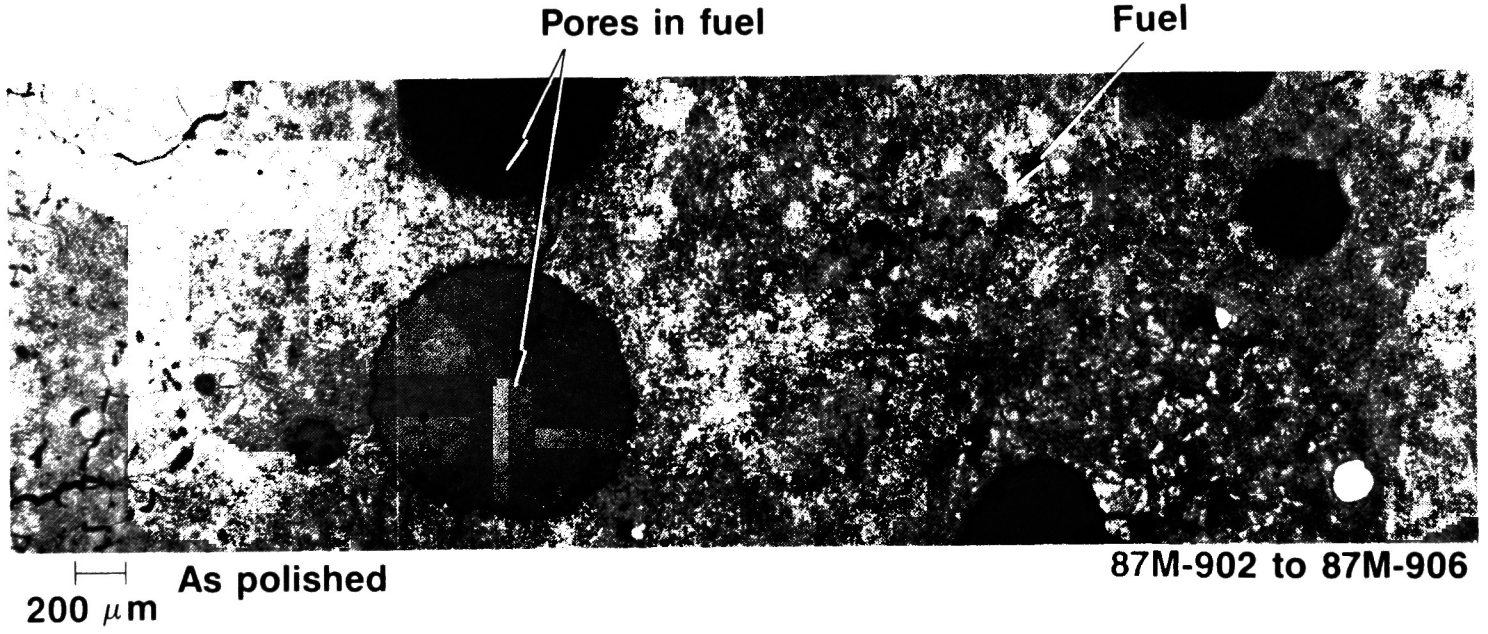

Figure 32. Pores in partially molten fuel pellet (G12-P4).

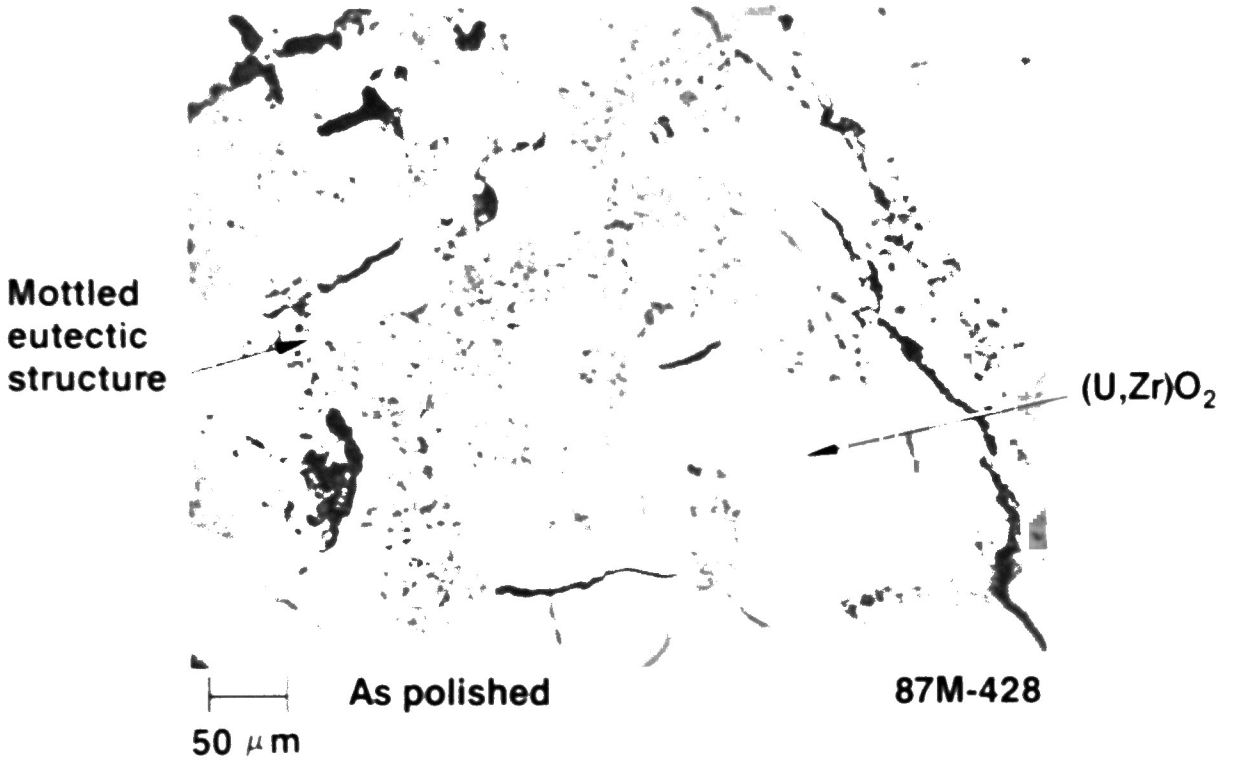

Figure 33. Mottled structure in $(U,Zr)O_2$ melt in central core region (G08-P10).

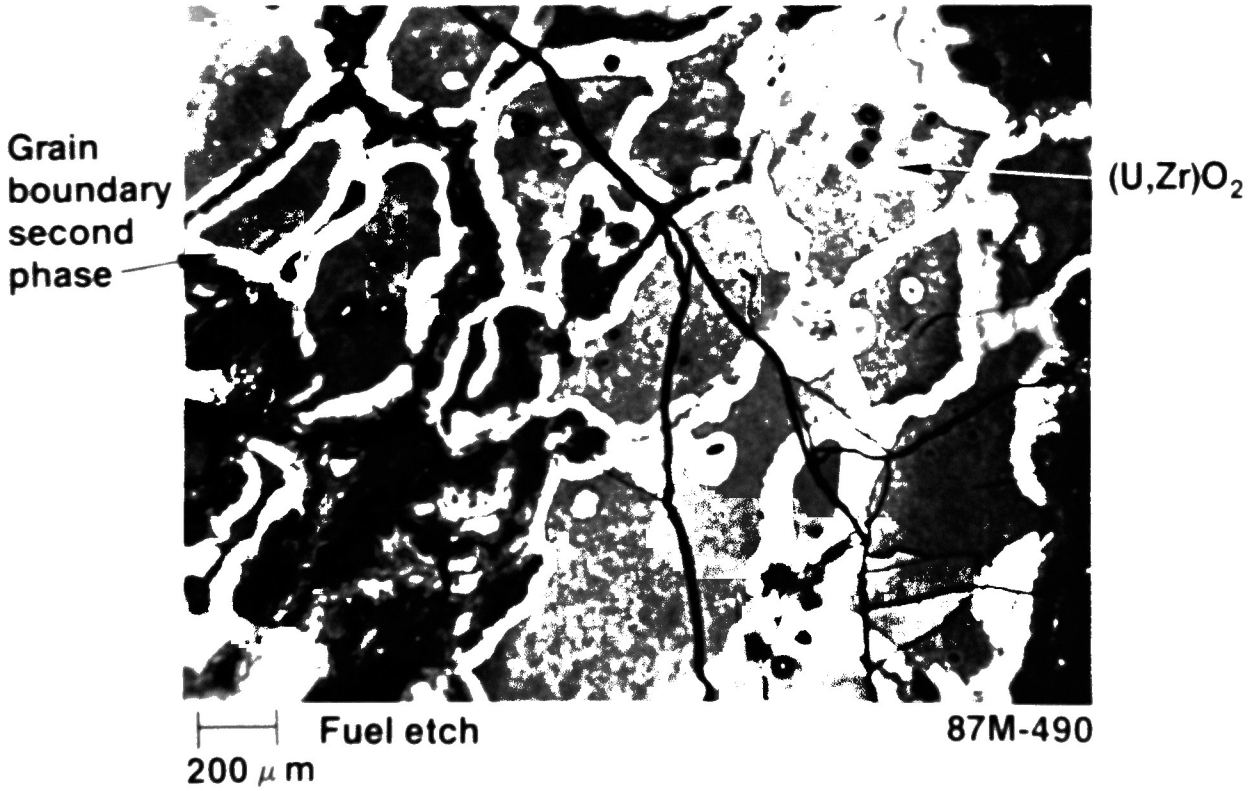

Figure 34. Second phase along $(U,Zr)O_2$ grain boundaries in central core region (G08-P10).

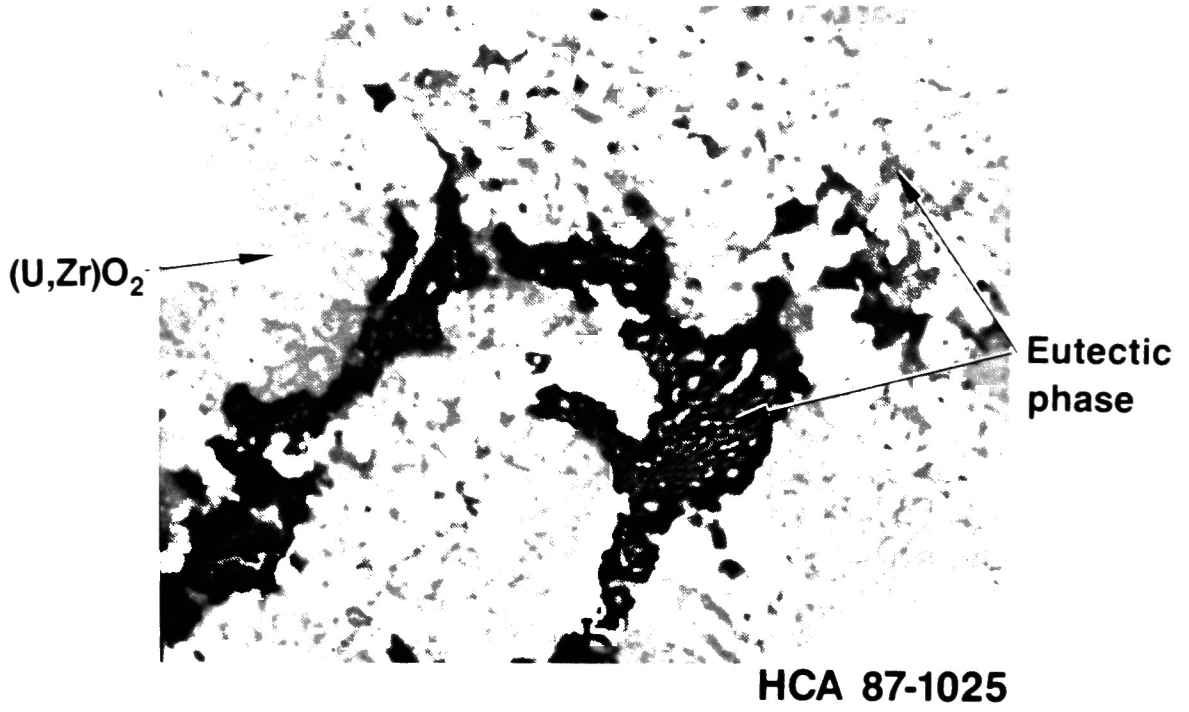

Figure 35. Backscattred electron image of iron, chromium, nickel eutectic phases in $(U,Zr)O_2$ grain boundaries (G08-P10).

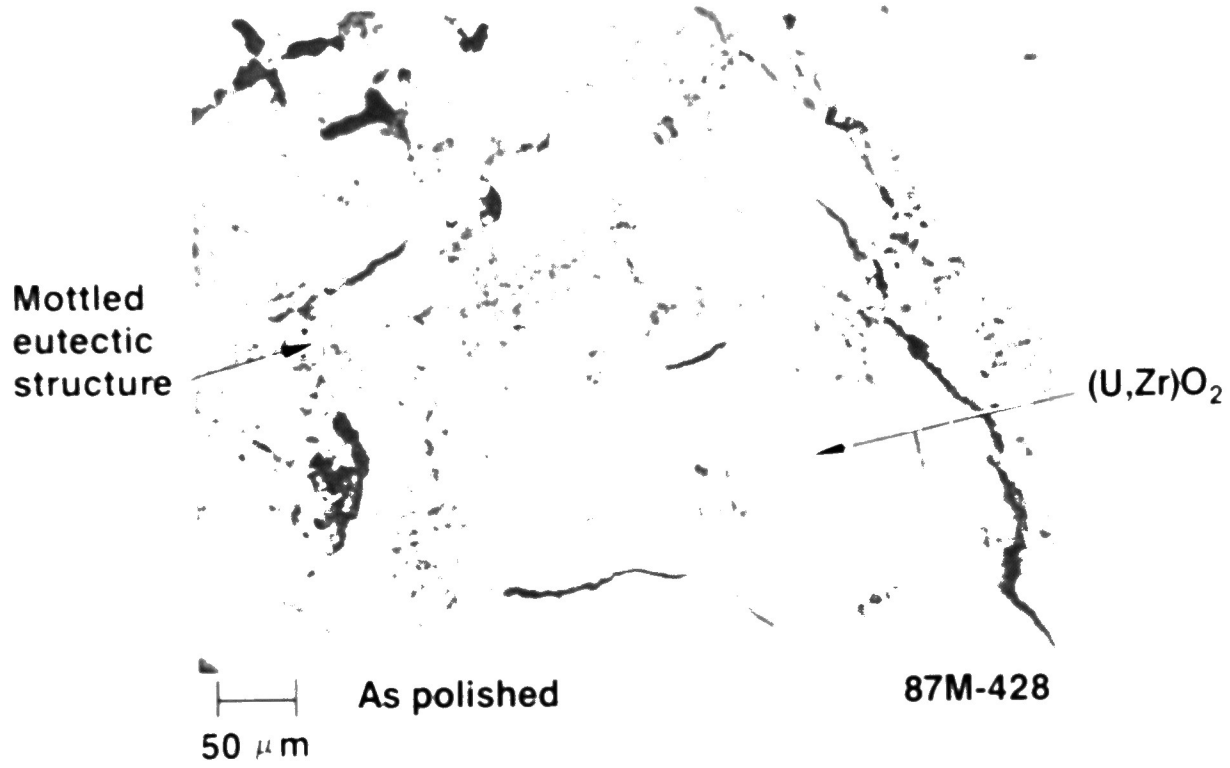

Figure 33. Mottled structure in $(U,Zr)O_2$ melt in central core region (G08-P10).

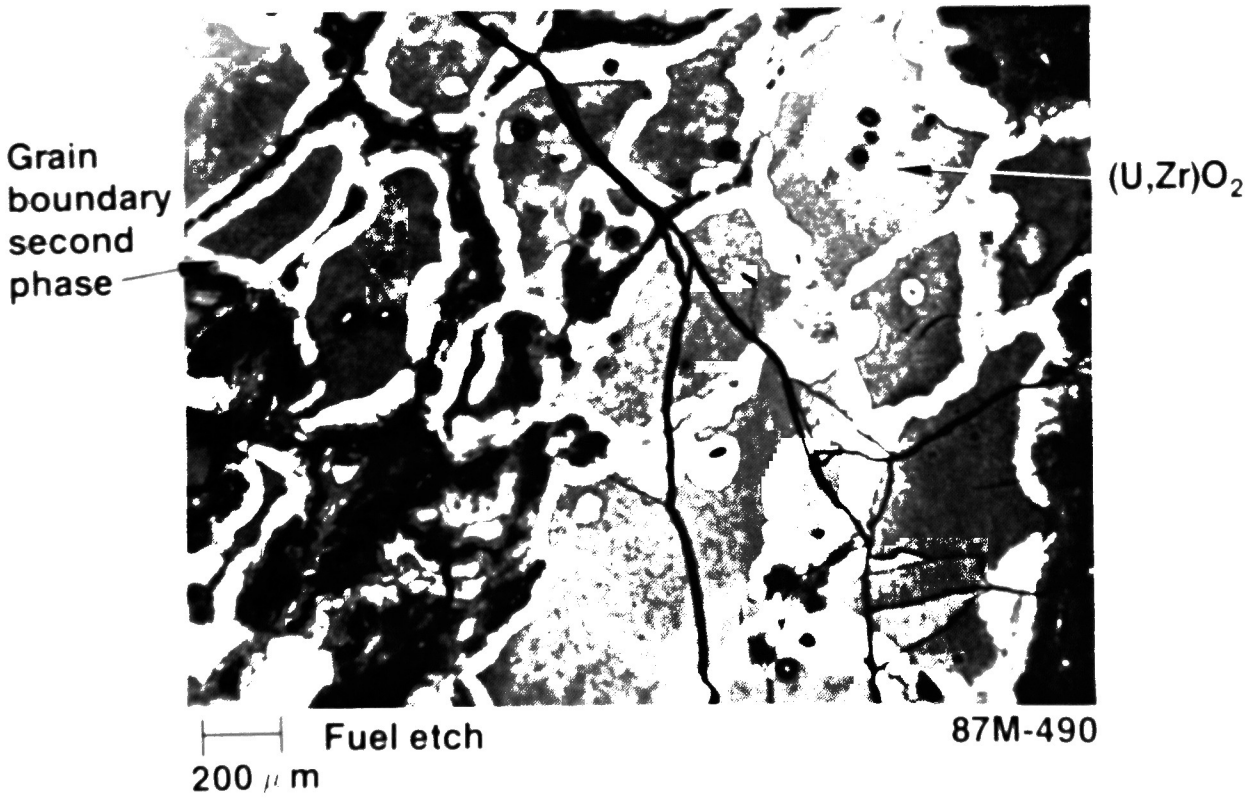

Figure 34. Second phase along $(U,Zr)O_2$ grain boundaries in central core region (G08-P10).

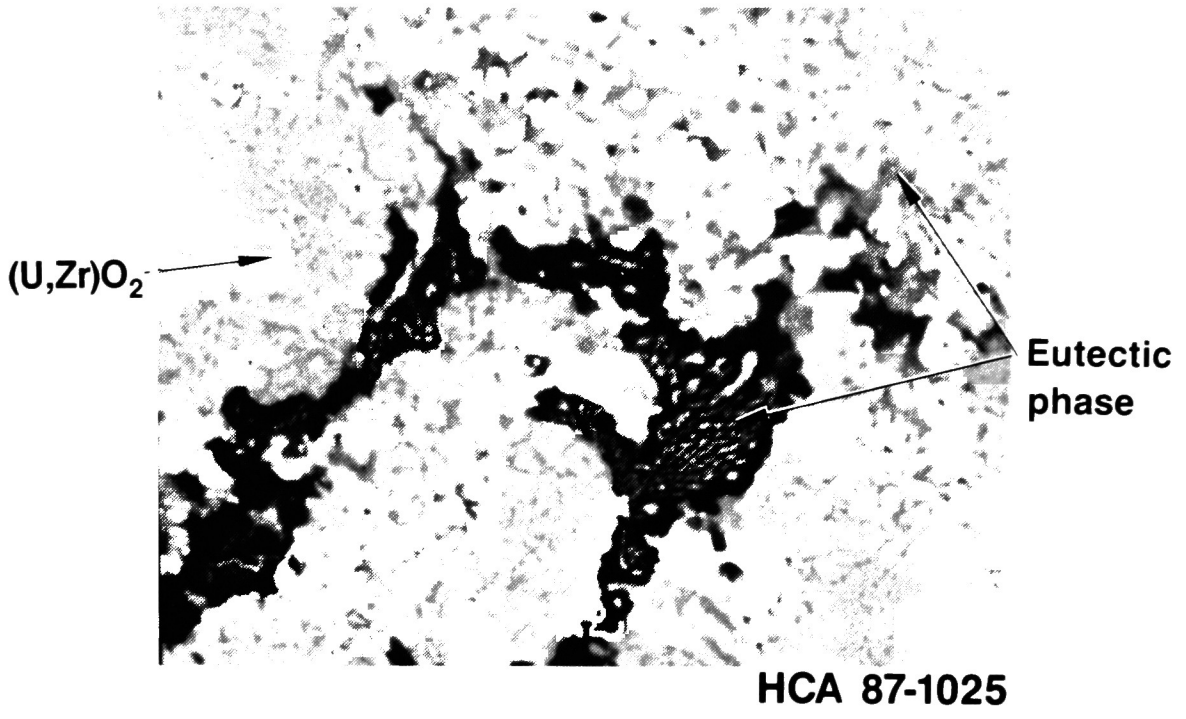

Figure 35. Backscattred electron image of iron, chromium, nickel eutectic phases in $(U,Zr)O_2$ grain boundaries (G08-P10).

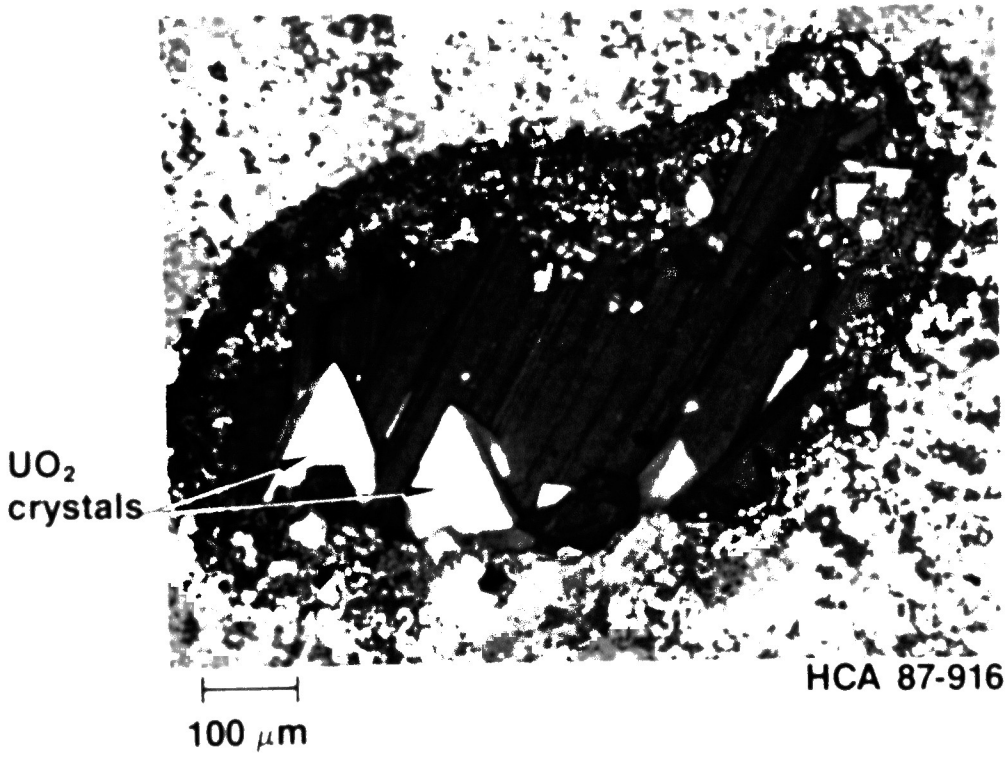

Figure 36. Backscattered electron image of UO_2 crystal growth inside pore in ceramic matrix (G12-P9).

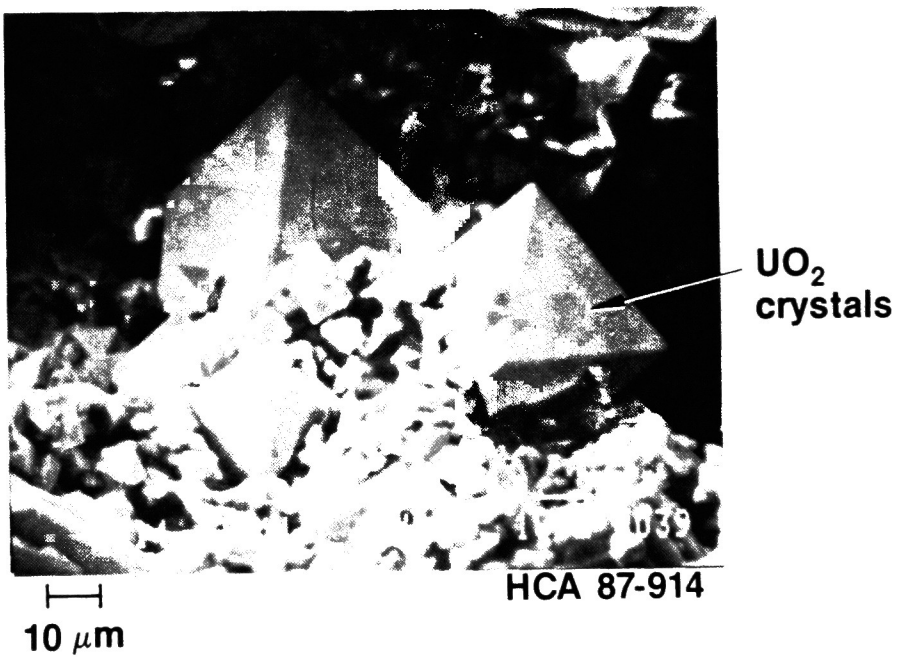

Figure 37. Secondary electron image of polyhedral UO_2 crystals in pores (G12-P9).

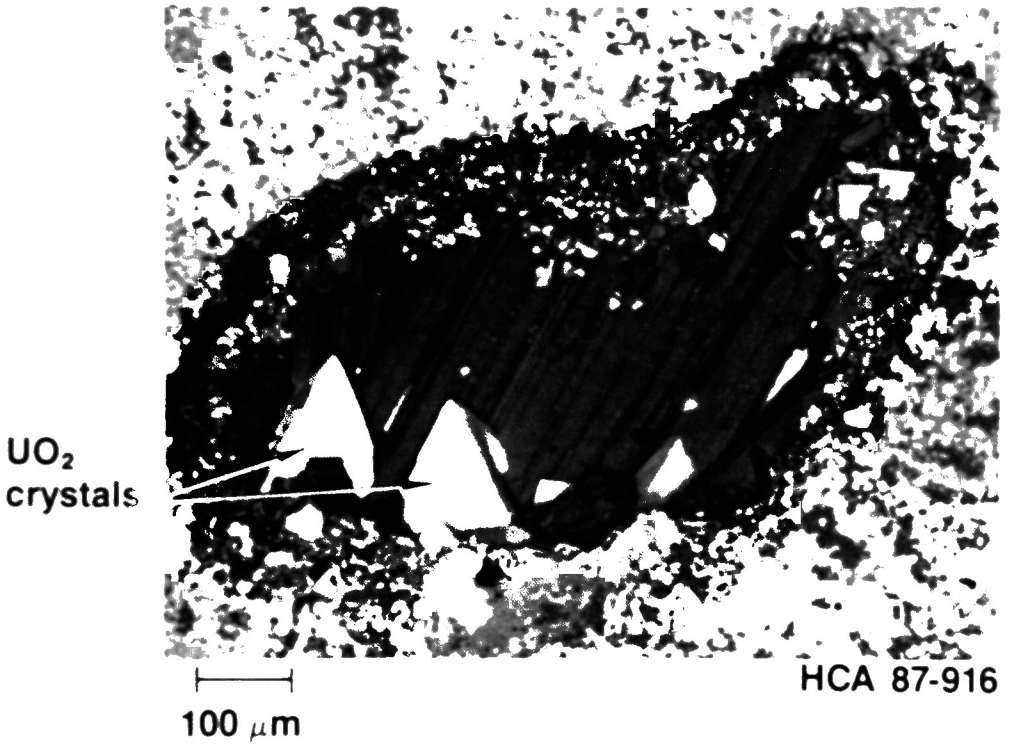

Figure 36. Backscattered electron image of UO_2 crystal growth inside pore in ceramic matrix (G12-P9).

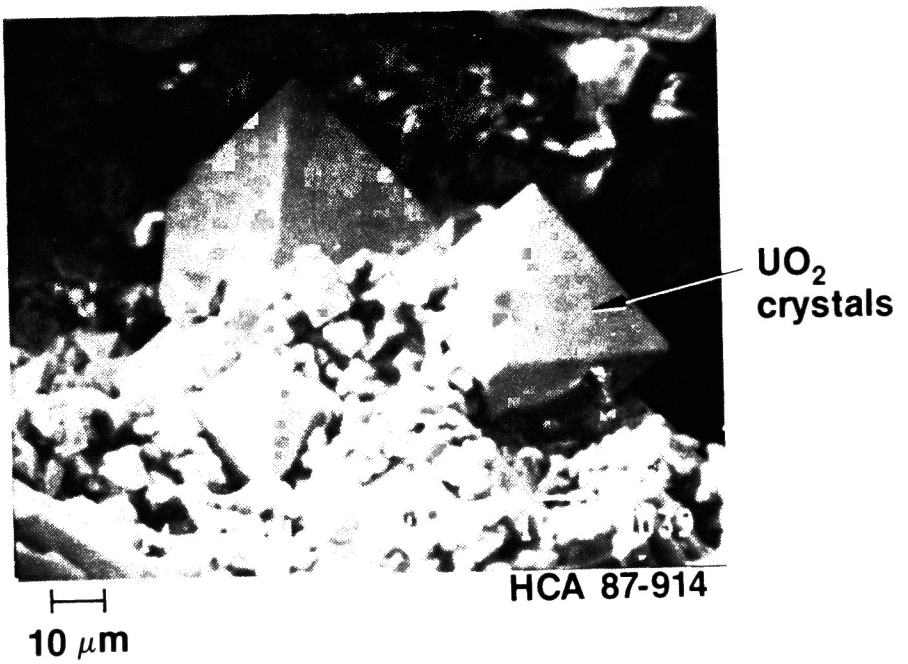

Figure 37. Secondary electron image of polyhedral UO_2 crystals in pores (G12-P9).

3.4.2 Central Core Bulk Composition

Elemental analyses were performed on dissolved microcores from particle samples from the central region of the reactor core. Analyses were performed for 17 elements that constitute the principal components of the TMI-2 core. For comparison purposes, Table 1 lists the average core composition of each of the core constituents and the average core composition of the TMI-2 core, including the oxygen content of the uranium, but excluding oxygen from the oxidation of zircaloy and structural materials. Data were obtained at all core locations sampled (i.e., K09, G08, D08, 009, G12, N05, 007, and D04). The elemental data for these samples are listed in Appendix G, Tables G11 through G17. At core location K09, all samples were composed principally of uranium (52 to 60 wt%) and zirconium (19 to 21 wt%), with the exception of K09-P4-D, which was composed mostly of zirconium (34 wt%) and lesser amounts of uranium (19 wt%) and iron (8.3 wt%).

At core location G08, most samples were again principally uranium and zirconium with the exceptions of G08-P7-C No. 1 and G08-P9-A No. 1, which had high concentrations of iron (~35 wt%) and nickel (~15 wt%). At the D08 sample locations, the bulk of the samples were again principally uranium (60 to70 wt%) with significant amounts of zirconium (16 to 20 wt%). The remaining samples were principally iron (50 to 58 wt%) and nickel (24 to 37 wt%) with lesser amounts of other structural material constituents. The remaining core locations, 009, G12, N05, and 007, were separable into two types of samples: those composed principally of uranium and zirconium, and those composed almost entirely of structural, metallic components. These data suggest that the central core region is relatively heterogeneous with two types of relatively immiscible constituents: the fuel and structural material components.

Table 33 lists the average composition and range of compositions for the central core region samples. The data indicate that the central core is composed principally of uranium and zirconium with metallic inclusions of control and structural materials. These data should be treated cautiously

TABLE 33. CORE CENTRAL REGION AVERAGE COMPOSITION[a]
(wt%)

	Average Concentration[b]	Range[c]
Ag	2.9	0.07 to 34.5
Al	0.34	0.09 to 1.33
B	0.07	0.03 to 0.23
Cd	0.16	0.004 to 0.83
Cr	1.4	0.04 to 6.6
Cu	0.14	0.05 to 0.59
Fe	14.5	0.26 to 58
Gd	0.08	0.01 to 0.12
In	0.89	0.05 to 7.6
Mn	0.05	0.01 to 0.10
Mo	0.89	0.01 to 3.7
Nb	0.16	0.02 to 0.58
Ni	6.8	0.05 to 37
Si	0.60	0.16 to 1.6
Sn	2.1	0.03 to 7.5
Te	0.06	0.01 to 0.24
U	54.0	1.2 to 93
Zr	16.4	0.01 to 37

a. This table presents the average of the examination results obtained from the particles in the central core region; however, due to the heterogeneity of the material and the small number of samples examined, these data must be used with caution.

b. The average concentration is calculated using only real values and is averaged without zero values.

c. Values below analytical detection limit not included in range.

because of the high degree of heterogeneity between the metallic and ceramic regions. In the following sections, each region is treated separately because of the substantial differences in composition.

3.4.2.1 Uranium Fuel and Zircaloy Cladding. The fuel material (uranium) concentrations in the central core region have a range from 1.2 to 93 wt%, as indicated in Table 33. However, if only the samples from the ceramic locations are considered, as identified in Table 34, the range is 52 to 70 wt%. For zirconium, the data from the ceramic region samples range from 0.01 to 37 wt% with an average of 16 wt%, which suggests that zirconium is probably not depleted in the central core ceramic fuel (i.e., core average concentration is 18 wt%).

Table 34 lists the U/Zr and Zr/Sn ratios in the central core samples. The average ratio of U/Zr for the ceramic samples is 4.0, which is slightly higher than the core average of 3.7. However, the U/Zr ratio data are biased by the data from G08-P10-A No. 2 (U/Zr = 11) and N05-P1-D No. 2 (U/Zr = 13), which have high U/Zr ratios and, consequently, lesser relative amounts of zirconium. These data suggest that the U/Zr component of the central core ceramic samples is similar to the core average. In the metallic phase, the U/Zr ratios range from 0 (no uranium) to 4.9; however, the bulk of the data are between 0.05 and 1.0, which suggests metallic inclusions with little relative amounts of uranium, as was observed in the crust layer samples. This is likely to be segregation on the basis of oxidation potential with uranium primarily in the the form of UO_2 in the ceramic regions.

In both the metallic and ceramic phases, there are significant amounts of zirconium and tin. The average tin concentration in the central core region samples is 2.1 wt%, which is significantly higher than the core average concentration of 0.3 to 0.35 wt%. These data suggest an accumulation of tin in this part of the core debris in the metallic samples. The ratio data in Table 35 indicate that the ceramic samples are generally somewhat depleted in tin relative to zirconium, as compared with the core average, whereas the metallic samples indicate accumulations

TABLE 34. CENTRAL CORE REGION FUEL MATERIAL (U, Zr, Sn) WEIGHT RATIOS

Sample ID	U/Zr Ratio[a]	Zr/Sn Ratio[b]
K09-P3-A		
No. 1	2.7	104
K09-P3-D		
No. 1	2.7	115
No. 2	2.8	131
K09-P3-F		
No. 1	2.8	131
G08-P5-B		
No. 1	3.1	--[c]
No. 2	3.2	--[c]
G08-P6-B		
No. 1	2.6	103
No. 2	2.7	--[c]
G08-P7-A		
No. 1	2.7	162
G08-P7-C		
No. 1[d]	0.22	5.8
No. 2	2.9	--[c]
G08-P8-A		
No. 1	2.8	--[c]
G08-P9-A		
No. 1[d]	1.0	0.26
G8-P10-A		
No. 1	4.3	445
No. 2	11	11.6
D08-P4-A		
No. 1[d]	--[d]	0.003
No. 2[d]	--[d]	--[d]
D08-P4-C		
No. 1	3.8	157
No. 2	3.8	--[c]
009-P1-A		
No. 1[d]	--[d]	--[d]
No. 2	4.2	258

TABLE 34. Continued

Sample ID	U/Zr Ratio[a]	Zr/Sn Ratio[b]
009-P1-B		
No. 1	4.0	158
G12-P2-B		
No. 1	3.5	--[c]
No. 2	3.8	--[c]
G12-P4-A		
No. 1	2.8	157
G12-P9-A		
No. 1	3.6	28
N05-P1-H		
No. 1	0.86	18
No. 2	4.2	20
N5-P01-D		
No. 1[d]	0.057	14
No. 2	13	2.5
007-P1-A		
No. 1[d]	--[d]	0.017
07-P6		
No. 1[d]	--[d]	--[d]
No. 2[d]	4.9	0.07
D4-P2-A		
No. 1[d]	--[d]	--[d]

a. The core average U/Zr ratio is 3.7 assuming oxidation of the zircaloy, and the ratio for a fuel rod is 4.0.

b. The average Zr/Sn ration in zircaloy cladding is 61.

c. Principally metallic samples (< 20 wt% U).

d. A component of the comparison was below the detection limit of the analysis method.

TABLE 35. CENTRAL CORE REGION CONTROL MATERIAL (Ag, In, Cd) WEIGHT RATIOS

Sample ID	Ag/In Ratio[a]	Ag/Cd Ratio[b]	In/Cd Ratio[c]
K09-P3-A			
No. 1	0.61	--[e]	--[e]
K09-P3-D			
No. 1	0.73	--[e]	--[e]
No. 2	0.50	23	46
K09-P3-F			
No. 1	1.0	--[e]	--[e]
G08-P5-B			
No. 1	5.9	--[e]	--[e]
No. 2	0.29	19	65
G08-P6-B			
No. 1	1.4	--[e]	--[e]
No. 2	0.56	30	54
G08-P7-A			
No. 1	1.4	--[e]	--[e]
G08-P7-C			
No. 1[d]	6.5	20	3.0
No. 2	1.0	--[e]	--[e]
G08-P8-A			
No. 1	0.42	34	80
G08-P9-A			
No. 1[d]	3.1	8.9	2.8
G08-P10-A			
No. 1	0.22	19	84
No. 2	3.7	122	33
D08-P4-A			
No. 1[d]	1.5	--[e]	--[e]
No. 2[d]	8.3	--[e]	--[e]
D08-P4-C			
No. 1	0.36	--[e]	--[e]
No. 2	0.69	--[e]	--[e]
009-P1-A			
No. 1[d]	1.8	92	51
No. 2	0.86	--[e]	--[e]

TABLE 35. Continued

Sample ID	Ag/In Ratio[a]	Ag/Cd Ratio[b]	In/Cd Ratio[c]
009-P1-B			
No. 1	1.2	--[e]	--[e]
G12-P2-B			
No. 1	0.45	18	40
No. 2	0.57	--[e]	--[e]
G12-P4-A			
No. 1	0.68	30	44
G12-P9-A			
No. 1	6.4	304	48
N05-P1-H			
No. 1	2.2	25	11
No. 2	--[e]	--[e]	--[e]
N05-P1-D			
No. 1[d]	3.2	73	23
No. 2	1.9	--[e]	--[e]
007-P1-A			
No. 1[d]	1.8	--[e]	--[e]
007-P6			
No. 1[d]	5.0	--[e]	--[e]
No. 2[d]	5.1	390	76
004-P2-A			
No. 1[d]	4.5	59	13

a. The average Ag/In ratio in a control rod is 5.3.

b. The average Ag/Cd ratio in a control rod is 16.

c. The average In/Cd ratio in a control rod is 3.0.

d. Principally metallic samples.

e. A component of the comparison was below the detection limit of the analysis method.

probably because the zirconium is easier to oxidize than tin, thereby causing the Zr/Sn ratio to be higher in the metallic phases.

3.4.2.2 Control Rod Materials. Control rod materials including the relatively volatile cadmium were measurable in most of the central core samples. Examination of the data in Tables G11 through G18 and 33 indicate that the least volatile control material, silver was measurable in both metallic and ceramic material samples at an average concentration of about 2.9 wt%, with a range of concentrations from 0.07 to 34 wt%. This is greater than the expected core average concentration of silver (1.9 wt%), and inspection of the data indicates accumulations of this element in the metallic regions in this part of the reactor core.

Indium was measurable in all samples at concentrations averaging 0.9 wt%, with the data ranging from 0.05 to 7.6 wt%. The core average concentration of this element is 0.3 wt%, which indicates that indium is concentrated in the central core region to a greater degree than silver.

Cadmium was measurable in only about half of the samples obtained from the central core. The concentrations ranged from 0.01 to 0.83 wt%, with an average concentration of about 0.16 wt%. This concentration is greater than the core average concentration of 0.12 wt%; however, the bulk of the element is located in the metallic regions.

Table 35 presents elemental ratios among silver, indium, and cadmium for the central core region samples. The Ag/In ratios range from 0.2 to 8, with the bulk of the data below the average ratio (5.3) for intact control rods. These data would suggest that indium is present at greater concentrations in this part of the core relative to silver. The higher density of silver relative to indium may be affecting the relative distribution of these elements, although the ratio difference may be an artifact of the precipitation of silver, as has been discussed.

The Ag/Cd ratios vary over a range of a factor of 20, excluding sample locations where cadmium was not detectable. The measured ratios are twice

those found in intact control rods, indicating that the cadmium has been partially depleted in the debris relative to silver. The average ratio is 79, which is substantially greater than the core average ratio of 16 (a factor of 5). The In/Cd ratios are greater due to the relatively greater amounts of indium in the debris. The ratios are generally factors of 10 to 30 greater than those found in intact control rods. The data for In/Cd are consistent with the Ag/Cd data and again indicate relatively less cadmium in the debris. The cadmium, as was previously noted, may be retained due to alloying with other less volatile components, which reduces the vapor pressure.

3.4.2.3 Poison Rod Materials. Poison rod materials measurable in the central core region included aluminum, boron, and gadolinium. Aluminum was measurable in all samples at concentrations averaging 0.3 wt%, which is similar to the core average concentration of 0.2 wt%. Boron from the poison rods and reactor coolant is present in most samples at concentrations between 0.03 and 0.23 wt%. Due to uncertainty in the quantity retained by core materials from interaction with the coolant, a core average cannot be calculated for boron. Gadolinium is also present in the central core in a range of concentrations from 0.01 to 0.12 wt%, with an average of 0.08 wt%. This concentration is greater than the average concentration of 0.01 wt%, which suggests accumulation of this element in the central core region. The concentrations of gadolinium are similar in both metallic and ceramic samples, suggesting that it may be present both as a metallic and the oxide.

3.4.2.4 Structural Materials. Measurements were made for all structural material constituents in the core (i.e., iron, chromium, nickel, manganese, niobium, and molybdenum). The average concentration data in Table 34 indicates that iron is the principal structural material present (average 14.5 wt%), and that it ranges up to 58 wt% in the metallic samples. Lesser concentrations of nickel (average - 6.8 wt%) and chromium (average - 1.4 wt%) are also present. Examination of the ratio data for the principal components of the metallic samples (Table 36) indicates that Fe/Cr, Fe/Ni, and Ni/Cr ratios are similar to stainless steel. The presence of molybdenum in the lower crust suggests that the Inconel grid spacers contributed to the formation of the crust.

TABLE 36. CENTRAL CORE REGION METALLIC MATERIAL (Fe, Cr, and Ni) WEIGHT RATIOS[a]

Sample ID	Fe/Cr Ratio	Fe/Ni Ratio	Ni/Cr Ratio	Ni/Mo Ratio
K09-P3-A				
No. 1	1.5	3.5	0.41	22
K09-P3-D				
No. 1	2.1	3.5	0.61	8.8
No. 2	2.1	4.6	0.46	7.8
K09-P3-F				
No. 1	2.4	2.0	1.2	22
G08-P5-B				
No. 1	2.0	2.6	0.76	24
No. 2	2.0	7.2	0.28	--[b]
G08-P6-B				
No. 1	2.3	4.8	0.48	--[b]
No. 2	2.1	4.5	0.47	7.1
G08-P7-A				
No. 1	2.3	5.1	0.45	--[b]
G08-P7-C				
No. 1[c]	7.5	2.2	3.4	11
No. 2	2.4	5.0	0.47	--[b]
G08-P8-A				
No. 1	2.1	5.0	0.42	--[b]
G08-P9-A				
No. 1[c]	7.3	2.2	3.3	11
G08-P10-A				
No. 1	3.6	17	0.21	3.8
No. 2	10	3.7	2.7	10
D08-P4-A				
No. 1[c]	8.7	2.4	3.7	11
No. 2[c]	1290	1.4	940	10
D08-P4-C				
No. 1	2.0	4.8	0.41	--[b]
No. 2	1.7	2.4	0.71	--[b]
009-P1-A				
No. 1[c]	8.5	2.3	3.7	11
No. 2	2.1	4.6	0.45	6.0

TABLE 36. Continued

Sample ID	Fe/Cr Ratio	Fe/Ni Ratio	Ni/Cr Ratio	Ni/Mo Ratio
009-P1-B				
No. 1	1.9	4.5	0.42	2.0
G12-P2-B				
No. 1	2.0	2.9	0.67	4.6
No. 2	2.4	7.1	0.34	3.3
G12-P4-A				
No. 1	2.4	5.2	0.46	10
G12-P9-A				
No. 1	5.4	1.9	2.9	31
N05-P1-H				
No. 1	1.6	0.80	2.0	--[b]
No. 2	1.6	8.2	0.20	--[b]
N05-P1-D				
No. 1[c]	11	2.3	4.8	9.7
No. 2	13	2.2	5.7	9.2
007-P1-A				
No. 1[c]	257	1.8	143	12
007-P6				
No. 1[c]	15	2.5	5.9	7.6
No. 2[c]	9.1	2.5	3.6	7.7
004-P2-A				
No. 1[c]	16	1.9	8.6	10

a. The elemental ratios for stainless steel and Inconel are:

	Stainless steel	Inconel
Fe/Cr	3.6	0.35
Fe/Ni	7.6	0.35
Ni/Cr	0.5	2.7
Ni/Mo	--	17.3

b. Component not detected.

c. Metallic samples.

3.4.3 Central Core Region Radiochemical Examinations

The radionuclide distribution in the central core region was determined for the samples discussed in Section 3.4.2. Results of the radiochemical analysis of the samples are listed in Appendix H, Tables H1 through H5. To provide information on the characteristic behavior of fission products, they have been categorized by the volatility of the chemical group and element, as discussed in Section 3.1.3.

Table 37 lists the average radionuclide concentrations, the range of concentrations, and the ratio of high to low values in the central core region samples. The ratios of high to low values are from 10^1 to 10^4, indicating a relatively wide range of radionuclide concentrations. However, the radionuclides with high to low ratios greater than 10^2 are only the metallic species (^{106}Ru and ^{125}Sb) that accumulate in the metallic portions of the crust.

3.4.3.1 Central Core Uranium-235 Enrichment. Measurements were performed to evaluate the concentrations of ^{235}U and ^{238}U in the central core and to determine ^{235}U enrichment. The ^{235}U and ^{238}U concentrations are listed in Appendix H, and the ^{235}U enrichments are listed in Table 38. Table 38, indicates a range of enrichments from 1.8 to 2.6; however, the bulk of the data is in the range from 2.2 to 2.4. These data suggest that the central core debris samples are mostly a composite of the 1.98% and 2.64% enriched assemblies.

3.4.3.2 Comparisons with ORIGEN2. The measured radionuclide concentrations in the central core region crust were compared with concentrations predicted by the ORIGEN2 Code in order to assess retention of radionuclides in the ceramic and metallic areas of the central core region crust. The ORIGEN2 data and analysis methods are discussed in Section 3.1.3 and Table 14 lists the ORIGEN2 values used for comparison with the core bore data.

TABLE 37. CENTRAL CORE REGION AVERAGE RADIONUCLIDE CONCENTRATIONS (microcuries/g sample on April 1, 1987)

Radionuclide	Average	Range	High/Low Ratio
^{60}Co	313	2.8 to 1,695	605
^{90}Sr	2,660	5.5 to 9,320	1,690
^{106}Ru	958	0.16 to 7,705	48,000
^{125}Sb	353	0.16 to 2,910	18,100
^{129}I	2.2 E-4	5.2 E-7 to 1.9 E-3	3,600
^{134}Cs	5.9	0.21 to 95	452
^{137}Cs	291	0.012 to 4,923	4.1E+5
^{144}Ce	232	60 to 3,534	59
^{154}Eu	52	1.9 to 780	410
^{155}Eu	72	7.8 to 1,055	135

[a] Detection limit value not included in range.

TABLE 38. CENTRAL CORE REGION URANIUM-235 ENRICHMENT

Sample ID	^{235}U Enrichment[a]
K09-P3-A	
No. 1	2.2
K09-P3-D	
No. 1	2.3
No. 2	2.3
K09-P3-F	
No. 1	--[b]
K09-P4-D	
No. 1	2.4
No. 2	4.4[c]
G08-P5-B	
No. 1	2.1
No. 2	2.2
G08-P6-B	
No. 1	2.3
No. 2	2.2
G08-P7-A	
No. 1	2.2
G08-P7-C	
No. 1	2.5
No. 2	2.3
G08-P8-A	
No. 1	2.2
G08-P9-A	
No. 1	--[b]
G8-P10-A	
No. 1	--[b]
No. 2	1.8
D08-P4-A	
No. 1	--[b]
No. 2	--[b]
D08-P4-C	
No. 1	--[b]
No. 2	--[b]

TABLE 38. Continued

Sample ID	^{235}U Enrichment[a]
009-P1-A	
No. 1	--[b]
No. 2	2.2
009-P1-B	
No. 1	--[b]
G12-P2-B	
No. 1	2.2
No. 2	2.2
G12-P4-A	
No. 1	2.4
G12-P9-A	
No. 1	2.1
N05-P1-H	
No. 1	2.2
No. 2	2.6
N05-P1-D	
No. 1	2.3
No. 2	2.5
007-P1-A	
No. 1	--[b]
007-P6	
No. 1	--[b]
No. 2	3.4[c]
D04-P2-A	
No. 1	--[b]

a. The core average ^{235}U enrichment is approximately 2.56% with the peripheral assemblies having an enrichment of 2.98 and the central assemblies having enrichments of 1.98% and 2.64%.

b. Not measured or detected.

c. Large uncertainty (>50%) associated with value.

A summary of the measured radionuclide retentions (based on uranium content) in the central core region is presented in Table 39 and the average retentions are listed in Table 40. The data listed in Table 39 indicate a wide range of retentions (accumulations), principally for the metallic radionuclides. The low volatile radionuclides have average retentions from 78 to 185%, which suggests that much of the central core region was formed from fuel material from a relatively high burnup region close to the center of the reactor core. Greater inaccuracies are expected from those samples with low uranium contents, as indicated in Table 39. The following sections discuss the radionuclide distributions for the principal low, medium, and high volatility groups.

3.4.3.3 Low Volatiles. The low volatiles for which radionuclide comparisons were performed are ^{144}Ce and ^{154}Eu. Tables 39 and 40 indicate a range for the low volatiles of a factor of <2 for most ceramic samples. The low volatiles were measurable in only one of the metallic samples. There is general consistency in the ceramic sample data that suggests that the relatively low volatile ^{144}Ce and ^{154}Eu have been retained entirely in the fuel material. The high retentions (i.e., >100%) suggest that the fuel material forming the central core debris came from a relatively high burnup region of the core. The sample with low cerium and europium retentions is from G08-P10-A No. 2, which has a high degree of uncertainty associated with the elemental analysis results.

3.4.3.4 Medium Volatiles. The fission products that are expected to have a medium volatility are ^{90}Sr, ^{125}Sb, and ^{106}Ru. Strontium-90 is expected to be the least volatile, as it should be present in oxide form at the oxidation potential conditions expected during the accident. The ^{90}Sr data, shown in Tables 39 and 40, indicate a range of concentrations with the lowest retentions associated with the metallic samples. The data generally suggest that a significant fraction of the ^{90}Sr has not been retained in the uranium fractions of metallic samples or in some of the ceramic samples. The apparent mobility of ^{90}Sr is discussed in Section 4.

TABLE 39. RADIONUCLIDE RETENTION IN THE CENTRAL CORE REGION[a]

Sample ID	Radionuclide Retention(%) 90 Sr	106 Ru	125 Sb	129 I	137 Cs	144 Ce	154 Eu
K09-P3-A No. 1	21	--[b]	3.6	0.50	0.65	194	154
K09-P3-D No. 1	110	5.1	8.2	2.9	0.64	153	179
No. 2	44	2.7	3.3	0.77	1.0	146	180
K09-P3-F No. 1	188	3.6	2.6	1.1	0.56	155	165
K09-P4-D No. 1[c]	160	1,180	1,700	31	0.14	160	260
No. 2	23	9.0	2.2	.094	0.60	139	170
G08-P5-B No. 1	62	8.5	2.1	0.37	0.38	85	109
No. 2	62	--[b]	29	0.37	12	--[b]	--[b]
G08-P6-B No. 1	95	2.9	3.8	0.85	0.56	152	166
No. 2	120	4.5	2.2	--[b]	0.34	132	156
G08-P7-A No. 1	97	0.15	--[b]	0.52	2.3E-4	--[b]	--[b]
G08-P7-C No. 1[c]	47	21,500	21,500	57	6.1	--[b]	--[b]
No. 2	109	23	3.2	.63	0.44	141	162
G08-P8-A No. 1	130	--[b]	2.4	0.64	0.61	143	183
G08-P9-A No. 1[c]	259	118,600	110,500	260	83	--[b]	--[b]
G08-P10-A No. 1	136	--[b]	--[b]	0.15	10	--[b]	--[b]
No. 2	28	46	202	7.5	2.6	36	24
D08-P4-A No. 1[c,d]	0.07	1,697	1,300	1.8	0.10	--[b]	--[b]
No. 2[c,d]	0.31	4,120	2,880	22	--[b]	--[b]	--[b]
D08-P4-C No. 1	--[b]	5.7	1.8	0.77	0.63	170	240
No. 2	48	--[b]	--[b]	.11	0.40	92	138

TABLE 39. Continued

Sample ID	Radionuclide Retention(%) 90 Sr	106 Ru	125 Sb	129 I	137 Cs	144 Ce	154 Eu
009-P1-A							
No. 1[c,d]	0.11	1,950	1,260	8.9	--[b]	--[b]	--[b]
No. 2	12	--[b]	3.8	0.99	0.14	66	99
009-P1-B							
No. 1	80	--[b]	18	9.0	0.17	99	165
G12-P2-B							
No. 1	40	0.45	.033	0.19	118	99	176
No. 2	0.16	--[b]	0.67	--[b]	0.12	106	162
G12-P4-A							
No. 1	132	--[b]	2.9	0.52	0.32	148	177
G12-P9-A							
No. 1	77	169	372	17.5	3.3	143	89
N05-P1-H							
No. 1	136	19	1,540	31	23	75	80
No. 2	202	9.6	14	10	36	142	173
N05-P1-D							
No. 1[c]	85	26,450	42,190	277	53	--[b]	--[b]
No. 2	192	1,370	738	132	101	126	100
007-P1-A							
No. 1[c,d]	0.06	2,200	1,760	4.4	0.07	--[b]	--[b]
007-P6							
No. 1[c,d]	0.15	2,720	2,290	20	--[b]	--[b]	--[b]
No. 2	98	--[b]	--[b]	--[b]	6.9	--[b]	--[b]
D04-P2-A							
No. 1[c,d]	0.45	815	0.16	31	0.03	--[b]	--[b]

a. Retention is calculated based on the uranium content of the sample material, as determined from the elemental analysis results in Appendix G. Additional figures are shown for calculational purposes beyond those statistically appropriate.

b. Not detected.

c. Contains significant amounts of metallic material (>30%).

d. Normalized to a value of 1, as no uranium was present in the sample (i.e., the analysis assumes the sample is composed entirely of uranium).

TABLE 40. AVERAGE RADIONUCLIDE RETENTION IN METALLIC AND CERAMIC SAMPLES

	Metallic Samples[a]	Ceramic Samples[b]
Radionuclide	Average	Average
^{90}Sr	59	86
^{106}Ru	34,400	107
^{125}Sb	27,600	129
^{129}I	186[c]	9.1
^{137}Cs	19	7.1
^{144}Ce	78[d]	125
^{154}Eu	185[d]	146

a. Nominal metallic samples are identified in Table E38.

b. Nominal ceramic samples include all other samples in the central core region, although there is some metallic material in all samples that may bias the results.

c. The ^{129}I retention is biased by the presence of a single high normalized retention value, which is high because of the presence of only a small amount of uranium for normalization.

d. Average based on only two values.

For ^{125}Sb, comparisons were performed with the concentrations of elemental constituents of the crust, and the only observed correlation was a general increase in metallic content with an increase in ^{125}Sb content. For samples with 100 wt% metallic content, identified in Table 39, the data were normalized to the total weight of the sample (i.e., assumes the sample was composed completely of uranium). Generally, these data indicated that the ^{125}Sb content was from 15 to 20 times that of intact fuel. Those sample results with much higher indicated retentions were based on trace quantities of uranium, which produces a much higher calculated retention (i.e., G08-P7-C, G08-P9-A, and N05-P1-D). These data suggest a retention mechanism for ^{125}Sb that is generally related to metallic material content.

Ruthenium-106 was measurable in most samples, generally low in ceramic samples and high in metallic samples and generally following a distribution similar to ^{125}Sb. These data indicate significant accumulation of ^{106}Ru in the metallic layers at concentrations between 20 and 40 times the concentration in intact fuel. The samples normalized to trace uranium content indicate much higher retentions, as they were biased by the low uranium content of the sample.

3.4.3.5 High Volatiles. The two high volatile radionuclides measurable were ^{137}Cs and ^{129}I. The ^{129}I was measurable in most samples at retentions lower than those found in intact fuel material. The presence of ^{129}I in the metallic samples at relatively high retentions is exaggerated by normalization to the low uranium content of the samples. In actual fact the radionculide concentrations in the ceramic and metal samples are similar and suggest that ^{129}I is distributed in the material, perhaps because of solubility, regardless of composition. These data suggest that ^{129}I is somewhat evenly distributed in the central core.

The ^{137}Cs retentions shown in Tables 39 and 40 indicate similar relative retentions to those of ^{129}I for both the metallic and ceramic samples. The data for the ceramic sections suggests only limited retention

of cesium at any location in the central core region at less than 10% retention.

3.5 Intact Core Component Examination Results

Distinct core components, defined as the intact fuel rods, control rods, and guide and instrument strings from the lower core region, were examined to evaluate possible damage to these components located in a relatively cold part of the reactor core. This summary was extracted from the visual examinations presented in Appendix C, the density measurements described in Appendix D, the metallographic examinations discussed in Appendix E, and the autoradiographic results presented in Appendix F. The bulk elemental and radiochemical analysis results are summarized in Sections 3.5.2. and 3.5.3

3.5.1 Visual and Metallurgical Examinations

Examinations of components were performed on (a) three fuel rod segments from the D04, G08, and K09 core locations; (b) four silver/indium/cadmium control rods from the D04, K09, N12, and 007 core locations; and (c) one instrument tube from the G08 core location. These examinations were performed to evaluate degradation of intact components in the lower region of the core which was probably covered with water, and to determine peak temperatures attained by these materials.

The metallographic examinations of all the intact fuel rods from the various core locations showed similar behavior. The fuel still retained the as-fabricated porosity within the grains, as shown in Figure 38, which indicates relatively low power conditions. The zircaloy cladding had not recrystallized and was still in the as-fabricated condition. A typical example of the zircaloy microstructure from the intact region just below the lower crust in the K09 core location is shown in Figure 39. This indicates cladding temperatures in this region were below the recrystallization temperature of 920 K. Minor amounts of zircaloy hydriding were also observed in the cladding, as shown in Figure 40. Based upon out-of-pile

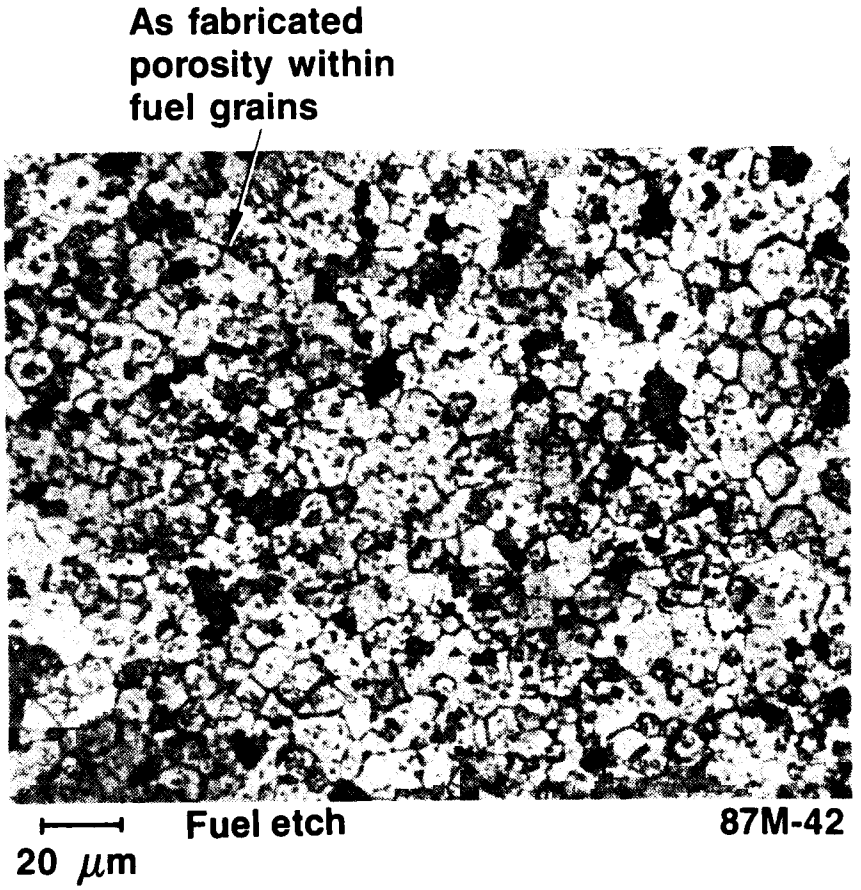

Figure 38. Fuel microstructure in fuel rod segment (D04-R9-2B).

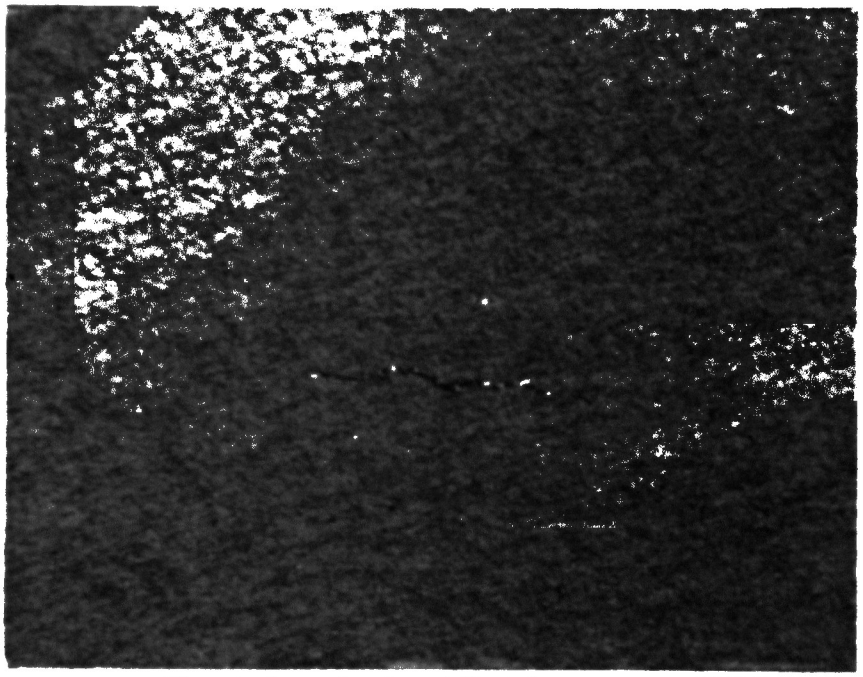

Figure 39. As-fabricated zircaloy cladding in intact region just below lower crust (K09-R5-5L).

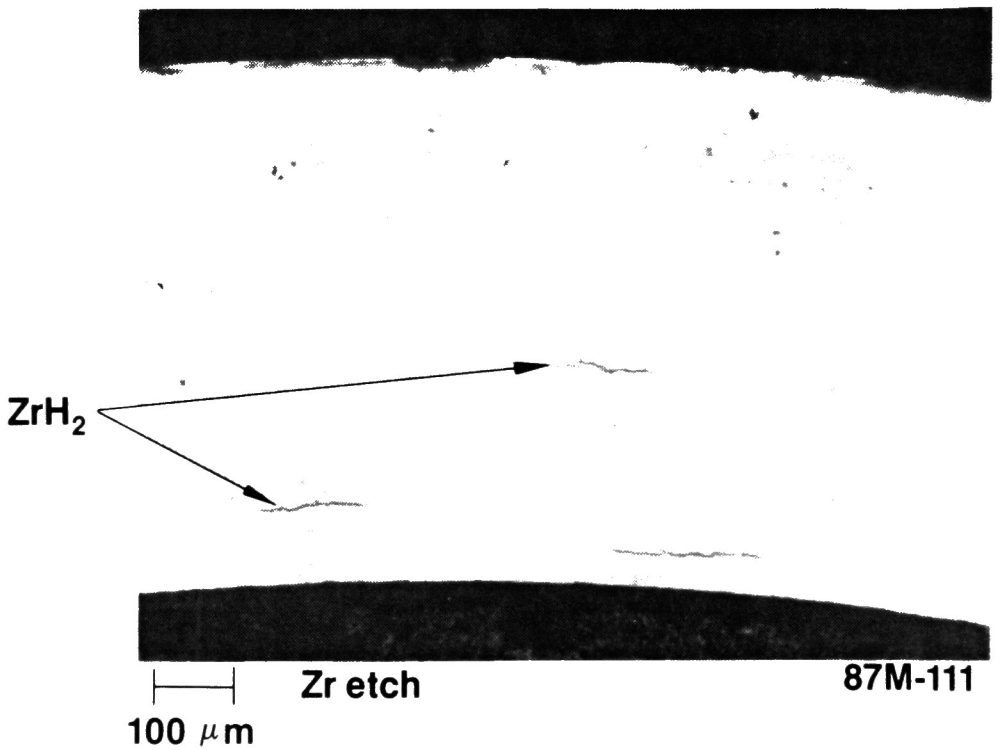

Figure 40. Zirconium hydrides in zircaloy cladding in intact region just below lower crust (K09-R5-5L).

zircaloy hydriding experiments,[17] the zirconium hydride concentrations in these regions were less than 25 ppm. No significant oxidation was apparent on the surface of the cladding.

Examination of control rods from various locations indicated that some of the Ag-In-Cd was intact and some was molten. Figure 41 shows intact Ag-In-Cd control material from near the bottom of an intact rod in central core location K09, whereas Figure 42 shows molten control rod material from near the upper end of an intact control rod segment from peripheral core bore location N12. The different behavior is attributable to variations in core location and axial height; the intact control material was approximately 38 cm above the bottom of the core bore, whereas the molten control material was approximately 117 cm above the bottom of the core bore. In the other two control rod segments that were examined, the Ag-In-Cd was molten 56 cm above the bottom of the core bore in core location O07, and may have been partially molten or recrystallized at approximately 11 cm in core bore location D04. The axial height of the D04 sample is nearly the same as for the zircaloy cladding sample (D04-R9-2B), which exhibited as-fabricated zircaloy structure with temperatures below 920 K. These data provide some indication of temperatures at specific reactor locations, and further details are provided in Appendix E.

Rod G08-R3 was determined to be an instrument tube installed without instrumentation. After the accident the tube contained previously molten metallic debris, as partially shown in Figure 43. Minor amounts of hydriding were observed in this instrument tube, similar to that observed on the fuel rod cladding, as well as an interaction zone on the inner surface of the tube. This interaction zone is also shown in Figure 43. Similar structures were observed on the surface of samples during zircaloy hydriding experiments 17, and this interaction zone may be due to localized concentrations of zirconium hydrides.

These metallographic examinations indicate that very little zircaloy oxidation occurred in these regions, which agrees with the ductile nature of these rods noted during the visual examinations. Temperatures varied as a

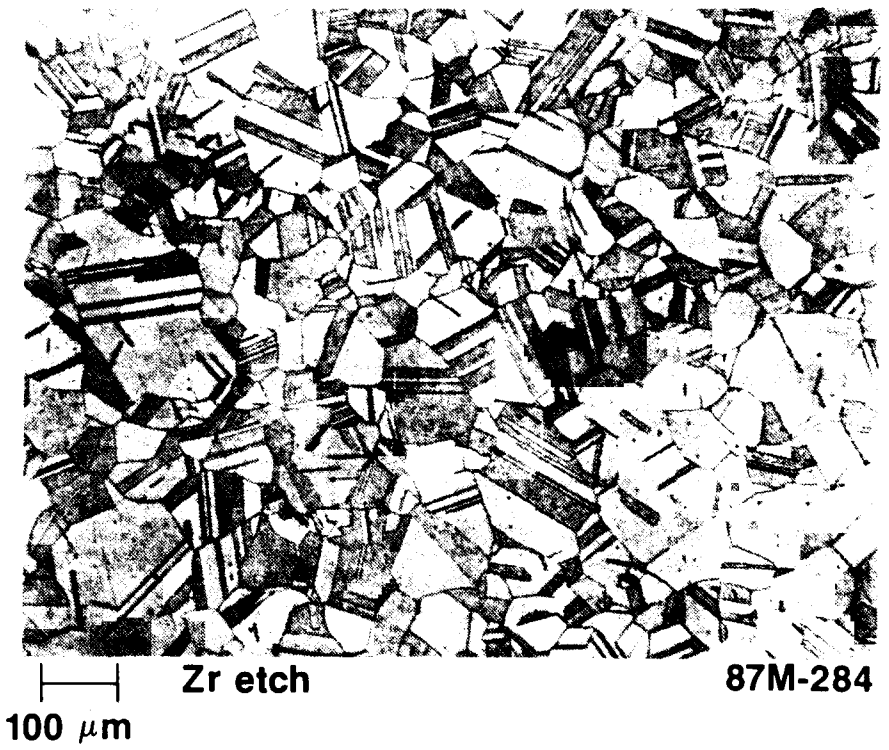

Figure 41. Intact Ag-In-Cd in control rod segment K09-R13-2B.

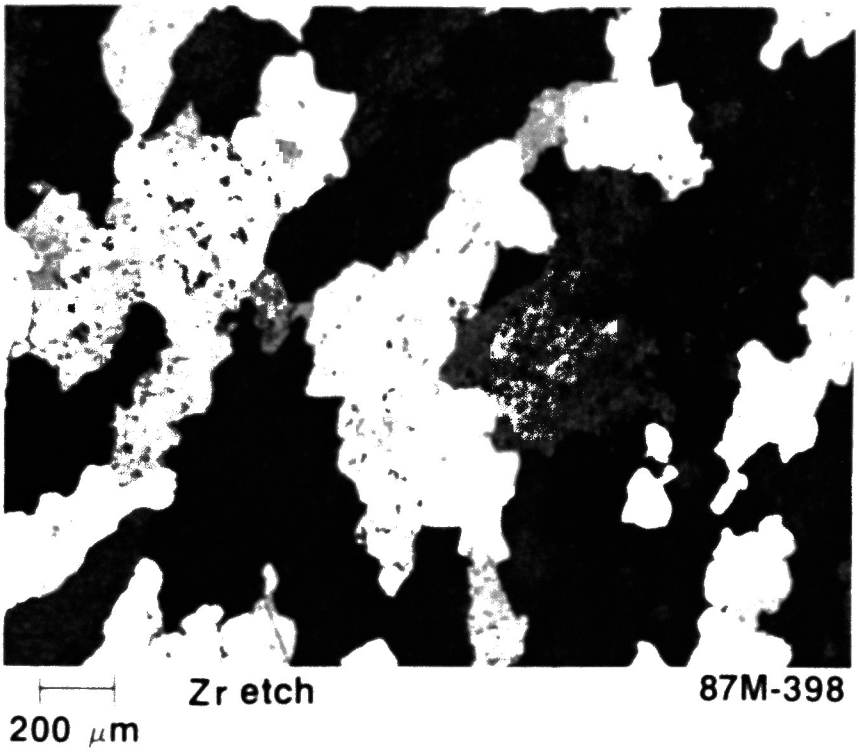

Figure 42. Molten control rod material near top of rod segment M12-87-10Y.

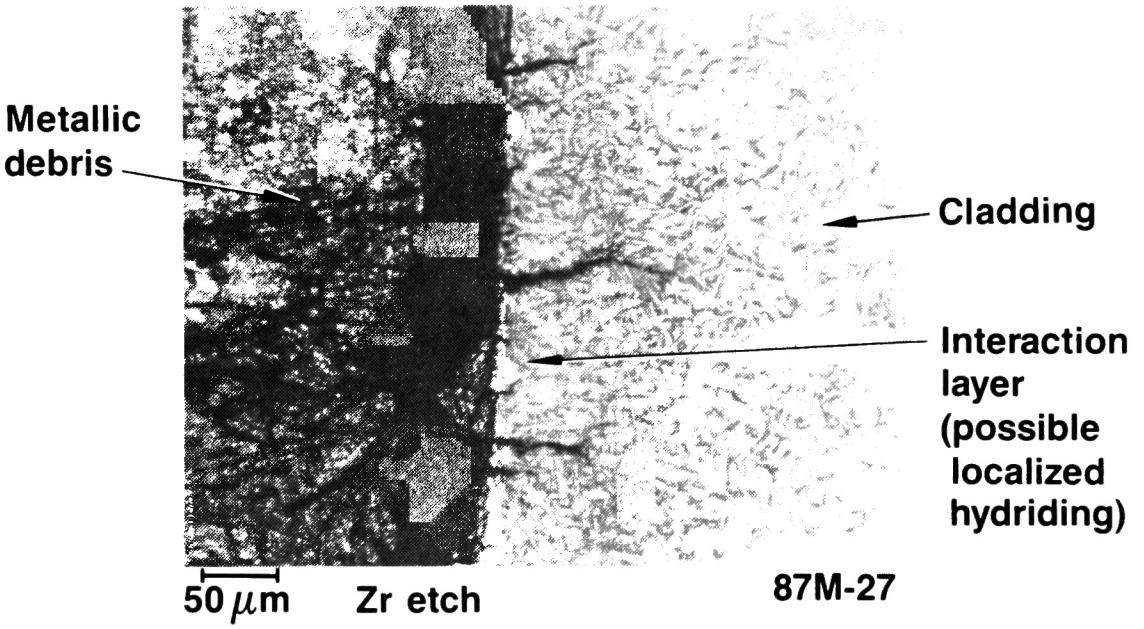

Figure 43. Cladding cracks at interaction zone of G08-R3 instrument tube.

function of reactor core position and axial heights, but in general the temperatures were relatively cool. Molten control rod material indicated temperatures in excess of 1073 K on the upper endtips of some of the intact control rod segments on the periphery of the core, whereas the as-fabricated condition of the zircaloy cladding in many parts of this region indicated temperatures were below the recrystallization temperature of 920 K. The extent of zircaloy hydriding was insignificant.

3.5.2 Lower Core Structural Material Bulk Composition

Elemental analyses were performed on several samples of structural material to evaluate possible changes in composition in the lower core region. Table 41 lists the composition of the three samples of debris. Analyses were performed for 17 elements that constitute the principal components of the TMI-2 core. G08-R11-2 and G12-R13-2 are samples of fuel material that had been contaminated with small amounts of control material, probably during sample acquisition. Visual examinations and measurement data indicate that G08-R3-2 is prior-molten material that flowed down into a guide tube. This sample is very similar in composition to the material in the lower crust and suggests that the lower crust material may have flowed downward into lower parts of the reactor core.

Elemental analyses were not performed on the structural material surfaces. Only the elemental composition of the matrix material could be measured because these samples were not exposed to high temperatures or differing environments as were the samples in the upper part of the lower core region.

3.5.3 Lower Core Structural Material Radiochemical Analyses

Examination of the surface deposits on the intact lower core structures was performed to evaluate the distribution of fission products on the surfaces. This analysis was performed by leaching the fission products from the surface using strong mineral acids that could dissolve the surface of the material. Table 42 lists the radionuclide concentrations measured for

TABLE 41. STRUCTURAL SAMPLE COMPOSITION[a]
(wt%)

	Concentration		
Element	G08-R3-2	G08-R11-2	G12-R13-2
Ag	0.33	--[b]	--[b]
Al	0.38	--[b]	--[b]
B	0.01	--[b]	--[b]
Cd	0.42	--[b]	--[b]
Cr	1.4	--[b]	--[b]
Cu	0.03	--[b]	--[b]
Fe	5.3	--[b]	--[b]
Gd	0.01	--[b]	--[b]
In	1.5	0.6[c]	0.6[c]
Mn	0.05	--[b]	--[b]
Mo	0.15	--[b]	--[b]
Nb	0.15	--[b]	--[b]
Ni	3.2	--[b]	--[b]
Si	0.06[d]	0.5[d]	0.5[d]
Sn	1.2	--[b]	--[b]
Te	0.02	0.3[c]	0.4[c]
U	4.2	78	79
Zr	40.6	--[b]	--[b]

a. Bulk composition of material present in intact cladding/guide tube materials.

b. Not detected.

c. High degree of uncertainty associated with result due to the presence of large amounts of U.

d. Probable contaminant introduced during cutting or dissolution.

TABLE 42. STRUCTURAL MATERIAL SURFACE RADIONUCLIDE CONCENTRATIONS (microcuries /cm^2 sample on April 1, 1987)

Radionuclide	G8-R3-2	G8-R3-4	G8-R3-6	N12-R7	K9-R5-4
^{60}Co					
	2.1±0.1E+1	7.0±0.1E-2	9.5±0.1E-2	5.0±0.1E-2	1.9±0.01E-1
Insol[a]	--[b]	1.4±0.1E0	5.2±0.1E-1	8.0±0.1E-1	1.35±0.1E0
^{90}Sr	3.4±0.3E0	8.8±0.7E-1	9.8±0.8E-2	4.1±0.3E-1	1.2±0.1E0
Insol[a]	--[c]	--[c]	--[c]	--[c]	--[c]
^{106}Ru	2.4±0.6E-1	1.8±0.2E-2	2.3±0.1E-2	6.3±1.1E-3	2.5±0.3E-2
Insol[a]	--[b]	<4.7E-2	1.6±0.4E-2	<1.7E-2	4.8±0.2E-1
^{125}Sb	6.4±1.8E-2	6.3±0.1E-2	5.1±0.1E-2	4.4±0.1E-4	6.8±0.2E-2
Insol[a]	--[b]	1.6±0.1E+1	5.4±0.1E0	1.4±0.1E+1	2.2±0.1E+1
^{129}I	--[d]	--[d]	--[d]	--[d]	--[d]
Insol[a]	--[c]	--[c]	--[c]	--[c]	--[c]
^{134}Cs	<1.5E-2	9.8±0.2E-3	1.2±0.1E-2	1.4±0.1E-2	5.3±0.1E-2
Insol[a]	--[b]	<4.9E-3	5.6±0.7E-3	<3.9E-3	1.8±0.1E-1
^{137}Cs	3.4±0.1E-1	3.3±0.1E-1	3.9±0.1E-1	6.1±0.1E-1	2.4±0.1E0
Insol[a]	--[b]	1.0+0.1E-1	2.3+0.1E-1	3.0+0.2E-2	1.1+0.1E+1
^{144}Ce	2.2±0.3E-1	1.1±0.2E-2	1.3±0.1E-2	9.3±0.9E-3	2.4±0.3E-2
Insol[a]	--[b]	<2.1E-1	<7.7E-2	<1.5E-1	2.5±0.4E-1
^{154}Eu	5.5±0.9E-2	3.4±0.3E-3	3.8±0.1E-3	1.3±0.1E-3	4.3±0.5E-3
Insol[a]	--[b]	<2.1E-1	<7.7E-2	<3.7E-3	2.5±0.4E-1
^{155}Eu	7.8±0.7E-2	4.1±0.6E-3	4.8±0.2E-3	2.1±0.2E-3	<9.4E-3
Insol[a]	--[b]	--[d]	--[d]	--[d]	9.9±1.2E-2
^{235}U	--[d]	--[d]	--[d]	--[d]	--[d]
^{238}U	--[d]	--[d]	--[d]	--[d]	--[d]

a. Activity not removed from sample determined by gamma spectroscopy of the sample after leaching.

b. Sample lost in analysis.

c. Not measured, as sample material not removable from the cladding.

d. Not detected.

the leach samples and the radionuclides retained on the material after leaching. A significant fraction of the activity was not removable by leaching, as indicated by the insoluble fractions of the total activity identified in the table. The data suggest that small amounts of fuel material may have been deposited on K09-R5-4 and that, with this exception, the surface concentrations are relatively consistent on the lower core surfaces. The data indicate that the ^{125}Sb deposition was highly insoluble in the nitric acid leaching solution used, and the measurable ^{60}Co was present principally in the matrix of the material.

If the average surface concentrations listed in Table 43 are extrapolated to the surface area (8.98 E+6 cm^2) of one-third of the fuel assemblies present in the reactor core (a highly conservative estimate of the surface area in the lower core region), the maximum surface deposition is from ^{137}Cs at 28 Ci of activity, which is substantially less than 1% of the ^{137}Cs core inventory. These data suggest that surface deposition of radionuclides on the intact fuel assemblies in the lower core region is insignificant and that the intact fuel assemblies did not participate in the accident. Evaluations of the radionuclide content of intact fuel pellets in the lower core region[18] indicate no loss of even the relatively volatile fission gases in this part of the reactor core.

3.6 Fission Gas Analyses

Fission gas analyses were performed on both samples of intact fuel and loose debris from the lower core region. These measurements, which included burnup evaluations of the intact pellets and mass spectrometric measurements of the fission gas content of both the intact pellets and loose debris, indicated that the intact fuel pellets at all locations in the lower core region (up to below the surface of the bottom crust) retained their complete inventories of volatile fission gases and radioiodine. However, in the loose debris from the upper crust and the central core region, the data indicate no retention of fission gases and only minor retention (<10%) of the ^{129}I. Table 44 lists the sample locations for both the the intact fuel pellets and fuel debris samples.

TABLE 43. CENTRAL CORE REGION AVERAGE RADIONUCLIDE CONCENTRATIONS (microcuries cm^3 sample on April 1, 1987)

Radionuclide	Average[a]	Low/High Value	Range
^{60}Co	5.1	0.6 to 21	35
^{90}Sr	1.2	0.09 to 3.4	38
^{106}Ru	0.16	0.006 to 0.48	80
^{125}Sb	11.5	5.4 to 22	4.1
^{129}I	--[b]	--[b]	--
^{134}Cs	0.07	0.014 to 0.23	16
^{137}Cs	3.1	0.34 to 13	39
^{144}Ce	0.11	0.011 to 0.27	25
^{154}Eu	0.06	0.0013 to 0.25	192
^{155}Eu	0.04	0.0021 to 0.09	43

a. Detection limit value not included in average or range.

b. Results below detection limit of analysis.

TABLE 44. SAMPLE LOCATIONS FOR INTACT PELLET AND DEBRIS FISSION GAS ANALYSES

Sample Identification	Core Location
Intact Fuel[a]	
D04-R9-4J	D04
D04-R9-6O	D04
G08-R9-2E	G08
N05-R2-2E	N05
N05-R2-8T	N05
Loose Debris[b]	
G12-P3-B	G12 debris particle
K09-P3-D	K09 debris particle

a. Contains full inventory of fission gases.

b. Contains no measurable fission gas.

4. CONTRIBUTIONS TO UNDERSTANDING THE TMI-2 ACCIDENT

This section describes the contributions of the lower core examinations to understanding the end-state condition of the TMI-2 core, the accident scenario, core damage progression, core materials behavior, and fission product behavior. A brief summary of the known end-state condition of the core is presented, followed by sections describing (a) damage progression in the lower core, (b) bulk core materials behavior, and (c) fission product behavior.

The observations made during the reactor defueling operations and the recent inspection of the lower core region during the core-boring operation have provided a clear description of the end-state core configuration (References 1 and 2). These data indicate four distinct regions within the core and three locations outside the core proper. The regions in the core are: the upper core void, the upper vessel debris bed, the prior-molten lower core region, and the standing fuel rod stubs. The regions outside the core are: the debris transported to the lower reactor vessel head, the debris located around the upper core support assembly (CSA), and the debris located on the lower CSA. Figure 1 in Section 1 shows the end-state condition of the reactor vessel based on the examinations performed to date, and Table 45 lists the core materials distribution in the various repositories.

- Upper Core Void. A cavity existed at the top of the original core region with a volume of approximately 9.2 m^3. The cavity volume represented ~26% of the original core volume and extended nearly across the full diameter of the upper core region. The average depth of the cavity was approximately 1.5 m, and in places it approached 2 m. Standing fuel rod assemblies remained at the core periphery, and none of the 177 original assemblies appeared to be totally intact. About 42 fuel assemblies had some full-length rods intact.

TABLE 45. ESTIMATED POSTACCIDENT CORE MATERIALS DISTRIBUTION

Core region	Estimated Quantity(kg)	Uncertainty[a] (%)	Percent of Total core(%)
Intact fuel assemblies (Partially or fully intact)	44,500	5	33.4
Central core region resolidified mass	32,700	5	24.5
Upper core debris bed	26,600	5	19.9
Prior-molten material on the Lower reactor vessel head	19,100	20	14.3
Lower core support assembly[b]	5,800	40	4.3
Upper core support assembly[b]	4,200	40	3.2
Outside the reactor vessel	450	--[c]	0.3

a. The uncertainty estimates are based on defueling. Those areas that have been defueled at this time have relatively low uncertainties, whereas those that have not have relatively high uncertainties.

b. The lower core support assembly is that portion of the reactor vessel below the core that includes the lower grid assembly and five flow distributor plates. The upper core support assembly is a coolant flow region outside the vertical baffle plates that make up the peripheral boundary of the core.

c. Estimates of the amount of fuel material outside the reactor vessel are based on nondestructive evaluations of reactor components in the reactor and auxiliary buildings. They range from 60 to ~430 kg.

- Upper Vessel Debris Bed. The upper vessel debris bed ranged from 0.6 to 1.0 m in depth, and rested on a solid crust located below the core midplane. The debris bed was sampled at 11 locations, ranging from the surface of the debris bed to 94 cm into the debris bed (Reference 15). Many of the particles examined contained regions of prior-molten U-Zr-O, indicating peak temperatures greater than 2200 K. Of these, some were prior-molten $(U,Zr)O_2$, indicating peak temperatures greater than 2800 K. There were a few examples of prior-molten material of almost pure UO_2, indicating temperatures up to 3100 K. However, based on the relatively unrestructured appearance of much of the fuel, considerable amounts of the upper debris bed fuel debris remained at fairly low temperatures (<2000 K) or was exposed to high temperatures for only a short time.

- Prior-molten material in the lower core region. As discussed in this document, the prior-molten part of the lower core region is composed of a central prior-molten region surrounded by crust layers of differing composition. Analyses were performed to determine the volume and mass of the crust layers. These analyses indicated that the upper crust had a nominal volume of 2.95 E+5 cm^3, an average density of 8.4 g/cm^3, and a nominal mass of 2450 kg. The lower crust, a crucible shaped crust had a nominal volume of 1.2 E+6 cm^3, density of 7.3 g/cm^3, and nominal mass of 8760 kg. The difference in the two masses is due principally to the volume of the lower crust, differences in crust thickness, and variation in the average density. Defueling information in Reference 2 indicated that the prior-molten portion of the central core region was composed of 24.5% of the total postaccident core mass of 133,500 kg, and that the upper and lower crusts were 1.8% and 6.6% of the total core, respectively.

- Standing fuel rods and fuel rod stubs. Table 45 lists the postaccident distribution of core materials at TMI-2. The largest fraction of the core materials (33%) is located in the intact fuel

rods in the periphery and the bottom of the reactor core. Examination of these damaged assemblies indicate that they have not lost any of their core materials inventory and were not subjected to high temperatures. Of these fuel assemblies, approximately 10.7% of the original total are located beneath the prior-molten part of the central core region, and 22.7% are located in the assemblies in the periphery of the core. Verification that the partially intact assemblies have retained their inventories of fission products is discussed in Reference 14.

- Reactor vessel lower plenum. Visual inspection of the lower plenum indicates that a substantial amount of prior-molten core material now rests on the reactor vessel lower head. Debris located on the head has a wide range of sizes, ranging from solid, irregularly shaped pieces >15 cm across to relatively fine gravel-like particles. Table 45 indicates that the lower vessel debris bed contains about 19,000 kg of material that, based on the examination of a very limited sampling of debris obtained from the south and southwest quadrants of the core, is a homogeneous mixture of prior-molten $(U,Zr)O_2$ with <1% of all structural and control materials, except iron, which ranges from 2 to 4 wt% in the debris.

- CSA debris. The lower CSA, which contains about 4% of the total core material, is that portion of the reactor vessel below the core that includes the lower grid assembly and five flow distributor plates. The upper CSA, which contains about 3% of the core material, is a coolant flow region outside the vertical baffle plates that makes up the peripheral boundary of the core. Although no sample examinations have been performed on this debris, it is expected to be similar in composition to the material that was relocated to the lower reactor vessel head.

The following sections contain discussions of how the lower core region examination results relate to understanding core damage progression, and the core materials and fission product distribution in the lower core region.

4.1 Core Damage Progression

The information from the core bore examinations has been used to develop a better understanding of how the accident progressed during the early stages of the accident based on the end-state condition[19]. Early in the accident, it is believed that the upper core was heated to ~1600 K around 150 min into the accident, when rapid oxidation of the zircaloy cladding occurred. Initially, an iron, nickel, and zirconium eutectic is expected to form at temperatures as low as 1200-1400 K followed by rapid oxidation of the zircaloy. The unoxidized iron, nickel, and zirconium eutectic then melted and partially dissolved the UO_2 pellets to form a eutectic with the UO_2. Upon cladding breach, the liquid U-Zr-O mixture and metallic zircaloy, which had been heated to melting, flowed downward along the fuel rods, melting the Inconel grid spacers and control rods, adding these materials to the complex liquid material. This material solidified between the fuel rods in the cooler, lower region of the core, beginning the development of the lower crust with a complex agglomerate of metallic and oxidized zirconium and structural materials.

As the lower crust continued to form, the steam flow was diverted from the central to the peripheral region of the core, as it flowed upward. The enhanced peripheral cooling caused the downward moving material to freeze at progressively higher elevations, resulting in the bowl-shaped lower crust (crucible). Because cooling was negligible inside the shell of the crucible, the enclosed relocating material eventually remained at high temperature. Due to the disparate melting points of uranium dioxide (3100 K) and the eutectic, the molten eutectic settled around the solid fuel pellets near the bottom of the crucible. The materials data from the lower core indicate that the composition of the lower crust is similar at all locations in the crucible, although there was some selective separation of constituents (e.g., silver from indium).

As the extent of the crucible grew, blockage of steam flow to the upper part of the core reduced the oxidation rate of the zircaloy. The rapid heatup of the upper ends of the fuel rods due to oxidation gave way to a much slower heatup due to decay heat. This heating allowed flow of metallics into the crucible. Inside the crucible, the heatup of the molten eutectic was accompanied by a slow dissolution of the fuel pellets that would be completely melted in due time. The submerged fuel rods or fuel pellets supported the remaining fuel rod segments above the surface of the molten core material. With the melting of the submerged fuel pellets, a corresponding slumping of the rod segments above the molten pool occurred. The liquid level of the pool increased; however, the liquid fraction in the pool would remain more or less constant until the upper rod segments slumped into the pool. The presence of a rubble bed above the consolidated region indicates that the slumping did not go to completion, but was arrested, most likely because of the formation of the top crust during the 2-B primary coolant pump transient.

During the slumping phase, the molten pool, with immersed fuel pellets and a significant amount of molten/gaseous structural materials, was at a temperature below, or at most, slightly above the liquidus temperature of the $(U,Zr)O_2$ mixture (~2800 K). This would have caused most of the structural materials found in the consolidated region to be present as entrained gases. Any appreciable superheat in the liquid above the liquidus temperature was dissipated in dissolving the fuel pellets. Because the inner surface of the shell of the crucible was also at the liquidus temperature, heat transfer from the molten pool to the crucible was negligible. At this stage, the thickness of the shell of the crucible was determined by the heat generation inside the shell and the boundary conditions at the inner and outer surfaces of the shell. The temperature at the inner surface was at the melting point of the material. The exact temperature at the outer surface depended on the heatup history of the fuel rod stubs below the crucible and the peripheral rods. The presence of rod stubs below the crucible and some intact peripheral assemblies would put the maximum temperature at most of the outer surface of the shell about 2300 K. With these conditions, calculations show that the equilibrium thickness of

the shell was about a 0.1 m, which is similar to that observed in the core-boring operations.

During the pump transient, starting at 174 min, some coolant may have been forced into the region above the liquid surface of the partially molten pool, causing the temperature of the surface to drop below the solidus temperature of the material. Solidification of the surface would have proceeded to form the top crust. With the formation of the top crust, the partially molten pool inside the crucible was sealed off from the rest of the core. The top crust was formed from the slumping of fuel rod segments or rubble in the upper core region. So long as there was an appreciable amount of fuel pellets inside the pool, heat transfer to the pellets was efficient, and the pool temperature was kept close to the melting point of the material. Volatile materials such as cadmium and ^{129}I were now trapped in the pool; however, the examination results indicate that most of the iodine was probably released before the crust formed. Because the inner surface of the crust surrounding the molten pool was also at the melting point, heat transfer from the pool to the crust was negligible and erosion of the crust did not occur. When all the fuel pellets inside the pool were melted (estimated to take about 10 min), the temperature of the pool began to increase above the melting point of the material. Concurrently, heat transfer to the crust was increased. Such heat transfer thermally ablated the inner surface of the shell of the crucible and progressively reduced its thickness until all the heat transferred to the shell was conducted to its outer surface and dissipated to the coolant or the rest of the core material.

As for the top crust, heat transfer to its inner surface from the pool initially slowed the crust's growth, then stopped its growth, and finally started to erode away the crust, similar to the erosion of the shell of the crucible. If the outer surface of the crust was kept at some constant temperature and constant decay heat level was maintained, equilibrium would be reached at about 205 minutes, after heat started to transfer from the crust to the pool.

4.2 Bulk Core Materials Distribution

Knowledge of the end-state distribution of core materials in the lower core provides information that is useful in understanding and modeling core damage progression. The following sections discuss the distribution of the three principal groups of core materials present in the TMI-2 core: the fuel materials, control materials, and structural materials. Specific issues addressed in the examination section are discussed and related to understanding the behavior of core materials during the TMI-2 accident.

To assess the distribution of core materials in the the lower core, it was necessary to estimate the mass of metallic and ceramic constituents in the various regions of the core. This was particularly difficult in the case of the metallic constituents of the crusts and the central consolidated region. Table 46 lists the ceramic and metallic masses of each region of the lower core and the method used to estimate them. The estimates of metal content have a high degree of uncertainty, but are the only estimates available.

4.2.1 Fuel Materials

The distribution of fuel materials in the lower core is shown in Table 47. The average uranium concentrations indicate relatively similar concentrations in all regions of the lower core with the exception of the lower crust. The lower crust contains only about half the expected amount of uranium, as compared with the core average, indicating the presence of significantly more structural components in this part of the core. However, the uranium content of the ceramic region of the crust is near the core average.

The average concentration data for zirconium indicate similar concentrations in all core regions (within 6%). These data suggest a

TABLE 46. ESTIMATED CERAMIC AND FUEL MATERIAL CONTENT OF THE LOWER CORE

Core region	Estimated Total Quantity(kg)[a]	Estimated Ceramic Content(kg)[b]	Estimated Metallic Content (kg)[b]
Upper crust	2450	637	1813
Central region	21490	490[c]	21000
Lower crust	8760	3854	4900

a. The estimated total quantities of material in each region were based on defueling estimates, the core boring visual inspections, density, and thickness measurements of the crusts. For the crust layers the associated uncertainties are approximately 50%. For the total mass of the central region determined from defueling records, the uncertainty is approximately 10%.

b. Estimates of the metallic and ceramic content of the crusts were based on the average elemental analysis results for the crust.

c. The estimated metal content of the central region was based on the metal content retained in the core bore samples extrapolated to the volume of the central core region. This method of estimating was necessary, as much of the friable ceramic content of the core bores was washed out of the bore during the coring operation, leaving the metallic components in the core bore. This method is inaccurate and provides an estimate that is biased low, as some metallics were probably swept out of the core during the core boring operation.

TABLE 47. FUEL MATERIAL DISTRIBUTIONS IN THE MOLTEN POOL[a] (wt%)

Quantity	Core Materials Distribution				
	Upper Crust	Lower Crust	Peripheral Crust	Central Region	Core Average[b]
Uranium					
Average concentration	49	34	46	54	66
Ceramic region average concentration	66	65	66	60	66
Metallic region average concentration	27	9.6	8.6	2.2	--
Average core materials inventory (%)[c]	1.3	3.6	1.2[d]	12	--
Zirconium					
Average concentration	9	22	16	16	18
Ceramic region average concentration	15	13	15	19	18
Metallic region average concentration	8.3	29	20	7.6	--
Average core materials inventory (%)[c]	1.5	8.5	1.8[d]	18.2	--
Tin					
Average concentration	1.1	1.5	1.3	2.1	0.3
Ceramic region average concentration	0.48	0.70	0.59	0.69	0.3
Metallic region average concentration	2.5	2.2	2.9	4.5	--
Average core materials inventory (%)[c]	8.4	36	8.7[d]	5.8	--

a. This table summarizes the average concentrations for each region of the lower core.

b. The core average data is the average concentration of all materials in the core, assuming oxidation of part of the zircaloy and metallics, as previously discussed.

TABLE 4-. Continued

c. The average core materials inventory is the amount of materials located in that region of the core as a percentage of the total core inventory, assuming nominal masses for the upper crust of 2450 kg, the lower crust of 8760 kg, and the central core region of 21,490 kg. The metal content of the central core region was determined based on the metal content of the central core bore samples.

d. The peripheral crust data is extrapolated to the mass of the entire upper crust 2450 kg for comparison purposes.

similar average distribution in the entire lower core region; however, when the samples are divided into metallic/ceramic groups, a different distribution is apparent.

The data in Table 47 indicate similar zirconium distributions in the ceramic regions; however, the metallic region samples indicate some apparent depletion of zirconium in the upper crust and the central consolidated region. These data would support the conclusion in Section 4.1 that some of the metallic zirconium melted and flowed downward to help form the lower crust.

The average concentrations of tin in the lower core are four to six times greater than the core average concentration (0.3 wt%). The metallic and ceramic average concentrations indicate that, although there is a significant concentration of the tin in the metallic region as might be expected from the chemical behavior of tin (i.e., a high free energy requirement for oxidation), the concentration in the ceramic region is generally twice the core average.

4.2.2 Control Materials

Table 48 lists the nominal control material distributions in the lower core region. The average concentrations of silver are almost twice as high in all parts of the lower core than the core average. The ceramic and metallic sample average data indicate that the bulk of the silver is present in the metallic region, consistent with the oxidation potential. However, the silver concentrations in the ceramic regions are near the core average. This is in contrast to the upper core debris bed, where the silver concentrations were significantly below the core average. Much of the silver in the upper core region apparently melted and flowed down to form the crust regions and metallic inclusions in the central core region. The data indicate that about half the total silver inventory is associated with the lower core region, with the greatest amounts in the lower crust and the central core consolidated region.

TABLE 48. CONTROL MATERIAL DISTRIBUTIONS IN THE MOLTEN POOL[a] (wt%)

Quantity	Core Materials Distribution				
	Upper Crust	Lower Crust	Peripheral Crust	Central Region	Core Average[b]
Silver					
Average concentration	3.2	4.5	2.9	2.9	1.8
Ceramic region average concentration	1.6	3.3	1.7	1.1	1.8
Metallic region average concentration	5.9	5.5	7.1	7.3	--
Average core materials inventory [c]	3.6	18	3.3[d]	12	--
Indium					
Average concentration (wt%)	1.0	1.1	1.2	0.88	0.3
Ceramic region average concentration (wt%)	0.83	0.61	0.88	0.54	0.3
Metallic region average concentration (wt%)	1.5	1.5	2.4	1.8	--
Average core materials inventory (%)[c]	6.6	23	7.5[d]	29	--
Cadmium					
Average concentration	0.09	0.07	0.14	0.16	0.1
Ceramic region average concentration	0.05	0.04	0.08	0.04	0.1
Metallic region average concentration	0.06	0.09	0.24	0.32	--
Average core materials inventory (%)[c]	1.0	4.3	2.4[d]	7.2	--

a. This table summarizes the average concentrations for each region of the lower core.

b. The core average data is the average concentration of all materials in the core, assuming oxidation of part of the zircaloy and metallics, as previously discussed.

TABLE 48. Continued

c. The average core materials inventory is the amount of materials located in that region of the core as a percentage of the total core inventory, assuming nominal masses for the upper crust of 2450 kg, the lower crust, 8760 kg, and the central core region, 21,490 kg.

d. The peripheral crust data is extrapolated to the mass of the entire upper crust (2450 kg) for comparison purposes, but should not be added to the upper crust data.

The average indium concentrations are similar in all parts of the lower crust with concentrations three to four times the core average. As in the case of silver, a significant accumulation is present in the metallic phases, although a significant amount is also present in the ceramic parts at concentrations two to three times the core average. These data indicate that, if extrapolated to the mass of the various regions of the lower core, approximately 48% of the core inventory of indium is present in the lower core region. This estimate has a relatively large uncertainty due to the heterogeneity of the debris and the possibility of selective sample material retention in the central core region from the core-boring operations.

The cadmium concentrations for the lower core are similar to or less than the core average concentration of 0.1 wt%. Lesser concentrations are present in the ceramic regions than in the metallic regions, which might be expected as cadmium has a high oxidation potential. The highest average concentrations of cadmium are in the central core region, and the correlation with metal content suggests that much of the relatively volatile cadmium was not released from the core, but was retained in the central molten part of the core alloyed with other metals. Approximately 30% of the core inventory of cadmium was retained in the lower core region.

4.2.3 Structural Materials

The structural material concentrations in the various parts of the previously molten material are shown in Table 49. The average iron concentrations are similar in the upper and lower crusts, and there are greater concentrations of iron in the central core region at two to five times the core average. Iron makes up large percentages of the metallic phases in all regions of the core, with the highest percentages in the central region particles.

The concentrations for chromium in Table 49 are similar at concentrations ranging from 1.4 to 1.7 wt% with the bulk of the material located in the metallic region samples. The concentration of chromium in the metallic phase is about 4.7 times that in the ceramic phase. This is a

TABLE 49. STRUCTURAL MATERIAL DISTRIBUTIONS IN THE MOLTEN POOL[a] (wt%)

Quantity	Core Materials Distribution				
	Upper Crust	Lower Crust	Peripheral Crust	Central Region	Core Average[b]
Iron					
Average concentration	11	11	6.4	14	3.0
Ceramic region average concentration	2.3	3.0	1.6	3.5	3.0
Metallic region average concentration	28	17	23	44	--
Average core materials inventory (%)[c]	8.6	23	4.6[d]	6.2	--
Chromium					
Average concentration	1.6	1.6	1.7	1.4	1.0
Ceramic region average concentration	0.69	0.46	1.1	0.70	1.0
Metallic region average concentration	3.3	2.5	3.8	3.4	--
Average core materials inventory (%)[c]	3.8	14.2	3.8[d]	14.5	--
Nickel					
Average concentration	5.2	5.5	2.7	6.8	0.9
Ceramic region average concentration	0.77	2.4	0.48	1.3	0.9
Metallic region average concentration	14	8.0	11	22	--
Average core materials inventory (%)[c]	13	45	6.4[d]	10	--

TABLE 49. Continued

Quantity	Core Materials Distribution				
	Upper Crust	Lower Crust	Peripheral Crust	Central Region	Core Average[b]
Molybdenum					
Average concentration	0.44	0.34	0.25	0.89	0.03
Ceramic region average concentration	0.10	0.12	0.05	0.21	0.03
Metallic region average concentration	1.1	0.51	0.75	2.1	--
Average core materials inventory (%)[c]	27	62	17[d]	28	--

a. This table summarizes the average concentrations for each region of the lower core.

b. The core average data is the average concentration of all materials in the core, assuming oxidation of part of the zircaloy and metallics, as previously discussed.

c. The average core materials inventory is the amount of materials located in that region of the core as a percentage of the total core inventory, assuming nominal masses for the upper crust of 2450 kg, the lower crust, 8760 kg, and the central core region, 21,490 kg.

d. The peripheral crust data is extrapolated to the mass of the entire upper crust (2450 kg) for comparison purposes.

smaller multiple than in the case of iron (11.2), and nickel (15.3). These ratios reflect the increasing oxidation potential from chromium to iron to nickel. The nickel data in Table 49 indicate higher concentrations in the central core metallic particles and upper and lower crust layers. The data range from two to six times the core average. The concentrations of nickel in the upper and lower crusts and the central consolidated region are similar and significantly higher than the peripheral crust. No rationale for this difference is apparent. The nickel, as might be expected due to its high oxidation potential, is more concentrated in the metallic phases, with only a few percent located in the ceramic samples.

The molybdenum data indicate that molybdenum is significantly concentrated in all metallic regions of the lower core at concentrations 10 to 20 times the core average. The average ratio of molybdenum concentrations in metallic to ceramic phases is similar to that of iron, as might be expected because the oxidation potential for the two metals is similar. The Ni/Mo ratio data from Section 3 indicate that the Ni/Mo ratios in the metallic phase are near those for Inconel (a factor of 2). These data suggest that the crust layers in the core contain a substantial contribution from the Inconel grid spacers.

4.3 Fission Product Behavior

The following sections discuss the examination results from the bulk fission product examinations performed on the lower core region samples. The sections are divided into low, medium, and high volatile radionuclide behavior. Because of the heterogeneity of the sample materials, and the wide range of concentrations in some of the core regions, a number of different correlations are presented that provide bounds on fission product retention and the inventory present in each of the repositories. The average retention data provide a lower bound on the retention of the radionuclide because these data are a comparison with the average content of 1 g of uranium. The normalized retention assumes that the fission product content is associated with the uranium content of the sample and is most appropriate for those radionuclides expected to stay with the fuel

material. The ceramic and metallic data are the distribution of the normalized data between the two types of samples. The fission product inventory lists the percentage of the total core inventory present in each region of the lower core based on the average concentration of the fission products in all samples.

Note that these are nominal values based on the examination results available; there are indications that, particularly for the central consolidated region, the samples are not representative of the bulk material. However, as discussed in the previous section, the difference between the composition of the metallic and ceramic samples is quite distinct; therefore, the normalized data for the ceramic samples in the consolidated region are probably the best indication of the properties of the materials in the lower core region that were preferentially washed out of the bores during core boring.

4.3.1 Low Volatiles

Table 50 lists the fission product retention and distribution in the lower core region for the three low volatile fission products measured (i.e., ^{144}Ce, ^{154}Eu, and ^{155}Eu). The average retention data for ^{144}Ce provide little information for the low volatile radionuclides because they are expected to remain in the matrix of the fuel material; however, the normalized retention indicates that the lower and peripheral crusts and the central consolidated region are composed of relatively high burnup fuel material from the central core region. In contrast, the average normalized retention in the upper crust is lower in some samples and suggests the possible loss of ^{144}Ce near the periphery of the core. Inspection of the individual sample retentions for the upper crust (Table 15) indicates that the retentions are generally lower for these samples and, in some cases, at less than 30% of the expected retention. It is suggested that ^{144}Ce probably was removed from the uranium through chemical or other interactions, such as very high temperatures, in the upper crust.

TABLE 50. LOW VOLATILE FISSION PRODUCT DISTRIBUTION IN THE MOLTEN POOL[a] - (%) retention

Quantity	Fission Product Distribution			
	Upper Crust	Lower Crust	Peripheral Crust	Central Region
^{144}Ce				
Average retention[b]	43	51	50	93
Normalized retention[c]	76	132	87	121
Ceramic region average retention	85	130	91	125
Metallic region average retention	49	134	59	78
Percent fission product inventory (%)[d]	1.4	5.9	1.6[e]	24
^{154}Eu				
Average retention[b]	57	61	57	114
Normalized retention[c]	98	143	102	149
Ceramic region average retention	105	149	105	146
Metallic region average retention	80	131	82	185
Percent fission product inventory (%)[d]	2.0	7.9	2.0[e]	32
^{155}Eu				
Average retention[b]	47	44	39	85
Normalized retention[c]	81	125	83	103
Percent fission product inventory (%)[d]	1.6	5.1	2.5[e]	22

a. This table summarizes the average retention and fraction of core inventory for each region of the lower core, assuming nominal masses for the upper crust of 2450 kg, the lower crust, 8760 kg, and the central core region, 21,490 kg.

b. The average retention data is calculated using uranium equivalent concentrations that provide a lower bound on fission product retention. (i.e., assumes total sample weight is uranium)

TABLE 50. Continued

c. The normalized retention data assumes that all fission product content is associated with the uranium content of the sample and provides an upper bound on retention.

d. The percent fission product inventory is the percent of the total amount of each fission product located in the core.

e. The peripheral crust data is extrapolated to the mass of the entire upper crust (2450 kg) for comparison purposes.

The normalized retentions for the ceramic samples are similar to those of the total normalized retention and indicate that the metallic region reduces the average retention only slightly (due to the relatively few metallic samples analyzed). The metallic region data indicate significant reductions (a factor of 2) in the retention of the low volatiles in the metallic regions with the exception of the lower crust. Uranium present in metallic melt could be UO_2 dissolved in Zr-Fe-Ni-Cr alloy. The UO_2 structure is destroyed in this process. $CeO_{2(x)}$ is more stable than UO_2 and may form an immiscible ceramic phase, thereby separating from the UO_2. The metallurgical data indicate that the fuel material in the lower crust had recrystallized from the melt as $(U,Zr)O_2$. It is interesting that the CeO_2 inventory is apparently retained during this process.

The inventory data indicate that approximately 31% of the core inventory of ^{144}Ce is located within the crusts in the lower core region. The intact fuel rods below this region account for another approximately 11% of the total. The data for the other regions in the lower core indicate that the lower crust contains about 6% of the total, with the upper crust approximately 1.5% of the total.

The ^{154}Eu and ^{155}Eu data indicate similar trends to those seen for the ^{144}Ce, except for variations in the measured retention values and total inventory for ^{154}Eu, which is due mostly to variations in the inventory data because of the relatively large uncertainty associated with the inventories of radionuclides produced by neutron capture by another radionuclide. In this instance, ^{155}Eu is produced by neutron capture by ^{154}Sm, a stable fission product.

4.3.2 Medium Volatiles

The nominal fission product distributions for the lower core region are listed in Table 51. The data for ^{90}Sr, the radionuclide in this category that exhibited the least mobility, indicates relatively low average and normalized retention data in the upper and peripheral crusts and the

TABLE 51. MEDIUM VOLATILE FISSION PRODUCT DISTRIBUTION IN THE MOLTEN POOL[a]

Quantity	Fission Product Distribution (%) Upper Crust	Lower Crust	Peripheral Crust	Central Region
^{90}Sr				
Average retention[b]	23	38	24	33
Normalized retention[c]	39	104	36	78
Ceramic region average retention	56	117	31	86
Metallic region average retention	15	94	58	59
Percent fission product inventory[d]	0.73	4.5	0.45[e]	8.3
^{125}Sb				
Average retention[b]	330	490	220	350
Normalized retention[c]	880	770	1690	9030
Ceramic region average retention	16	29	80[f]	129[f]
Metallic region average retention[g]	640	860	1960	1060
Percent fission product inventory[d]	8.3	43.4	7.4[e]	10

TABLE 51. Continued

Quantity	Fission Product Distribution (%) Upper Crust	Lower Crust	Peripheral Crust	Central Region
^{106}Ru				
Average retention[b]	193	330	97	510
Normalized retention[c]	770	990	1070	14,100
Ceramic region average retention	50	34	47	107
Metallic region average retention[g]	370	580	420	1,240
Percent fission product inventory[d]	4.6	29.7	3.4[e]	11.2

a. This table summarizes the average retention and fraction of core inventory for each region of the lower core assuming nominal masses for the upper crust of 2450 kg, the lower crust, 8760 kg, and the central core region, 21,490 kg.

b. The average retention data is calculated using uranium equivalent concentrations that provide a lower bound on fission product retention.

c. The normalized retention data assumes that all fission product content is associated with the uranium content of the sample and provides an upper bound on retention.

d. The percent fission product inventory is the percent of the total amount of each fission product located in the core.

e. The peripheral crust data is extrapolated to the mass of the entire upper crust (2450 kg) for comparison purposes.

f. Result biased high by a single high value with some metallic content.

g. Normalized to average retention rather than normalized retention, which is appropriate for the radionuclides associated with the metal content of the debris.

central consolidated region. In contrast, the data for the lower crust indicate approximately 100% retention of the ^{90}Sr in the fuel material. The retention data indicate generally higher ^{90}Sr retentions in the ceramic parts of the samples, but that there has been some transport of the ^{90}Sr to the metallic region samples.

The ^{125}Sb data in Table 51 indicate average and normalized retentions much higher than the core average at all locations in the lower core region. ^{125}Sb content in the lower core is on the average 2.2 to 4.9 times the average concentration found in intact fuel. When these data are normalized to uranium content, the ratio changes to 7.7 to 90 times those found in intact fuel. However, this comparison is inappropriate as the bulk of the ^{125}Sb is located in the metallic regions at high concentrations and is not associated with the fuel material present in the crusts or consolidated region. The ceramic sample data for ^{125}Sb indicate that the concentrations are relatively low (generally less than 50% of the average inventory). The data for the peripheral crust and central region are biased by the presence of metallic material in several mostly ceramic samples.

The ^{106}Ru data listed in Table 51 follow a similar distribution to that observed for the ^{125}Sb data. Much of the ^{106}Ru is found in association with metallic samples at concentrations 4 to 12 times those of intact fuel. The reaction mechanisms allowing this behavior are discussed in Reference 18. It is more likely that the metallic materials were present in the consolidated region before or during the time that ruthenium and antimony were released from the fuel. This must be true for these fission products to be segregated in the metallic phases.

4.3.3 High Volatiles

The retentions for the high volatiles (^{129}I and ^{137}Cs) are listed in Table 52. The average and normalized data indicate that ^{129}I is found in all core regions, and that it is also found in the metallic regions of the core. These data suggest that there may be reaction mechanisms that cause accumulation of ^{129}I in the metallic sections. The fraction of core inventory found in association with the lower core region prior-molten material is 2.4%, which indicates that, although some retention of this species occurs, most is released.

TABLE 52. HIGH VOLATILE FISSION PRODUCT DISTRIBUTION IN THE MOLTEN POOL[a]

Quantity	Fission Product Distribution (%) Upper Crust	Lower Crust	Peripheral Crust	Central Region
^{129}I				
Average retention[b]	8.1	30	2.8	8.1
Normalized retention[c]	19	66[f]	14	65
Ceramic region average retention	7.2	98[f]	3.5	9.1
Metallic region average retention	35	93	52	186
Percent fission product inventory[d]	0.27	3.5	0.1[e]	2.1
^{137}Cs				
Average retention[b]	13	12	2.7	3.0
Normalized retention[c]	26	31	12	10
Ceramic region average retention	4.9	35	3.2	7.1
Metallic region average retention	28	27	41	19
Percent fission product inventory[d]	0.41	1.4	0.1[e]	0.87

a. This table summarizes the average retention and fraction of core inventory for each region of the lower core assuming nominal masses for the upper crust of 2450 kg, the lower crust, 8760 kg, and the central core region, 21,490 kg.

b. The average retention data is calculated using uranium equivalent concentrations that provide a lower bound on fission product retention.

c. The normalized retention data assumes that all fission product content is associated with the uranium content of the sample and provides an upper bound on retention.

TABLE 52. Continued

d. The percent fission product inventory is the percent of the total amount of each fission product located in the core.

e. The peripheral crust data is extrapolated to the mass of the entire upper crust (2450 kg) for comparison purposes.

f. Result biased by two high retention values.

5. CONCLUSIONS AND OBSERVATIONS

The metallographic examinations of the TMI core bore samples indicated that the upper and peripheral crust material, as well as the material from the central consolidated region, were very similar. Samples from these regions can basically be described as a mixture of metallic and ceramic melts, with some segregation of metallic and ceramic phases. This segregation is due in some cases to immiscible metallic melts, particularly Ag-In and Fe-Cr-Ni, and sometimes the segregation is simply due to melts flowing over and through previously solidified melt material. Examples of metallic melts flowing through cracks in the solidified ceramic melt material are certainly evident in samples from the upper crust, which suggests that metallic melts from higher in the reactor core flowed down over the solidified upper crust. This also indicates that the melt progression was incoherent and took place over time.

Fuel liquefaction by zircaloy melts was observed in regions of the upper crust, which indicates temperatures in excess of 2200 K; however, the presence of $(U,Zr)O_2$ melt regions indicates that temperatures in some regions of the upper and peripheral crusts exceeded 2810 K prior to solidification. Localized temperatures within material in the center of the consolidated region exceeded the 3120 K melting point of the UO_2 fuel, as evidenced by large voids and porosity in some fuel pellet remnants. Average temperatures in the central consolidated region were certainly above 2810 K, in order to form the molten $(U,Zr)O_2$ that eventually flowed out of a breach in the crust and relocated to the lower vessel head.

In contrast to the other regions, the lower crust consisted primarily of metallic melts which flowed down and surrounded intact fuel pellet stacks. This metallic melt material can be assumed to represent material which relocated early in the melt progression. The lowest extent of this material probably solidified near the lowest water level during the accident. Oxidized cladding remnants were dissolved by these metallic melts, and any unoxidized zircaloy (no significant zircaloy oxidation was observed in the intact rod regions just below the lower crust) would

probably have liquefied as a result of eutectic interactions between the zircaloy, silver, iron, and nickel. These interactions become significant above approximately 1400 K, with complete solidification of these materials expected by approximately 1200 K. Minor amounts of fuel liquefaction by the metallic melts were observed, which suggests localized maximum peak temperatures of approximately 2200 K. Based upon this information, a best estimate average temperature for the lower crust material is approximately 1300-1500 K.

The thickness of the crust varied from 4.5 to 11.5 cm, with the greatest thickness measured in the upper crust. These data suggest a relatively uniform crust thickness, which might be expected if it is assumed that this crust contained a molten pool of material of relatively uniform temperature. The density of samples from the upper and peripheral crusts varied from 7.6 to 9.7 g/cm^3, which reflects a consolidated mixture of $(U,Zr)O_2$ and metallic materials, whereas the density of the lower crust varied from 7.0 to 7.6 g/cm^3, which reflects the presence of significant amounts of zircaloy melt. The density of samples from the central consolidated region ranged from 5.5 to 8.8 g/cm^3, which reflects the segregation of immiscible metallic and ceramic melts.

The condition of the intact rod segments below the lower crust indicates that very little zircaloy oxidation occurred in this region, and that the rods remained ductile. Temperatures varied as a function of reactor core position and axial heights, but in general the temperatures were relatively cool. Molten control rod material indicated temperatures in excess of 1073 K on the upper endtips of some of the intact control rod segments on the periphery of the core, whereas the as-fabricated condition of the zircaloy cladding in many parts of this region indicated that temperatures were below the recrystallization temperature of 920 K. The fuel rod lengths varied from approximately 60 cm near the center of the core to approximately 120 cm near the periphery of the core. These data suggest that the lowest water level during the accident was approximately 60 cm above the lower end fitting in the center of the reactor core. The presence of longer rod segments in the peripheral regions suggests that the lower

crust solidified in a hemispherical shape, reflecting the cooler temperatures which would generally be expected in the peripheral regions for a given axial elevation.

The radiochemical examination data indicated that the upper and peripheral crusts were primarily ceramic material with some metallic material. The examinations indicated that the metallic portion of the upper crust was mostly made up of structural materials with lesser amounts of zirconium. For zirconium, the data from the ceramic regions range from 10 to 20 wt%; the average is 13 wt%, which indicates that zirconium is depleted in the upper crust relative to the core average concentration of 18 to 19 wt%.

Control materials were measurable in both metallic and ceramic material samples of the upper and peripheral crusts at an average concentration of about 3 wt%, which is greater than the expected core average concentration of silver (1.9 wt%). Indium and cadmium were both also measurable with indium at approximately 3 times the core average concentration. The Ni/Mo ratios in the upper crust suggest that the Inconel grid spacers contributed to the formation of the crusts along with some stainless steel.

The bulk of the uranium enrichment data for the upper crust suggests that the upper crust is a composite of the 1.98% and 2.64% enriched assemblies with a very homogeneous distribution of the fuel material from the two assembly enrichments in the upper crust. Also, the high relative retentions for the low volatile fission products suggest that the fuel material forming the upper crust came from a relatively high burnup region of the core and that the upper crust was not formed by fuel material from the upper periphery of the core.

The ^{90}Sr data for the upper crust indicate a wide range of concentrations with no apparent distinction between metallic and ceramic samples. The data indicate mobility of this radionuclide with no obvious correlation with elemental composition or other radionuclide characteristics. Comparisons with the elemental analysis results were also

performed for ^{125}Sb and ^{106}Ru. These comparisons indicate a general increase in metallic content generally correlated with large increases in ^{125}Sb and ^{106}Ru content.

Examinations for the high volatiles ^{129}I and ^{137}Cs indicate retention of these fission products in both metallic and ceramic materials. Comparisons indicate retentions in the ceramic phase that are approximately 5%, whereas in the metallic phase the uranium-based, normalized retentions are about 35%. However, the concentration data are similar in both types of material, which indicates that the high concentrations in the metal phases are an artifact of the normalization to uranium content which is low in the metallic samples.

The lower crust generally is composed of relatively intact columns of fuel pellets embedded in a metallic mixture. The intact columns contain some veins of metallic materials that extend into the cracks in some fuel pellets. The elemental data indicate that zirconium is concentrated in the crust and that tin is not transported with the zirconium and may tend to form accumulations separate from the zirconium in the lower crust. The average concentration data for the lower crust indicates that iron is the principal structural material present (average 11 wt%) and that it ranges up to 34 wt% in the metallic regions of the crust. Lesser concentrations of nickel (average 5.5 wt%) and chromium (average 1.6 wt%) are also present (zirconium is 30 wt% in the metallic region).

The presence of significant amounts of molybdenum in the lower crust at ratios appropriate for Inconel suggests that Inconce was a significant contributor to the formation of the crust.

The average retention of low volatiles for the ceramic and metallic regions of the lower crust are between 130 and 134%. These high concentrations (i.e., >100% retentions) indicate that the fuel material forming the lower crust came from a relatively high burnup region of the core.

For the medium volatiles, the data generally suggest that the bulk of the ^{90}Sr has been retained in the ceramic regions with only small amounts present in the metallic regions of the lower crust. For ^{125}Sb and ^{106}Ru, comparisons were performed with the concentrations of elemental constituents of the crust; no correlations were observed with the exception that a general increase in metallic content generally correlated with an increase in ^{125}Sb and ^{106}Ru content.

The samples obtained from the central core region debris are quite heterogeneous; many samples are either metallic or ceramic, and some samples are a mixture of the two types of material. Examination of the data indicate that the least volatile control material, silver, was measurable in both metallic and ceramic material samples at an average concentration of about 2.9 wt%, with a range of concentrations from 0.07 to 34 wt%. Also, indium was measurable in all samples at concentrations averaging 0.9 wt% (core average 0.3 wt%), with the data ranging from 0.05 to 7.6 wt%. Cadmium was measurable in only about one-half of the samples obtained from the central core, principally the metallic ones. It is suggested that cadmium alloyed with other materials at relatively low concentrations, which reduced the vapor pressure substantially and caused retention in the reactor vessel.

The low volatile radionuclides have relatively consistent average retentions from 78 to 185%, which suggests that much of the central core region was formed from fuel material from a relatively high burnup region close to the center of the reactor core. The data generally suggest that a fraction of the ^{90}Sr has not been retained in the uranium fractions of either the ceramic or metallic samples.

6. REFERENCES

1. E. L. Tolman et al., TMI-2 Accident Scenario Update, EGG-TMI-7489, December 1986.

2. G. R. Eidem et al., "TMI-2 Defueling Conditions and Summary of Research Findings," Proceedings of IAEA/NEA International Symposium on Severe Accidents in Nuclear Power Plants, Sorrento Italy, March 21-25, 1988.

3. J. Adams and R. Smith, Lower Plenum Video Data Survey, EGG-TMI-7429, July 1987.

4. E. L. Tolman et al., TMI-2 Accident Evaluation Program, EGG-TMI-7048, September 1986.

5. M. L. Russell et al., TMI-2 Accident Evaluation Program Sample Acquisition and Examination Plan for FY-1987 and Beyond, EGG-TMI-7521, February 1987.

6. E. L. Tolman et al., TMI-2 Core Bore Acquisition Summary Report, Rev. 1, EGG-TMI-7385, February 1987.

7. M. L. Russell et al., TMI-2 Accident Evaluation Program Sample Acquisition and Examination Plan for FY-1988 and Beyond, EGG-TMI-7992, February 1988.

8. B. G. Schnitzler and J. B. Briggs, TMI-2 Isotopic Inventory Calculations, EGG-PBS-6798, August 1985.

9. Nuclear Safety Analysis Center, TMI-2 Accident Core Heat-Up Analysis, NSAC-25, June 1981.

10. C. V. McIsaac and D. W. Akers, TMI-2 Core Bore Gamma-Ray Spectroscopy Measurements, EGG-TMI-8058, June 1988.

11. M. L. Russell, TMI-2 Core Horseshoe Ring Examination, GEND-INF-083, October 1987.

12. J. Esteban, Core Materials, Melting Points, and Interactions, in publication.

13. J. M. Broughton, Private Communication, EG&G Idaho, Inc., May 1985.

14. D. W. Akers et al., "Verification of the ORIGEN2 Code Analyses for the TMI-2 Reactor Core," Proceedings of the ACS Symposium on Nuclear Reactor Severe Accident Chemistry, Toronto Canada, June 6-11, 1988.

15. D. W. Akers et al., TMI-2 Core Debris Grab Samples--Examination and Analysis, GEND-INF-075, September 1986.

16. C. S. Olsen et al., Examination of Debris from the Lower Head of the TMI-2 Reactor, GEND-INF-084, June 1988.

17. Barry Z. Hyatt, Metallographic Hydride Standards for LWBR Zircaloy 4 Seed Tubing Based on Out-of-Pile Corrosion Tests, WAPD-LC(BB)-89, February 1974.

18. D. W. Akers, "Fission Product Behavior in the TMI-2 Reactor Core," ANS TMI-2 Topical Meeting, October 27 to November 1, 1988.

19. P. Kuan, "TMI-2 Consolidated Region Crust Behavior," TMI-2 Topical Meeting, to be published.

TABLE 45. ESTIMATED POSTACCIDENT CORE MATERIALS DISTRIBUTION

Core region	Estimated Quantity(kg)	Uncertainty[a] (%)	Percent of Total core(%)
Intact fuel assemblies (Partially or fully intact)	44,500	5	33.4
Central core region resolidified mass	32,700	5	24.5
Upper core debris bed	26,600	5	19.9
Prior-molten material on the Lower reactor vessel head	19,100	20	14.3
Lower core support assembly[b]	5,800	40	4.3
Upper core support assembly[b]	4,200	40	3.2
Outside the reactor vessel	450	--[c]	0.3

a. The uncertainty estimates are based on defueling. Those areas that have been defueled at this time have relatively low uncertainties, whereas those that have not have relatively high uncertainties.

b. The lower core support assembly is that portion of the reactor vessel below the core that includes the lower grid assembly and five flow distributor plates. The upper core support assembly is a coolant flow region outside the vertical baffle plates that make up the peripheral boundary of the core.

c. Estimates of the amount of fuel material outside the reactor vessel are based on nondestructive evaluations of reactor components in the reactor and auxiliary buildings. They range from 60 to ~430 kg.